THE ROLE OF AUTOPHAGY IN CONTROL OF GLUCOSE HOMEOSTASIS

A Dissertation

by

ZHENG SHEN

Submitted to the Graduate and Professional School of
Texas A&M University
in partial fulfillment of the requirements for the degree of

DOCTOR OF PHILOSOPHY

Chair of Committee,	Shaodong Guo
Committee Members,	Annie Newell-Fugate
	Linglin Xie
	Yuxiang Sun
Head of Department,	David Threadgill

December 2021

Major Subject: Nutrition

ABSTRACT

Blood glucose homeostasis is essential for human growth, physical activities, and health. The present study proposes a possible mechanism for autophagy-mediated hepatic glucose production (HGP) during starvation, which is likely to be in a FoxO1-dependent manner. HGP assay showed that autophagy deficiency induced by either chloroquine (CQ) or siRNA-ATG7 significantly suppressed the HGP in wild type (WT), but not in liver-specific FoxO1 knockout (L-FKO) mouse hepatocytes. Similarly, the glucagon tolerance test and pyruvate tolerance test showed that upon inhibition of autophagy, only WT mice but not L-FKO mice exhibited a significant reduction in glucose production compared to the WT or L-FKO mice without autophagy deficiency. Western blot results further revealed that under autophagy deficiency, the protein amount of FoxO1 was remarkably reduced, accompanied with a significant decrease of FoxO1 nuclear localization. Notably, the reduction of FoxO1 protein amounts induced by autophagy deficiency was independent of FoxO1-S253 and FoxO1-S273 phosphorylation, as the reduction of FoxO1 persisted in hepatocytes isolated from FoxO1-S253$^{A/A}$ and FoxO1-S273$^{D/D}$ knock-in (KI) mice. Even proteasome inhibitor MG132 did not prevent FoxO1 from decreasing under autophagy deficiency, suggesting that the FoxO1 degradation was unlikely the major cause. In addition, autophagy deficiency did not change FoxO1 mRNA level, meaning that the reduction of FoxO1 was likely happening in post-transcriptional activities. The HPLC results unveiled that autophagy deficiency significantly altered hepatic amino acid pools and amino acid transportation including ATF4-LAT1 axis. With an addition of exogenous amino acid

mixture, we successfully restored the FoxO1 protein amount and HGP even under autophagy deficiency. Meanwhile, amino acid supplementation-induced restoration of FoxO1 and HGP was abolished by protein synthesis inhibitor cycloheximide (CHX), suggesting that the alteration of amino acid pools caused by autophagy deficiency impaired FoxO1 protein synthesis. The present study highlights an important role of autophagy involved in glucose homeostasis, which is to maintain the hepatic amino acid pools under starvation, subsequently supporting the activity of FoxO1 in control of the HGP.

DEDICATION

This study is wholeheartedly dedicated to my beloved parents, Rui Jiang and Qigang Shen, who have offered tremendous support and encouragement during my entire life. Thanks mom and dad for always believing in me and for encouraging me to chase my goal.

ACKNOWLEDGEMENTS

I would like to express special gratitude to my brilliant PhD supervisor and committee chair, Dr. Shaodong Guo, who has demonstrated how a great scientist could be, and he is always providing me with tremendously valuable guidance and inspiration throughout my PhD study. I would also like to sincerely thank my committee members Drs. Annie Newell-Fugate, Linglin Xie, and Yuxiang Sun for their priceless advice on my research. I highly appreciate all their help for me.

I would also like to thank my close friends Drs. Yufei Zhang and Tinyi Chu, for their continuous encouragement and inspiration throughout my undergraduate and postgraduate study.

My deepest thanks are given to my dear colleagues in Dr. Guo lab, including Dr. Quan Pan, Dr. Wanbao Yang, Dr. Xiaopeng Li, Dr. Hui Yan, Dr. May Yunmei Chen, Mr. Nicolas Hesseltine, Dr. Wang Liao, Dr. Wendy Zhou, Mr. Wiki Weiqi Ai, and Ms. Wen Jiang for their support and encouragement throughout the five years of my PhD study. A special thank is given to Mr. Thomas Peikert who helped proofreading of this article.

CONTRIBUTORS AND FUNDING SOURCES

Contributors

This work was supervised by the dissertation committee consisting of Professor Shaodong Guo (advisor), Professor Linglin Xie and Professor Yuxiang Sun of the Department of Nutrition, and Professor Annie Newell-Fugate of the Department of Veterinary Physiology and Pharmacology.

The amino acids determination in the primary hepatocytes and liver tissue lysate samples by the HPLC method in Chapter IV was conducted by Mr. Gayan Nawaratna and Mr. Wenliang He from Guoyao Wu's lab in the Department of Animal Science, Texas A&M University.

Retro-orbital (RO) injection was conducted by Dr. Wanbao Yang. The mouse tissue collection was performed with the lab colleagues in Guo Lab of the Department of Nutrition (Dr. Quan Pan, Dr. Wanbao Yang, Dr. Xiaopeng Li, Dr. Wang Liao, Mr. Wiki Weiqi Ai and Ms. Wen Jiang).

All other work conducted for this dissertation was completed by the PhD student, independently.

Funding Sources

The graduate study was partially supported by graduate teaching assistantship from the Department of Nutrition, Texas A&M University.

This work was mainly supported by National Institutes of Health grants (R01 DK095118 and R01 DK120968), American Diabetes Association Career Development

Award (1-15-CD-09), the faculty startup funds from Texas A&M University Health Science Center and AgriLife Research, and the U.S. Department of Agriculture National Institute of Food and Agriculture grant (Hatch 1010958) to Shaodong Guo (Principal Investigator).

NOMENCLATURE

AAV8	Adeno-associated virus serotype 8
ALA	Alanine
ARG	Arginine
ASN	Asparagine
ASP	Aspartate
ATF4	Activating transcription factor 4
ATG7	Autophagy-related gene 7
Beta-ALA	Beta-alanine
CaMKK-β	Calcium/calmodulin-dependent protein kinase β
CHX	Cycloheximide
CIT	Citrulline
CQ	Chloroquine
CREB	cAMP response element-binding protein
F2,6P2	Fructose-2,6-bisphosphate
FBPase	Fructose bisphosphatase
FoxO1	Forkhead box protein O1
G6Pase	Glucose 6-phosphatase
GCG	Glucagon
GCGR	G-protein coupled glucagon receptor
GD	Gestational diabetes

GLU	Glutamate
GLN	Glutamine
GLY	Glycine
HCQ	Hydroxychloroquine
HGP	Hepatic glucose production
HIS	Histidine
HPLC	High performance liquid chromatography
IDF	International diabetes federation
ILE	Isoleucine
IP	Intraperitoneal
IRS1/2	Insulin receptor substrate 1 and 2
LEU	Leucine
L-FKO	Liver-specific FoxO1 knockout
LYS	Lysine
MET	Methionine
MG132	Proteasome Inhibitor Cbz-leu-leu-leucinal
PCK	Phosphoenolpyruvate carboxykinase
PKCε	The epsilon isoform of protein kinase C
ORN	Ornithine
PHE	Phenylalanine
RO	Retro-orbital
RT-qPCR	Reverse transcription quantitative real-time PCR

SER	Serine
$S253^{A/A}$ KI	FoxO1-S253A knock-in
$S273^{D/D}$ KI	FoxO1-S273D knock-in
siR-ATG7	siRNA-ATG7
SLC7A5/LAT1	Solute carrier family 7 member 5/L-type amino acid transporter
T1D	Type 1 diabetes
T2D	Type 2 diabetes
TAU	Taurine
TCA	Tricarboxylic acid
THR	Threonine
TRP	Tryptophan
TYR	Tyrosine
VAL	Valine
VDCCs	Voltage-dependent calcium channels
VLDL	Very-low-density lipoprotein
WT	Wild type

TABLE OF CONTENTS

Page

LIST OF FIGURES

Page

LIST OF TABLES

Page

CHAPTER I

INTRODUCTION AND LITERATURE REVIEW

Carbohydrates, as the main fuel of human body, are playing an essential role in supporting human health, growth, and development. In order to keep our cells and organs functioning properly, our blood glucose level is maintained in between 80 mg/dL and 120 mg/dL (about 4.4 mM to 6.7 mM) [1-3]. In particular, a physiological range of blood glucose level is extremely important for ensuring a constant glucose supply to our erythrocytes and central nervous system (CNS)[4-9]. Erythrocytes do not contain mitochondria, therefore the energy supply in erythrocytes is solely from glycolysis and pentose phosphate pathway in which glucose is the substrate[9-11]. Likewise, glucose is the major energy source (~80%) of our brain, even though the brain is able to utilize ketone bodies as the alternative energy source[12, 13]. On top of that, our muscle contraction requires large amount of adenosine triphosphates (ATPs) generated from oxidative phosphorylation in which reducing equivalents (e.g., NADH, $FADH_2$) produced from glycolysis and tricarboxylic acid (TCA) cycle are the principal substrates[7, 14, 15]. In contrast, patients with hypoglycemia have a high chance to develop cognitive dysfunction like coma and seizure[6, 16].

In order to maintain a proper blood glucose level, our body evolved a sophisticated regulatory machinery in which insulin and glucagon are playing the central roles. Glucagon, which is synthesized and secreted from pancreatic α-cells, is a peptide hormone consisting of 29 amino acids which folds into a short alpha helix secondary structure[17, 18]. When our body is under fasting conditions, the relatively low blood glucose level (usually less than 99 mg/dL or 5.5 mM) triggers α-cells to secrete glucagon into circulation.

Glucagon not only promotes glycogenolysis and gluconeogenesis in the liver to produce glucose, but also triggers lipolysis in adipose tissues, resulting in the generation of fatty acids as the non-carbohydrate substrate for gluconeogenesis[19-21]. On the other hand, when our body is under the feeding conditions, insulin, which is playing as a counter-regulatory hormone on glucagon, is synthesized and secreted from pancreatic β-cells. With the help of insulin signaling, glucose disposal and lipogenesis are promoted in insulin-sensitive organs/tissues (e.g., the liver, skeletal muscle, and adipose tissues), resulting in a decrease of blood glucose level and increase of glycogen and lipid storage[20, 22, 23].

After decades of studies, more and more new intracellular mechanisms involved in glucose homeostasis are unveiled. In particular, autophagy, which is the dynamic process of eukaryotic cells breaking down intracellular components such as misfolded proteins, protein aggregates or damaged organelles by lysosomal degradation, is found to play an indispensable role in energy balance[24, 25]. Forty years ago, it was first demonstrated that glucagon could be a potential inducer of autophagy[26]. Recently, it has been reported that glucagon promotes autophagy by triggering Ca^{2+}- calcium/calmodulin-dependent protein kinase β (CaMKK-β) signaling cascade under starvation[27-30]. Considering the activities of autophagy is elevated under fasting and regulated by glucagon, we would like to further investigate the potential contribution of autophagy to hepatic glucose production (HGP). In the present study, we found that autophagy is an important mechanism to sustain the protein level of forkhead box protein O1 (FoxO1) which is a critical transcription factor regulating gluconeogenic gene expression, subsequently supporting HGP under starvation conditions.

Hormonal regulation in the liver

Glucagon promotes HGP in the fasting state

Glucagon is the major hormone promoting HGP during starvation via glycogenolysis and gluconeogenesis. In terms of the regulation of glycogenolysis, glucagon interacts with a glucagon receptor which is a member of the G-protein coupled family of receptors (GCGR) located on the plasma membrane of hepatocytes, leading to the activation of adenylate cyclase (AC)[31, 32]. AC catalyzes the conversion of ATP to cyclic adenosine monophosphate (cAMP) at the inner surface of the plasma membrane[33, 34]. Elevation of cAMP concentration initiates the conformational changes of cAMP-dependent protein kinase (PKA) which in turn becomes active and catalyzes the phosphorylation of phosphorylase kinase B (inactive form), generating phosphorylase kinase A (active form). Phosphorylase kinase A (PPK) further catalyzes the phosphorylation of glycogen phosphorylase B (inactive form) to generate glycogen phosphorylase A (active form). Activated glycogen phosphorylase (PYG) catalyzes the phosphorolytic cleavage of the 1-4 linkage of glycogen, releasing glucose-1-phosphate (G1P). G1P is then converted to glucose-6-phosphate (G6P) which eventually turns into glucose under the catalyzation of glucose-6-phosphatase (G6Pase)[35-37].

Apart from glycogenolysis, glucagon-activated PKA stimulates gluconeogenesis by using non-carbohydrate carbon substrates, such as pyruvates, lactates and amino acids. In the gluconeogenic signaling pathways, PKA has three important phosphorylation targets, fructose-2,6-bisphosphatase (FBPase-2), cAMP-response element binding protein (CREB) and FoxO1[7, 38, 39]. Particularly, FBPase-2 is a bifunctional enzyme which is not

only responsible for the conversion of fructose-2,6-bisphosphate (F2,6P2) to fructose-6-phosphate (F6P) in the gluconeogenic pathway, but also able to reverse this enzymatic reaction as phosphofructokinase-2 (PFKase-2) in its dephosphorylated state during glycolysis[7]. In the fasted state, glucagon activates PKA, which in turn catalyzes the phosphorylation of PFKase-2 at serine 32 to activate its phosphatase domain (i.e., turning into FBPase-2). FBPase-2 cleaves the phosphoric monoester bonds of F2,6P2 to generate F6P. Decrease of F2,6P2 concentration releases the inhibitory effect of F2,6P2 on fructose-1,6-bisphosphatase (FBPase-1), favoring the generation of F6P in the process of gluconeogensis[7]. In addition, PKA catalyzes the phosphorylation of CREB at serine 133, which initiates the recruitment of CREB-binding protein (CBP) and CREB-regulated transcriptional coactivators 2 (CRTC2), forming a CREB-CBP-CRTC2 complex in the nucleus. This complex binds to cAMP response element (CRE) of the promoter regions of target genes including gluconeogenic genes *g6pc* and *pck1*, leading to upregulation of G6Pase and phosphoenolpyruvate carboxykinase (PCK) which are two key enzymes contributing to gluconeogenesis[38-40]. Finally, recent studies revealed that PKA catalyzes the phosphorylation of FoxO1 at serine 276, which improves FoxO1 stability and nuclear localization[35, 41]. Under this circumstance, more FoxO1 are able to stay in the nucleus and bind to the insulin response element (IRE) of the promoter regions of *g6pc* and *pck1*, resulting in promotion of gluconeogenesis (Figure 1)[38, 42-44].

Insulin suppresses HGP in the feeding state

In the feeding state, insulin is a principal hormone responsible for the upregulation of glycolysis and lipogenesis, and downregulation of gluconeogenesis and glycogenolysis

in the liver, leading to reduction of HGP, promotion of glucose disposal in insulin-sensitive tissues/organs (e.g., skeletal muscle), and storage of lipids in adipose tissues[22, 23, 45]. In the liver, insulin signaling starts from the interaction between insulin and an insulin receptor (IR) which is a transmembrane receptor in the plasma membrane of hepatocytes. Upon this ligand-induced initiation, tyrosine residues of IR undergo autophosphorylation and activation, triggering downstream signaling cascades starting from the recruitment of insulin receptor substrate 1 and 2 (IRS1/2)[46, 47]. IRS1/2 are members of cytoplasmic adaptor proteins typically responsible for insulin signaling. Notably, IRS1 is reported to have a dominant role in controlling of the insulin signaling cascade compared to IRS2 in the liver, probably because IRS1, but not IRS2, can regulate gene expression responsible for both glucose and lipid metabolisms[48, 49]. There are several tyrosine phosphorylation sites in the C-terminal of IRS1/2. Once these tyrosine phosphorylation sites become phosphorylated by IR, they serve as binding sites for the Src homology-2 (SH2) domain in the regulatory subunit (p85) of phosphatidylinositol 3-kinase I class (PI3K-1), leading to the formation of a PI3K-1 heterodimer between regulatory subunit p85 and catalytic subunit p100[50-53]. Then PI3K-1 heterodimer travels to the inner cell membrane in which the catalytic subunit p100 catalyzes the phosphorylation of phosphatidylinositol 4,5-bisphosphate (PIP_2), forming phosphatidylinositol-3,4,5-triphosphate (PIP_3). PIP_3 can not only interact with pleckstrin homology (PH) domain of phosphoinositide-dependent kinase-1 (PDK1) and protein kinase B (AKT) which can be subsequently phosphorylated by PDK1 in threonine 308 (T308), but also recruit the mammalian target of rapamycin complex 2 (mTORC2) to phosphorylate hydrophobic motif (HM) sites of AKT at serine

473 (S473)[54]. AKT with both S473 and T308 phosphorylation turns into a fully activated state, which in turn catalyzes the phosphorylation of FoxO1 in serine 256 (S256) (equivalent to S253 in mouse FoxO1), leading to FoxO1 nuclear exclusion followed by ubiquitination and proteasome degradation in the cytoplasm[55, 56]. Meanwhile, AKT catalyzes the phosphorylation of glycogen synthase kinase 3 (GSK3) at serine residues, leading to GSK3 inhibition, which makes more glycogen synthases (GS) stay at dephosphorylated (active) state to promote glycogenesis (Figure 1)[38, 46, 57]. Lastly, insulin signaling triggers the phosphoprotein phosphatase to dephosphorylate FBPase-2, which in turn activates PFKase-2 to convert F6P to F2,6P2. F2,6F2 serves as an allosteric activator of PFKase-1, favoring the process of glycolysis[7].

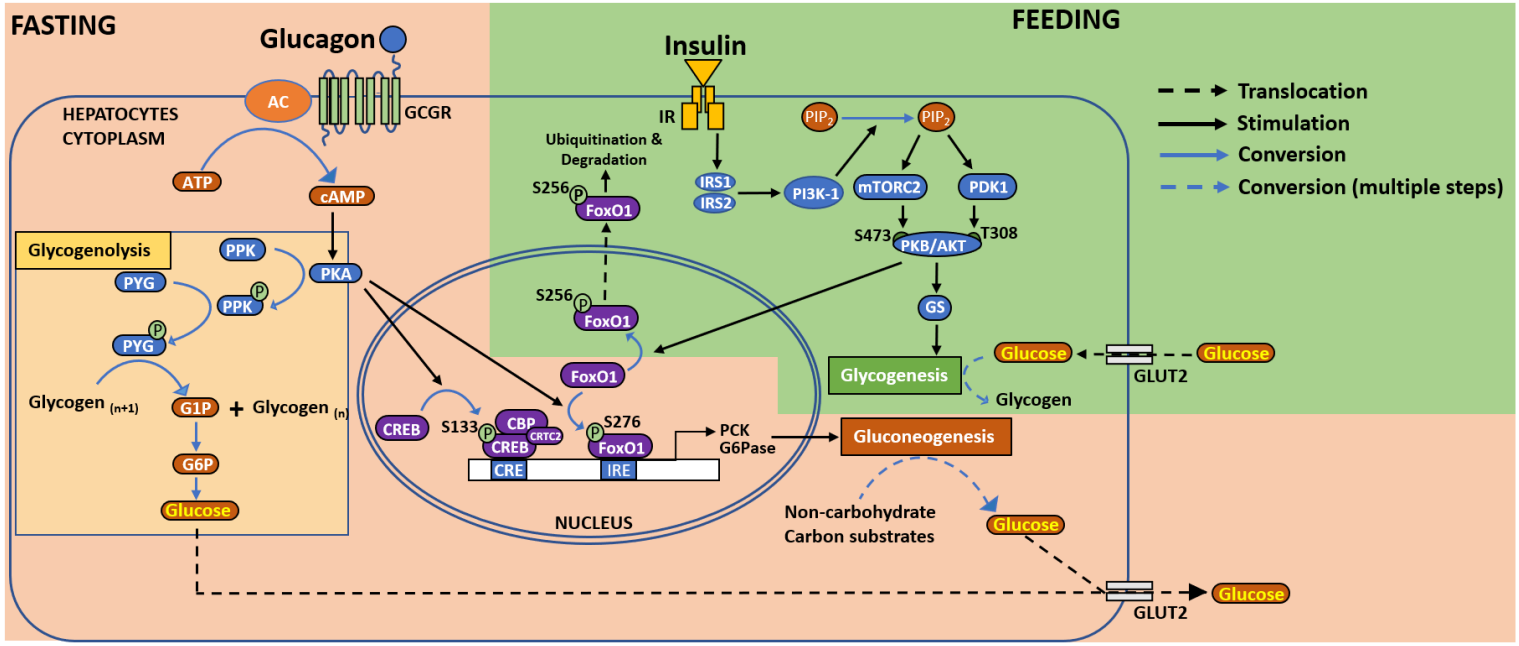

Figure 1. Hormonal regulation on HGP.

Hepatic glucose production (HGP) is regulated by insulin and glucagon in opposite directions depending on the nutritional condition. In the feeding conditions, insulin inhibits HGP after binding to an insulin receptor (IR), triggering intracellular IRS-PI3K-AKT signaling cascade which not only stimulates glycogenesis via glycogen synthase (GS)-dependent pathway, but also suppresses gluconeogenesis by catalyzing FoxO1-S256 phosphorylation. Phospho-FoxO1-S256 undergoes nuclear exclusion and degradation in the cytoplasm. In addition, insulin promotes glycolysis by activating PFKase-1 (not shown in this figure). In the fasting conditions, glucagon stimulates HGP after binding to a glucagon receptor (GCGR), triggering cAMP-PKA signaling cascade. PKA promotes glycogenolysis via PPK-PYG pathway. Meanwhile, PKA phosphorylates CREB and FoxO1 at S133 and S276 (equivalent to S273 in mouse FoxO1) respectively, promoting the formation of the CREB-CBP-CRTC2 complex and FoxO1 nuclear localization, which subsequently induces the gluconeogenic gene expression. In addition, PKA activates fructose bisphosphatase-2 (FBPase-2) which decreases the concentration of fructose-2,6-bisphosphate (F2,6P2), releasing the inhibitory effects of F2,6P2 on FBPase-1, favoring gluconeogenesis (not shown in this figure). In hepatocytes, the glucose uptake and secretion are facilitated by glucose transporter 2 (GLUT2).

Dysfunction of hormonal regulation causes metabolic disorders

As the hormonal regulation controlled by insulin and glucagon is essential for glucose homeostasis, dysfunction of the hormonal regulation causes many metabolic syndromes, such as dysinsulinemia, dyslipidemia and hyperglycemia, which could subsequently develop into diabetes mellitus (DM, or "diabetes" for short)[1, 45, 58]. DM is considered as one of the leading global health issues. According to the report from the International Diabetes Federation (IDF), there were about 463 million people between the ages 20-79 years around the world having diabetes in 2019, and this data is predicted to rise to 578 million in 2030, then 700 million in 2045 if there are insufficient actions being taken to tackle this issue[59].

Type 1 diabetes (T1D)

In the US, about 1 to 2 million people (5-10% of diabetic patients) are suffering from Type 1 diabetes (T1D)[2, 3]. T1D is also called insulin-dependent diabetes, which is classified as an autoimmune disorder[2, 60-62]. In T1D patients, the pancreatic β-cells, which are the only cells that are able to generate and secrete insulin, are falsely recognized as invaders of patients' body, and destroyed by the immune system, leading to insufficient insulin production in circulation, which is namely hypoinsulinemia[62]. Moreover, as insulin is one of the strongest suppressors of glucagon secretion in pancreatic α-cells, hypoinsulinemia can cause excess secretion of glucagon, resulting in hyperglucagonemia. Under these circumstances, the body not only fails to efficiently promote glucose disposal in muscle and adipose tissues, but also suffers from excess HGP, bringing constant hyperglycemia after meal[21, 45, 63].

The development of T1D is primarily due to genetic predisposition. It is reported that over 50 loci in our chromosomes are found to be associated with the development of T1D. In particular, the major contributor that counts for about 50% of the genetic risk of T1D development, is located in the major histocompatibility complex (MHC) region on chromosome 6 which is responsible for the proteins involved in adaptive and innate immunity[61, 62, 64, 65]. Considering the close association between T1D and genetic disorders, T1D is often diagnosed at the early age of patients, although T1D can sometimes be diagnosed in adulthood[66-69]. In order to keep the blood glucose level under control, T1D patients are required to keep monitoring their own blood glucose level and take insulin injections several times a day[69-71].

Type 2 diabetes (T2D)

Type 2 diabetes (T2D) accounts for more than 90% of the prevalence of diabetes in the US[3, 72, 73]. Compared to the T1D patients who cannot generate sufficient insulin due to autoimmunity-induced destruction of pancreatic β-cells, the T2D patients are mainly suffering from insufficient insulin sensitivity, namely insulin resistance[22, 23, 45, 74, 75]. Although the patients with insulin resistance may not necessarily develop T2D eventually, insulin resistance is still considered as the primary cause of T2D[58, 76]. There are three major risk factors for the development of insulin resistance: sedentary lifestyle, excess energy consumption and aging. Pathogenetically speaking, these risk factors promote ectopic lipid accumulation in insulin-responsive tissues/organs (i.e., the liver, skeletal muscles, and adipose tissues) which is believed to be one of the main causes of insulin resistance[45, 77, 78]. For instance, excess amounts of lipid accumulated in the liver exceeds the capacity

of lipid exportation via very-low-density lipoprotein (VLDL). These excess hepatic lipids activate the epsilon isoform of protein kinase C (PKCε) which in turn inhibits the phosphorylation of IRS1/2, leading to inactivation of AKT. As a result, neither the promotion of glycogenesis mediated by glycogen synthase, nor the suppression of gluconeogenesis mediated by FoxO1 phosphorylation and degradation can be efficiently triggered by insulin signaling, inducing hyperglycemia[52, 79-81].

Although the pancreatic β-cells are not destroyed by the immune system in T2D, the insulin secretion would actually be impaired along with the progression of T2D from insulin resistance[82-84]. In general, the hyperinsulinemia is observed at the early stage of insulin resistance, followed by hypoinsulinemia when insulin resistance is progressing to T2D[85-87]. Mechanically speaking, as the insulin resistance-induced hyperglycemia persists, a high glucose level keeps the opening of voltage-dependent calcium (Ca^{2+}) channels (VDCCs) in pancreatic β-cells, leading to a Ca^{2+} influx which in turn drives the Ca^{2+}-dependent exocytosis of insulin from β-cells, causing insulin over-production[58, 82, 88-91]. In addition, the β-cell mass is markedly expanded under the stimulation of hyperglycemia[92, 93]. The stimulation of insulin secretion and β-cell mass expansion are two typical compensatory mechanisms in response to insulin resistance-induced hyperglycemia[94, 95]. However, prolonged exposure of β-cells to hyperglycemia (and probably hyperlipidemia) gradually exhausts the function of β-cells. Glucose toxicity and lipid toxicity trigger oxidative stress and inflammation in β-cells, damaging the organelles (particularly the mitochondria) and upregulating pro-apoptotic genes expression which subsequently lead to β-cells dysfunction and destruction[92, 96-100]. Under these circumstances, the secretion of

insulin is significantly reduced, and the β-cell mass is remarkably truncated. It was reported that the total volume of β-cells in obese nondiabetic individuals was about 40% larger than normal weight nondiabetic individuals, indicating an expansion of β-cell mass at the early stage of insulin resistance; but the β-cell volume dropped approximately 30% in obese diabetic individuals comparing with normal nondiabetics, indicating a shrinkage of β-cell mass when insulin resistance proceeds to T2D[92]. Similar to hyperglucagonemia in T1D, the dysfunction of β-cells in T2D makes the secretion of glucagon from pancreatic α-cells out of control which in turn continuously enhances the HGP even under fed state.

There are quite a few therapeutic strategies to tackle T2D. Improvement of lifestyle, dietary habits (e.g., diet containing low carbohydrate and high fiber) and regular physical activity are the three top recommended strategies because these methods are beneficial for control of weight gain and glucose consumption without drug intervention. On top of that, metformin, glucagon-like peptide 1 (GLP-1)-based therapies (e.g., dipeptidyl peptidase 4 (DPP-4) inhibitors, GLP-1 receptor agonists) and insulin injection are several well-recognized T2D medications[72, 101-105].

Gestational diabetes (GD)

Apart from T1D and T2D, there is a third type of diabetes called gestational diabetes (GD) which refers to diabetes that are developed during pregnancy. In the US, around 10% of pregnant women are diagnosed with GD[2, 106, 107]. The development of GD is closely related to the changes of metabolism during pregnancy. In brief, the demand of calories in pregnant women is significantly increased compared to non-pregnant women[108-110]. In particular, a certain amount of energy sources (i.e., blood glucose) needs

to be transported to the fetus through the placenta, driven by the concentration gradient between maternal and fetal blood glucose level[111, 112]. In order to keep the maternal blood glucose at a relatively high level to maintain the blood glucose concentration gradient, the placenta generates placental hormones, such as human placental lactogen (HPL) to reduce the insulin sensitivity of the mother's tissues/organs, leading to insulin resistance and hyperglycemia in pregnant women[113-115]. To counterbalance the elevated blood glucose level, the mother's β-cell mass substantially expands, and performs hypersecretion of insulin which could be twice as much as its level in non-pregnant women[116-118]. If the pregnant woman's β-cells fail to secret sufficient amount of insulin, GD would be developed[119].

Fortunately, GD usually disappears after delivery because the "initiator" placenta is removed shortly after the baby is born, and the insulin sensitivity of the mother is restored afterwards[108, 116]. Nevertheless, during the pregnancy, GD can also be well controlled through proper weight management, healthy diet and regular physical activities similar to the treatment for T2D patients[120-122]. If the GD patients' blood glucose level is still beyond the acceptable range after taking the aforementioned actions, insulin could be prescribed. Since the main reason for the development of GD is insufficient insulin secretion, injection of insulin is considered as the safest medication to treat GD[123]. In addition, metformin is considered as an alternative safe hypoglycemic agent for GD patients[121, 124, 125].

Autophagy and energy balance

Introduction to autophagy

Energy homeostasis in our body cannot be well-regulated without a balance between anabolic pathways and catabolic pathways. For instance, the gluconeogenesis is a type of anabolic pathways, while the glycolysis is a type of catabolic pathways. Apart from these classic pathways involved in energy homeostasis, another type of catabolic process, autophagy has also been reported to be very important for energy balance in the past few decades[25, 126-128]. In general, autophagy, which is typically found in eukaryotic cells, sequesters intracellular components (e.g., damaged proteins, protein aggregates, polysaccharides, organelles or lipids), namely autophagy substrates, then delivers them to lysosomes for degradation[129-131]. After being processed by lysosomes, these autophagy substrates return to simple carbon sources such as amino acids, glucose or fatty acids which can be easily utilized by the cells for ATP production or protein synthesis[132]. Autophagy is usually activated under the nutrient deprivation conditions, producing a limited amount of carbon sources which are essential for cell survival. Therefore, autophagy is considered as one of the important pro-survival mechanisms in eukaryotic cells[24, 133-135].

Autophagy is generally categorized into three different types based on the ways of delivery of autophagy substrates to lysosomes: macroautophagy, microautophagy, and chaperone-mediated autophagy[127, 136, 137]. Macroautophagy is the most common type of autophagic activities in which the autophagy substrates are required to be internalized by double-membrane vesicles called autophagosomes. The autophagosome then fuses with

lysosome to form autolysosome in which the autophagy substrates are degraded by lysosomal enzymes (e.g., proteolytic enzymes, lipolytic enzymes and carbohydrate splitting enzymes)[138-141]. By contrast, in microautophagy, there is no specific double-membrane vesicle facilitating the delivery of autophagy substrates. Instead, the autophagy substrates (along with the surrounding cytoplasm) are directly taken by lysosomes through inward invagination[142-145]. Last, if the autophagy substrates are cellular proteins carrying KFERQ- or KFERO-like motifs, these substrates can be identified by cytosolic chaperones called heat shock cognate 71 kDa proteins (Hsc70) and form a chaperone complex which subsequently has a specific binding with lysosomal-associated membrane protein 2A (LAMP2A), followed by lysosomal degradation[146-149]. Since macroautophagy is the most common and well-investigated type of autophagy, the present study is going to further study the involvement of macroautophagy (referred to as autophagy hereinafter) in the HGP.

General process of autophagy

To study the relationship between autophagy and HGP, it is critical to understand the process of autophagy. The general process of autophagy can be summarized into several steps: 1) formation of autophagy precursors, namely omegasomes; 2) formation of autophagosomes; 3) formation of autolysosomes; 4) lysosomal degradation, and 5) efflux of degraded products to the cytoplasm[130, 150-152]. The upstream protein of autophagy pathway is uncoordinated-51 like kinase-1/2 (ULK1/2) which contains two specific phosphorylation sites that can be catalyzed by different kinases[153, 154]. Under the fed state or less stress conditions, high nutrient environments or increase of insulin signaling

upregulates the activity of mammalian target of rapamycin complex 1 (mTORC1) which catalyzes the phosphorylation of ULK1/2 at serine 757 and inactivates the activities of ULK1/2, resulting in suppression of autophagy[155, 156]. On the other hand, under stress conditions (e.g., starvation), the concentration of intracellular AMP-activated protein kinase (AMPK) is increased, which in turn catalyzes the phosphorylation of ULK1/2 at serine 555, leading to ULK1/2 activation[127, 157, 158]. Activated ULK1/2 recruits autophagy-related protein 13 (ATG13), ATG101 and FAK family-interacting protein of 200 kDa (FIP200) to form the ULK 1/2 complex which is able to translocate to a specific discrete region of the endoplasmic reticulum (ER) rich in ATG9, followed by the recruitment of the beclin1-class III phosphatidylinositol 3-kinase (PI3K C-III) complex and formation of the omegasome[159, 160]. PI3K C-III then alters the lipid composition of omegasomal membrane, promoting the maturation of omegasome (formation of phagophore) which starts to engulf intracellular components and eventually turns into autophagosome[160, 161]. There are two parallel ubiquitin-like conjugation systems involved in the maturation of autophagosome, the ATG5-ATG12-ATG16 complex and ATG7/ATG3-driven lipidated LC3-I (i.e., LC3-II)[162-164]. Being facilitated by these two systems, the mature autophagosome fuse with the lysosome, forming autolysosome in which the lysosomal degradation of autophagy substrates is initiated[138]. When the autophagy substrates are broken down into simple molecules such as amino acids or monosaccharides, these simple molecules are relocalized to the cytosol and ready for recycling as energy sources or building blocks for protein synthesis (Figure 2)[140, 165].

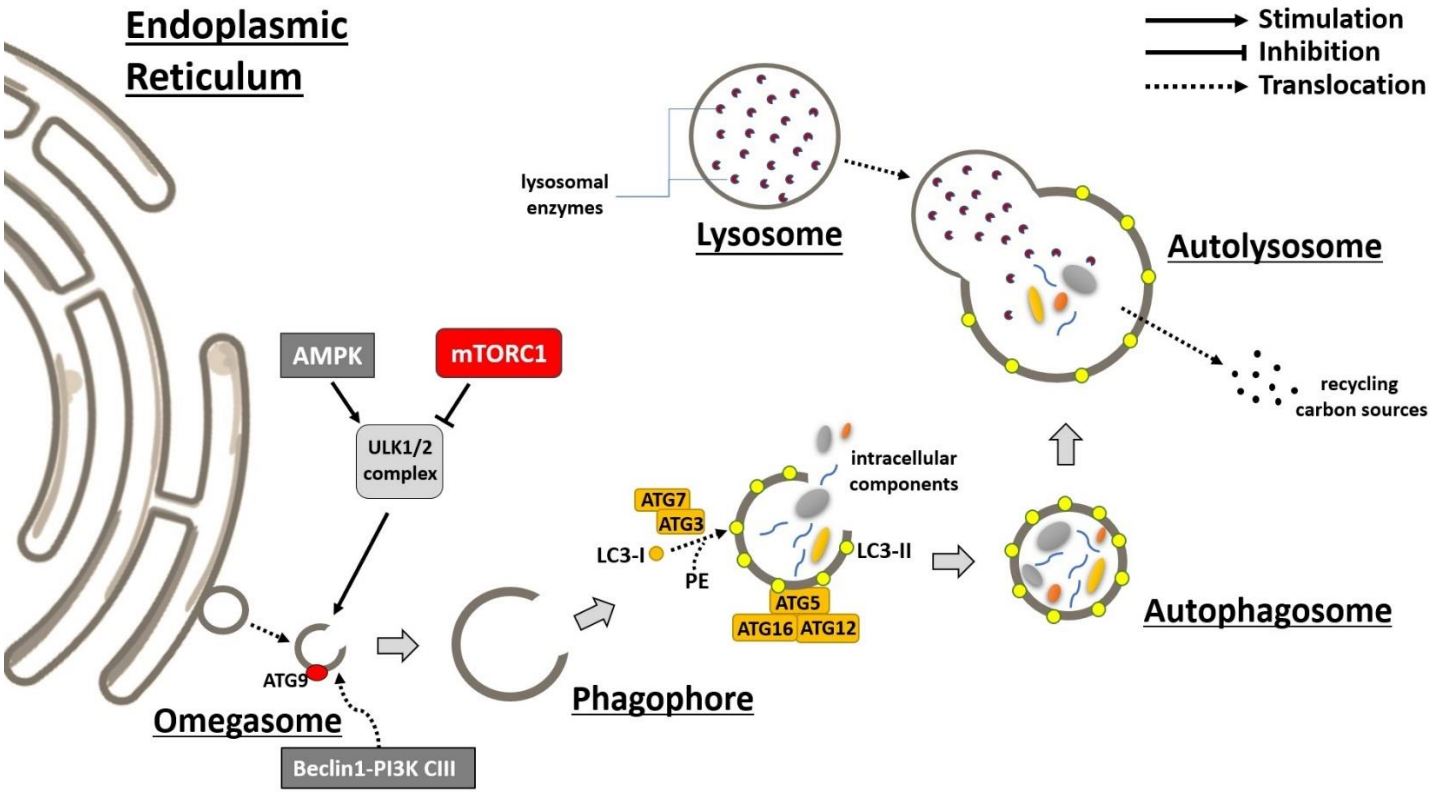

Figure 2. The general process of autophagy in the eukaryotic cells.
The initiation of autophagy is controlled by ULK-1/2-mediated signaling which can be either promoted by AMPK or inhibited by mTORC1. Upon activation, the ULK1/2 complex moves to a region of endoplasmic reticulum (ER) in which ATG9 is abundantly found. Then this ER region starts to recruit a beclin1-PI3K C-III complex and form omegasomes. Along with the alteration of lipid composition catalyzed by PI3K, the omegasome is converted into a phagophore. The phagophore then performs internalization of cellular components, turning into mature autophagosome after coupling with the LC3-II and ATG5-ATG12-ATG16 conjugation systems. Mature autophagosome fuses with the lysosomes, forming an autolysosome in which cellular components are hydrolyzed by lysosomal enzymes, subsequently producing carbon sources ready for recycling.

Autophagy activity is tightly related to the nutrient state and hormonal signals

Considering autophagy is one of the most important pro-survival cellular mechanisms in the eukaryotic cells, we believe that there is a great potential in studying the regulation of autophagy in order to find new scientific evidence to manage our energy homeostasis, or develop therapeutic strategies to tackle metabolic disorders such as insulin resistance and diabetes. Indeed, starvation, especially amino acid (AA) deprivation has been demonstrated to be a strong stimulus of autophagy in eukaryotic cells in which the mTOR-dependent signaling pathway is found to be playing a pivotal role[30, 128, 136, 166-168]. In particular, Ca^{2+}-CaMKK-β signaling cascade is proposed to be an important pathway mediating mTOR-dependent autophagy activation[30, 128, 169]. Although there is another signaling cascade being proposed to be involved in the initiation of autophagy, namely mitogen-activated protein kinase (MAPK)/extracellular signal-regulated kinase (ERK) kinase (MEK)-ERK1/2 signaling cascade, the exact mechanism of this cascade, and the crosstalk between MEK-ERK1/2 cascade and Ca^{2+}-dependent cascade require further study[30, 133, 170-173].

Glucagon/AA deprivation-induced Ca^{2+}-CaMKK-β signaling cascade

As the most abundant mineral in the human body, calcium (Ca^{2+}) is extremely important for the maintenance of our body structure (such as bone mass and teeth construction), secretion of synaptic neurotransmitter, and muscle contraction[169, 174]. One of the reasons making Ca^{2+} so important in neurons and skeletal muscle cells is because the neurons and skeletal muscle cells can generate an action potential (namely excitable cells) which is tightly associated with the changes of cytosolic Ca^{2+} concentration. These

changes of cytosolic Ca^{2+} concentration can be achieved by regulating the opening of Ca^{2+} channel located in the plasma membrane, or in the intracellular compartments like endoplasmic reticulum (ER) and mitochondria[175, 176]. Nevertheless, even in non-excitable cells which cannot generate action potentials (e.g., hepatocytes), upon stimulation from glucagon or amino acid deprivation, the change of Ca^{2+} concentration is still actively involved in many cellular actions including autophagy activity[177-179]. For instance, glucagon or AA deprivation triggers PKA to catalyze the phosphorylation and activation of inositol l,4,5-trisphosphate (InsP3) receptors (namely InsP3-gated Ca^{2+} channel) located in the ER membrane, resulting in a release of Ca^{2+} from the ER lumen to the cytosol[29, 31]. The increase of cytosolic Ca^{2+} concentration not only induces the Ca^{2+} influx in the mitochondria where Ca^{2+} facilitates the activation of dehydrogenases and promotion of the TCA cycle, but also upregulates the activity of CaMKK-β. Activated CaMKK-β catalyzes the phosphorylation of AMPKα at threonine 172 (T172), which in turn activates ULK-1/2 complex via stimulating an mTORC inhibitor tuberous sclerosis complex (TSC), or by direct interaction with ULK-1/2 complex, which subsequently initiates autophagy (Figure 3)[28, 29, 169].

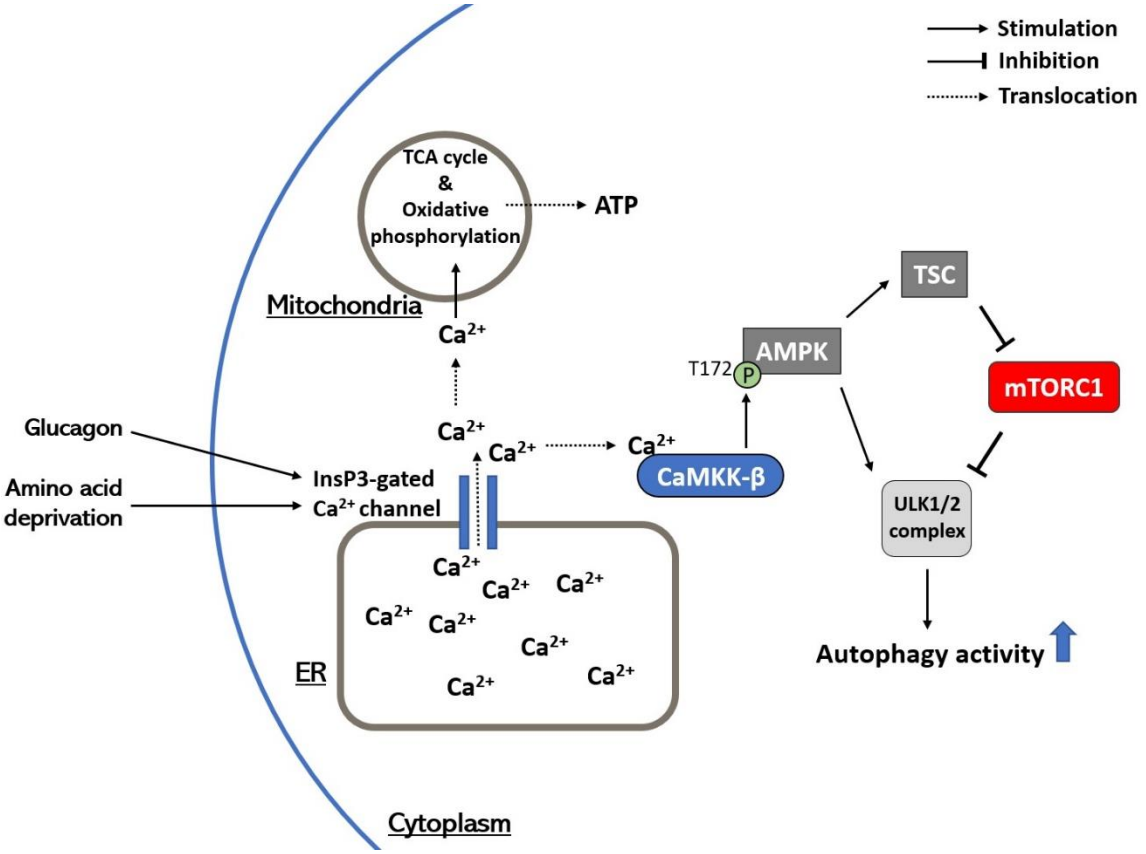

Figure 3. Glucagon/Amino acid deprivation induces autophagy through Ca^{2+}/CaMKK-β signaling cascade in non-excitable cells.
Under the stimulation of glucagon or amino acid deprivation, more Ca^{2+} is released from the ER lumen to the cytoplasm through the InsP3-gated Ca^{2+} channel. An increase of cytosolic Ca^{2+} concentration promotes the activity of CaMKK-β in the cytosol, which in turn catalyzes the phosphorylation of AMPK at T172, leading to activation of the ULK1/2 complex either by the TSC-mTORC1 pathway, or by direct interaction. Meanwhile, the influx of cytosolic Ca^{2+} to the mitochondria is promoted. Ca^{2+} facilitates the activity of hydrogenase in the mitochondria, resulting in promotion of the TCA cycle and ATP production.

FoxO1-mediated regulation of autophagy

As mentioned in previous sections, FoxO1, which could be significantly upregulated or downregulated under the stimulation of glucagon or insulin respectively, is an important transcription factor controlling the expression of gluconeogenic genes in the liver[38]. Indeed, there are quite a few studies having demonstrated that FoxO1 plays an important

role in the regulation of autophagy through different mechanisms[180-182]. For instance, it is reported that serum starvation triggers a dissociation of FoxO1 from nicotinamide adenine dinucleotide (NAD^+)-dependent deacetylase sirtuin 2 (SIRT2), promoting an interaction between acetylated FoxO1 (Ac-FoxO1) and ATG7, which in turn induces the activity of autophagy[181]. Under the induction of starvation, human colorectal carcinoma cell line HCT116 transfected with dysfunctional SIRT2 (i.e., SIRT2(168A)) demonstrated an upregulation of autophagy, while the autophagy in HCT116 transfected with normal SIRT2 was blocked[181]. Moreover, in terms of FoxO1-mediated regulation of autophagy in the epigenetic level, it is reported that the gene expression and nuclear accumulation of FoxO1 can be upregulated by histone deacetylase inhibitors (HDACIs), leading to an increase of Ac-FoxO1 in the nucleus. Ac-FoxO1 binds to the promoter regions of mTOR suppressor (SESN3) genes and autophagy-related genes (ATGs), which in turn not only facilitates the initiation of autophagy by suppressing mTOR, but also promotes the progress of autophagy via upregulation of ATGs[183].

Recently, there is evidence starting to unveil that autophagy, in turn, is able to regulate the protein turnover of FoxO1, and subsequently control gluconeogenesis in the liver, although more studies are required to illustrate the exact mechanisms[184]. Previous studies demonstrated that autophagy can selectively degrade circadian protein cryptochrome 1 (CRY1) which triggers ubiquitination and degradation of FoxO1 through direct binding to FoxO1 and the recruitment of an E3 ligase. Therefore, autophagy-mediated degradation of CRY1 promotes the stability and nuclear translocation of FoxO1[185, 186]. In the present study, we continue on investigation of autophagy in the

regulation of the HGP. Surprisingly, our data demonstrated that the autophagy supports the HGP by sustaining the protein level of FoxO1, and the autophagy-mediated intracellular amino acid pool is one of the underlying mechanisms.

Aims and hypothesis

Although there are several mechanisms which have been proposed to illustrate the underlying mechanisms of the regulation of autophagy upon the stimulation of glucagon/starvation, there is limited evidence showing the contributions of autophagy to HGP during starvation or under the stimulation of glucagon[184]. Hence, the overall goal of present study is to investigate the possible contribution of autophagy to the HGP, particularly under the stimulation of glucagon and/or starvation. **We hypothesize that autophagy is critical to maintain the intracellular amino acid pools, which in turn sustains the protein level and activity of FoxO1, subsequently support HGP under the present of glucagon and/or starvation**. This hypothesis will be verified by addressing the following specific aims:

Aim 1: To investigate the effects of autophagy on HGP

We hypothesize that maintaining normal autophagy activity is critical for the HGP. We will inhibit the autophagy activity by using chloroquine (CQ) or siRNA-ATG7 (siR-ATG7) in our *in vitro* study, and hydroxychloroquine (HCQ) and adeno-associated virus vector serotype 8 (AAV8)-shRNA-ATG7 (shR-ATG7) in our *in vivo* study. We will evaluate the effects of inhibition of autophagy on total HGP, gluconeogenesis and glycogenolysis to narrow down the possible affected glucose production pathways. We will also conduct the western blotting assay to investigate the possible affected signaling

pathways, including CREB-mediated and FoxO1-mediated signaling pathways, to find the potential affected transcription factor. We will perform the HGP assay *in vitro* by using mouse primary hepatocytes. We will also use our transgenic mouse model to evaluate the capability of glucose production *in vivo* through pyruvate tolerance test and glucagon tolerance test. Liver-specific FoxO1 knockout (L-FKO) mice generated by breeding floxed $FoxO1^{L/L}$ mice with albumin-Cre mice will be used in this study. Floxed $FoxO1^{L/L}$ mice will be used as the control mice.

Aim 2: To identify possible mechanisms involved in autophagy deficiency-induced reduction of FoxO1.

Our preliminary data indicated that autophagy deficiency caused suppression of HGP, and FoxO1 is a possible target involved in autophagy-mediated HGP. Thus, we hypothesize that autophagy deficiency will lead to an alteration of FoxO1 activity, which in turn interferes with HGP. We will investigate several possible mechanisms that are related to FoxO1 expression, phosphorylation and stability, and nuclear localization. mRNA level of target genes (including FoxO1) will be evaluated by quantitative reverse transcription-polymerase chain reaction (RT-qPCR). FoxO1 phosphorylation, nuclear localization and stability will be evaluated by western blotting assay , immunohistochemistry and immunofluorescence staining. Primary hepatocytes isolated from FoxO1-$S253^{A/A}$ and Foxo1-$S273^{D/D}$ knock-in (KI) mice will be used to study the association between autophagy and FoxO1 phosphorylation and stability.

Aim 3: To investigate the association between autophagy-mediated amino acid pools and FoxO1 activity

We hypothesize that the alteration of cellular amino acid pools caused by the inhibition of autophagy could be one of the possible reasons leading the alteration of the FoxO1 protein amount. We will evaluate the amino acid pools in our primary hepatocytes as well as the liver samples determined by high-performance liquid chromatography (HPLC) method conducted in Dr. Guoyao WU's lab. We will also add exogenous amino acids which are significantly affected under autophagy deficiency to hepatocytes to test if the FoxO1 and HGP can be restored upon autophagy deficiency, and use protein synthesis inhibitor cycloheximide (CHX) to evaluate the activity of protein synthesis.

Significance and rationale

Maintaining a balanced blood glucose level is essential to our survival, health, growth, and development. Dysregulation of blood glucose homeostasis could make people at risk of getting many metabolic disorders, including obesity, insulin resistance and diabetes[20, 37]. Statistically speaking, the IDF reported that around 31 million people were suffering from diabetes in the US in 2019, making the US the 3rd country for the number of people with diabetes in 2019[59]. Large numbers of diabetic patients could cause substantial economic burden and medical expenditure for both individuals and the whole country[73]. In the past century, many scientists have dedicated themselves to the investigation of the regulation of glucose homeostasis as well as the pathogenesis of diabetes, and proposed many fabulous molecular mechanisms to help us develop effective therapeutic medications that are potentially useful to treat blood glucose-related metabolic disorders.

However, there are still many areas regarding glucose homeostasis remaining elusive. Since the discovery of the mechanism of autophagy established by Dr. Yoshinori Ohsumi, autophagy-related studies have emerged as a hot research topic in the field of molecular biology[131, 187, 188]. So far quite a few mechanisms regarding the regulation of autophagy under starvation have been proposed, however, the evidence showing the contributions of autophagy to HGP upon the stimulation of glucagon and/or starvation is still limited. The present study is trying to highlight that the contribution of autophagy to HGP is through supporting FoxO1 protein activities, which emphasizes the importance of maintenance of cellular amino acid pools. We not only further solidify the necessity of autophagy in the regulation of glucose homeostasis, but also provide a potential impact on the development of therapeutic strategies for the patients with metabolic disorders, especially insulin resistance and diabetes. Last but not least, several amino acids that could significantly altered by autophagy deficiency could be potentially useful for the development of dietary guideline for the patients with an autophagy deficiency-related disorder in hepatic glucose production.

CHAPTER II

AUTOPHAGY-MEDIATED HEPATIC GLUCOSE PRODUCTION REQUIRES FOXO1

Introduction

The process of autophagy is precisely controlled by two ubiquitin-like conjugation systems, the ATG5-ATG12-ATG16 complex and ATG7/ATG3-driven lipidated LC3-I (i.e., LC3-II)[162-164]. Both systems are essential for the maturation of autophagosomes and the fusion between autophagosomes and lysosomes (which eventually develop into autolysosomes). Therefore, the activity of autophagic flux can be evaluated through monitoring the activities of proteins (namely autophagy markers) involved in the above conjugation systems. For instance, LC3 is one of the well-recognized indicators of autophagic flux[163, 189]. In brief, when autophagic activity is inactive, LC3 is predominantly located in the cytoplasm and kept in a non-lipidated form (namely LC3-I, without forming a covalent bond to phosphatidylethanolamine (PE)). However, once the autophagy is activated, ATG7 will cooperate with ATG3 to catalyze the lipidation of LC3-I, resulting in formation of LC3-II which is no longer suspending in the cytoplasm, but bound to both inner sites and outer sites of autolysosomal membrane. During lysosomal degradation, the LC3-II located in the inner sites is degraded by lysosomal enzymes while the LC3-II located in the outer sites remains intact and will be released to the cytoplasm afterwards[190-193]. These phenomena indicate that we can evaluate the progress of autophagy by monitoring the change in the amount of LC3-II via immunoblotting, or distribution of LC3 in the cytoplasm via immunofluorescence.

As mentioned above, LC3-II located in the inner site of autolysosomal membrane will eventually undergo lysosomal degradation. In order to prevent the LC3-II from degradation, we used chloroquine (CQ) to stop the development of autolysosome, leading to the inhibition of lysosomal degradation in the late stage of autophagy[138, 194]. In this case, we could visually observe an accumulation of LC3-II from the immunoblotting assay, or an increase of cluster of LC3 from the immunofluorescence assay in CQ-treated groups, compared to the groups without CQ treatment[195, 196]. Alternatively, we used siRNA-ATG7 to specifically knock down the expression of ATG7. Since ATG7 is required for the formation of LC3-II, knocking down ATG7 by siRNA-ATG7 suppresses the development of autolysosomes, causing the inhibition of autophagy. However, it is worth emphasizing that in the siRNA-ATG7-treated groups, the level of LC3-II is reduced compared to the siRNA-scramble-treated groups, because the formation of LC3-II is interrupted and the majority of LC3 is kept in LC3-I form [196-198].

Considering that the mammalian LC3 family contains three isoforms, LC3A, LC3B and LC3C, it is important to determine a proper isoform of LC3 as our autophagic marker. It is reported that LC3C is absent in mice, therefore, we narrow down our potential targets to LC3A and LC3B[199, 200]. According to previous reports, both LC3A and LC3B participate in the progress of autophagy in a similar localization during starvation[201]. mRNA expressions of LC3A and LC3B are shown to be vastly different depending on the target tissues, organs, and cell lines in mice. Nevertheless, both LC3A and LC3B are expressed in the mouse livers[202]. On top of that, regarding the localization of LC3A and LC3B, it is reported that LC3A mainly accumulates in the perinuclear area, while LC3B

is evenly distributed throughout the cytoplasm[201], indicating that LC3B is a better autophagic marker than LC3A regarding evaluation of autophagic flux in the present study[203].

In the present chapter, we inhibited the autophagy activity by using an autophagy inhibitor CQ and siR-ATG7 in our *in vitro* study, and using hydroxychloroquine (HCQ, a less toxic CQ metabolite) and AAV8-shRNA-ATG7 in our *in vivo* study[204, 205], then evaluated the total HGP, glycogenolysis and gluconeogenesis in both primary hepatocytes and mice. FoxO1, alongside with CREB, is an important transcription factor regulating gluconeogenic gene expression in hepatocytes (e.g., *pck1* and *g6pc*), which subsequently controls HGP[35, 38, 42, 55]. We found that inhibition of autophagy significantly suppressed HGP, and it was in a FoxO1-dependent manner.

Materials and methods

Ethics statement

Animal protocols were approved by the Institutional Animal Care and Use Committee (IACUC) at the Texas A&M University. All mice were kept in the laboratory animal resources and research facility (LARR), and housed in standard cages under 12hr-light/12hr-dark cycle with access to food and drinking water ad libitum as previously described[41, 44, 206]. Necessary procedures (e.g., performing euthanasia by means of isoflurane vaporizer) were conducted to minimize the discomfort, distress, and pain of the mice during the experiments.

Generation of liver-specific FoxO1-knockout mice

Liver-specific FoxO1-knockout (L-FKO) mice were generated by breeding floxed FoxO1 ($FoxO1^{fl/fl}$) mice with albumin-Cre mice as previously described[44, 207]. The Cre recombinase induced by the mouse albumin enhancer/promoter did not show any influence on animal performance, as previously reported[41, 44, 50]. $FoxO1^{fl/fl}$ littermates were used as wild type (WT) mice in the present study. The genetic background of mice littermates was confirmed through genotyping DNAs extracted from mice tails with GoTaq® Green Master Mix (Promega, Madison, WI, USA). Eight to 12-week-old male WT and L-FKO mice were used for all our animal studies.

Isolation of mouse primary hepatocytes

Mouse primary hepatocytes were isolated from 8- to 12-week-old male mouse liver and cultured in DMEM (containing 5.5mM glucose) supplemented with 10% fetal bovine serum (FBS) as previously described[41, 44, 208]. In brief, WT or L-FKO mice were first

anesthetized with isoflurane, then their liver and intestines were exposed by cutting open the peritoneal cavity. To start the liver perfusion, a catheter (25G needle) connected to a perfusion pump (speed: 250ml/hr) was inserted into the portal vein, immediately followed by cutting through the vena cava to relieve the pressure. The mouse liver was perfused with perfusion buffer I and II consecutively to become fully digested (Table 1). The digested liver was then transferred to a petri dish containing cold fasting DMEM (without FBS) in which the liver could be mechanically broken apart by gently scraping with forceps. The medium (containing single hepatocytes) was centrifuged at 1700rpm, 2min, followed by removal of the supernatant. The cell pellets were resuspended in 8ml of cold fasting DMEM prior to mixing with 10ml of cold Percoll solution (9 ml of cold Percoll® + 1 ml of HBSS (10x)). After centrifugation (1800rpm, 6min) and removal of the supernatant, the remaining cell pellets were mainly the isolated mouse primary hepatocytes. Mouse primary hepatocytes ($3.0*10^5$ cells per well for 6-well plate, collagen coated) were then cultured in complete DMEM (containing 10%FBS) under 37 ℃, 5% CO_2 environment for at least 3 hours to wait for the cell attachment. Once primary hepatocytes successfully attached onto the culture plates, the culture medium would be replaced by fresh DMEM, after which treatment of hepatocytes begins.

Table 1. Recipe of liver perfusion buffer I and II.

Name of reagent	Amount
Liver perfusion buffer I (50ml)	
HBSS (1x)*****	48.725ml
EGTA (50mM)	500µl
Glucose (1.0M)	275µl
Penicillin-Streptomycin (Cat# P0781, MilliporeSigma)	500µl
Liver perfusion buffer II (40ml)	
HBSS (1x)*****	39.32ml
$CaCl_2$ (1.0M)	60µl
Glucose (1.0M)	220µl
Penicillin-Streptomycin (Cat# P0781, MilliporeSigma)	400µl
Collagenase (Type II) (Cat# 17101015, Fisher Scientific)	22mg

**Note: ***HBSS (1x): HBSS (500ml, Cat# 14175095, ThermoFisher) with HEPES (1190mg, Car# BP310500, Fisher Scientific), pH=7.4, 37 °C, filtered with Olympus bottle top vacuum filters (Cat# 25-233, Genesee) prior to use.

Induction of autophagy deficiency in mouse primary hepatocytes

Either chloroquine (CQ, 50µM, dissolved in ddH_2O) or siRNA-ATG7 (siR-ATG7, 100nM, dissolved in RNAse-free H_2O) was used to induce autophagy inhibition in mouse primary hepatocytes. In the CQ-treated experiment, attached primary hepatocytes were first starved in fasting DMEM (with 2% FBS) for 2 hours prior to replacing the DMEM with a fasting buffer (120 mmol/L NaCl, 5.0 mmol/L KCl, 2.0 mmol/L $CaCl_2$, 25 mmol/L $NaHCO_3$, 2.5 mmol/L KH_2PO_4, 2.5 mmol/L $MgSO_4$, 10 mmol/L HEPES, 0.5% BSA, dissolved in ddH2O, pH=7.4, filtered with vacuum filters prior to use) in which autophagy was stimulated. The CQ stock solution was added in the buffer to make the final concentration of CQ 50µM. After 3 hours of CQ-treatment, a significant accumulation of LC3-II could be observed by protein immunoblotting, or a large amount of LC3 clusters could be observed by protein immunofluorescence, compared to the control group

(without CQ-treatment), indicating an inhibition of autophagy as previously reported[189, 195, 196]. In the siR-ATG7-treated experiment, siRNA-ATG7 was transfected into primary hepatocytes with Lipofectamine 3000 (Invitrogen, Carlsbad, CA, USA) following the manufacturer's instruction. After transfection, the transfection culture medium was replaced by the fasting buffer. Three hours after medium replacement, a significant reduction of LC3-II could be observed by protein immunoblotting compared to the control group (transfected with scramble siRNA), indicating an inhibition of autophagy as previous reported[189, 196].

Hepatic glucose production (HGP) assay

In the CQ-treated groups, attached primary hepatocytes were first starved in fasting DMEM (with 2% FBS) for 2 hours prior to replacing the DMEM with an HGP buffer (120 mmol/L NaCl, 5.0 mmol/L KCl, 2.0 mmol/L $CaCl_2$, 25 mmol/L $NaHCO_3$, 2.5 mmol/L KH_2PO_4, 2.5 mmol/L $MgSO_4$, 10 mmol/L HEPES, 0.5% BSA, 10 mmol/L lactate and 5 mmol/L sodium pyruvate, pH=7.4, dissolved in ddH2O, filtered with vacuum filters prior to use). The CQ stock solution was added to the HGP buffer to make the final concentration of CQ 50μM. After 30min of CQ pre-treatment, glucagon (100nM) would be added to the HGP buffer to stimulate HGP based on the group requirement. In the siR-ATG7-treated groups, siR-ATG7-transfected primary hepatocytes were grown in the HGP buffer. Glucagon (100nM) would be added to the HGP buffer based on the group requirement. After 3 hours of incubation, the HGP buffer was collected, and the glucose concentration in the buffer was determined by Amplex™ Red Glucose/Glucose Oxidase Assay Kit (Invitrogen, Carlsbad, CA, USA) following the manufacturer's instruction.

Induction of autophagy deficiency in mice

Either hydroxychloroquine sulfate (HCQ, 60mg/kg body weight, dissolved in saline vehicle (0.9% (w/v) NaCl)) or shRNA-ATG7 cloned in an adeno-associated virus serotype 8 vector (AAV8-shRNA-ATG7, dissolved in saline vehicle) was used to induce autophagy inhibition in our WT and L-FKO mice. In the study with HCQ treatment, the HCQ solution was administered via intraperitoneal (IP) injection to 8- to 12-week-old male mice (5-6 mice each group) after overnight (16 hours) fasting. The control group received the same volume of normal saline. Mice were ready for tolerance tests 4 hours after the HCQ injection[138, 140, 209, 210]. In the study with AAV8-shRNA-ATG7 treatment, AAV8-shRNA-ATG7 (VectorBuilder, Chicago, IL, USA) was administered via retro-orbital (RO) injection to 8- to 12-week-old male mice (5-6 mice each group) at the concentration of 10^{11} genome copies/mouse. The control groups received the same amount of AAV8-shRNA-scramble. Mice were ready for tolerance tests 8 days after the AAV8 injection.

Pyruvate tolerance test

A pyruvate tolerance test was performed after an overnight (16 hours) fasting. In the study with HCQ treatment, WT and L-FKO mice received HCQ (60mg/kg body weight) via IP injection after overnight fasting, followed by an additional 4 hour-waiting period for a proper induction of the autophagy inhibition, as previously reported[140, 196]. The control groups received the same volume of normal saline IP injection. Four hours later, blood glucose concentration was recorded as the initial time point (i.e., 0^{th} min). Then a pyruvate solution (2g/kg body weight, dissolved in normal saline) was administered to each mouse by IP injection. In the study with AAV8-shRNA-ATG7 treatment, pyruvate

tolerance test was performed on the mice after 7 days since AAV8 RO injection. After overnight (16hr) fasting, the fasting blood glucose levels of WT and L-FKO mice were recorded as the initial time point (i.e., 0^{th} min). Then the pyruvate solution was administered to each mouse by IP injection. The blood glucose level was measured at 15^{th}, 30^{th}, 60^{th}, 90^{th}, 120^{th} min after pyruvate injection, using the CONTOUR NEXT ONE Blood Glucose Monitoring System (Ascensia Diabetes Care, Parsippany, NJ, USA).

Glucagon tolerance test

The glucagon tolerance test was performed after an overnight (16 hours) fasting. In the study with HCQ treatment, WT and L-FKO mice received HCQ (60mg/kg body weight) via IP injection after overnight fasting, followed by additional 4 hour-waiting period for a proper induction of autophagy inhibition, as previously reported[140, 196]. Four hours later, blood glucose concentration was recorded as the initial time point (i.e., 0^{th} min). Then the glucagon solution (16mg/kg body weight, dissolved in normal saline) was administered to each mouse by IP injection. In the study with AAV8-shRNA-ATG7 treatment, glucagon tolerance test was performed on the mice after 13 days since AAV8 RO injection. After overnight (16hr) fasting, the fasting blood glucose levels of WT and L-FKO mice were recorded as the initial time point (i.e., 0^{th} min). Then glucagon solution was administered to each mouse by IP injection. The blood glucose level was measured at 15^{th}, 30^{th}, 60^{th}, 90^{th}, 120^{th} min after glucagon injection, using the CONTOUR NEXT ONE Blood Glucose Monitoring System (Ascensia Diabetes Care, Parsippany, NJ, USA).

Determination of protein concentration

For *in vitro* study, primary hepatocytes were lysed by a RIPA lysis buffer (Cat# 20-188, MilliporeSigma, Atlanta, GA, USA) containing a protease and phosphatase inhibitor cocktail (Cat# PPC1010, MilliporeSigma) and sodium orthovanadate (Na_3VO_4, Cat# S6508, MilliporeSigma). For *in vivo* study, liver tissue fragments (about 50mg) were lysed by the RIPA lysis buffer containing protease and phosphatase inhibitor cocktail and Na_3VO_4, then proceeded to homogenization by using IKA T8 homogenizer (12-18V DC, 100W). Cells or tissue lysates were then centrifuged at 14000rpm, 4°C for 15min, and the supernatant was collected. Protein concentration was determined by using Pierce™ BCA Protein Assay Kit (Cat# 23225, ThermoFisher) following the manufacturer's instruction.

Protein immunoblotting

Western blotting was conducted as previously described[41, 44, 208]. In brief, protein samples were first normalized with an Alfa Aesar™ laemmli SDS sample buffer (reducing, 6X) (Cat# AAJ61337AD, Fisher Scientific) based on the concentration of protein samples, and denatured under 95.5°C for 10min. Protein samples (25-40µg) were then resolved in a polyacrylamide gel (7.5-15%) by using the Mini-PROTEAN® Tetra Vertical Electrophoresis Cell (Cat# 1658004, Bio-Rad), and electro-blotted onto the Amersham Hybond western blotting membranes, (0.45µm PVDF) (Cat# 10061-492, VWR) by using Trans-Blot Turbo Transfer System (Cat# 1704150, Bio-Rad). Membranes were incubated with primary antibodies (Table 2) in a 5% BSA solution (5% w/v in TBST) overnight at 4°C, followed by incubation with secondary antibodies (anti-rabbit IgG, horseradish peroxidase (HRP) linked, Cat#7074, Cell Signaling Technology) in 5% BSA solution on

the second day. Clarity Western ECL Substrate (Cat#1705061, Bio-Rad) was used to react with HRP linked secondary antibody to generate light signals (i.e., band intensity) which were captured by the ChemiDoc™ Imaging System (Cat# 12003153, Bio-Rad). The band intensity was quantified by the ImageJ software (NIH, 1.8.0v) and expressed as a ratio to GAPDH (internal control).

Immunofluorescence staining

Mouse primary hepatocytes were cultured ($5*10^4$ cells/well) in a collagen coated Thermo Scientific™ Nunc™ Lab-Tek™ II Chamber Slide™ System (Cat#125657, Fisher Scientific). The immunofluorescence assay was conducted following immunocytochemistry and immunofluorescence protocol (Abcam). In brief, after experimental treatment, culture medium was discarded, followed by an addition of fixing reagent (100% methanol, pre-chilled at -20°C) and incubation at room temperature for 15min. Fixed cells were then permeabilized by a permeabilizing reagent (PBS with 0.2% TritonX-100) at room temperature for 15min. After discarding the permeabilizing reagent, blocking solution (PBS with 0.1% Tween-20, 1% BSA and 22.52mg/ml glycine) was added to each well to block the cells at room temperature for 1 hour. After this blocking step, cells were incubated with primary antibodies (Table 2) in an antibody dilution buffer (1% BSA w/v in PBS, with 0.1% Tween-20) overnight at 4°C. After overnight incubation with primary antibodies, cells were incubated with secondary antibodies (Cat#4412S, anti-rabbit IgG (H+L), F(ab')2 fragment (Alexa Fluor® 488 Conjugate), Cell Signaling Technology) at room temperature for 1 hour (in the dark). Finally, cells were mounted by ProLong™ Gold Antifade Mountant with DAPI (Cat# P36935, Invitrogen) and covered

with coverslip. Images were captured by using SPE confocal microscopy (Leica Biosystems, Wetzlar, Germany).

Statistical analysis

All data was presented as mean ± standard error of the mean (SEM), unless otherwise stated. Student t-test (with Welch's correction) was used to compare the means of two treatment groups. Two-way ANOVA (coupled with post-test, Tukey's test) was used to compare the means of more than two treatment groups if there were two independent variables (e.g., treatments) among the groups. $p<0.05$ was considered as statistically significant. *denotes $p<0.05$; **denotes $p<0.01$; ***denotes $p<0.005$; ****denotes $p<0.0001$. Statistical analysis was performed in GraphPad Prism software (Version 9.2.0).

Table 2. Primary antibodies for immunoblotting and immunofluorescence.

Name	Company	Cat#	Host	Dilution	Application
AKT	Cell Signaling	4691	Rabbit	1:1000	WB[a]
ATF4	Cell Signaling	11815	Rabbit	1:1000	WB
ATG7	Cell Signaling	8558	Rabbit	1:1000	WB
CREB	Cell Signaling	9197	Rabbit	1:1000	WB
FoxO1	Cell Signaling	2880	Rabbit	1:1000	WB
				1:100	IF[b]
G6PC	Abcam	ab83690	Rabbit	1:1000	WB
GAPDH	Cell Signaling	5174	Rabbit	1:2000	WB
Histone	Cell Signaling	9715	Rabbit	1:1000	WB
LAT1/SLC7A5	Alomone	ANT-105	Rabbit	1:200	WB
LC3B	Cell Signaling	3868	Rabbit	1:200	IF
				1:1000	WB
PCK1	Abcam	ab70358	Rabbit	1:1000	WB
pAKT-S473	Cell Signaling	9271	Rabbit	1:1000	WB
pCREB-S133	Cell Signaling	9198	Rabbit	1:1000	WB
pFoxO1-S256	Cell Signaling	9461	Rabbit	1:1000	WB

Note: [a]WB=Western blotting; [b]IF=Immunofluorescence

Results

Inhibition of autophagy suppresses HGP in vitro

To investigate whether autophagy was playing a crucial role in HGP *in vitro*, we isolated mouse primary hepatocytes and conducted an HGP assay upon inhibition of autophagy. Primary hepatocytes were cultured in the HGP buffer (the recipe was given in Materials and Methods), and either chloroquine (CQ) or siRNA-ATG7 (siR-ATG7) was applied to induce the inhibition of autophagy as previously reported[189, 195, 196]. CQ is reported to inhibit the maturation of autolysosome, leading to a decrease of lysosomal degradation in the late stage of autophagy[138]. Our immunofluorescence (IF) results showed that LC3 puncta (green) were significantly increased after 3 hours of CQ treatment compared to the groups without CQ treatment (Figure 4). Consistently, western blotting results showed that the amount of LC3B-II was significantly increased upon the treatment of CQ (Figure 7A and B). These results indicated that the late stage of autophagy (i.e., lysosomal degradation) was inhibited. Similarly, the development of autolysosomes can be inhibited by siRNA-ATG7 because knocking down ATG7 results in suppression of LC3 lipidation, leading to inhibition of the fusion between autophagosomes and lysosomes[211]. Our western blot results showed that both ATG7 and LC3B-II/I ratio were significantly reduced in the siR-ATG7-treated groups, indicating an inhibition of autophagy (Figure 7C and D).

The HGP buffer contains the glucogenic substrates sodium pyruvate and lactate which can be consumed by primary hepatocytes and converted to glucose through gluconeogenesis[38, 212]. In WT mouse primary hepatocytes without CQ treatment or siR-

ATG7 treatment, glucagon significantly increased HGP by 42.8% and 28.8%, respectively, compared to their corresponding control groups (Figure 5A and B, white bars). However, in WT mouse primary hepatocytes with CQ treatment or siR-ATG7 treatment, the promotive effect of glucagon on HGP was significantly reduced (only a 20.1% increase of HGP in the CQ-treated group, and no significant increase of HGP in the siR-ATG7-treated group), indicating that inhibition of autophagy alleviated glucagon-induced HGP (Figure 5A and B, white bars).

Since both glycogenolysis and gluconeogenesis are counted as HGP, we wanted to identify which pathway was majorly affected by autophagy deficiency. We removed the glucogenic substrates (i.e., sodium pyruvate and lactate) from the HGP buffer, then determined the glucose production with or without inhibition of autophagy. The HGP results showed that after removing glucogenic substrates, the HGP was not affected by inhibition of autophagy in WT mouse primary hepatocytes (Figure 5C, green bars). This result indicated that the inhibition of autophagy mainly impaired the gluconeogenesis, rather than glycogenolysis.

Inhibition of autophagy suppresses glucose production in vivo

Since our *in vitro* results showed that inhibition of autophagy suppressed HGP, particularly in gluconeogenesis, we wanted to verify these phenomena *in vivo* to ensure it was physiologically relevant. We used either hydroxychloroquine (HCQ) which is a less toxic derivative of CQ[138, 204, 205, 213], or adeno-associated virus vector serotype 8-shRNA-ATG7 (AAV8-shR-ATG7)[189, 214-216] to induce inhibition of autophagy in the liver of our WT mice. HCQ was administered via intraperitoneal (IP) while AAV8-shR-ATG7 was

administered via retro-orbital (RO) injection. The control groups received the same volume of normal saline or AAV8-shR-scramble, respectively. Western blot results showed that 4 hours after HCQ injection, the LC3B-II protein was significantly accumulated in the HCQ-treated WT mice's livers (Figure 8A and B). Meanwhile, seventeen days after AAV8 injection, the levels of both ATG7 and LC3B-II/I ratio were significantly reduced in the AAV8-shRNA-ATG7-treated mice's livers (Figure 8F and G). Since we injected AAV8 through retro-orbital sinus, we extracted proteins from other tissues, including the heart, adipose tissues and skeletal muscle and verified that the shRNA-ATG7 delivered by AAV8 was mainly directed to the liver (Figure 8C, D and E). Above results indicated that an inhibition of autophagy in the mouse liver was successfully induced *in vivo*.

In order to evaluate the capability of glucose production in WT mice with the inhibition of autophagy, we conducted pyruvate tolerance test and glucagon tolerance test on our mice with either HCQ or AAV8-shR-ATG7 treatment. Mice were fasted for at least16 hours, then received pyruvate or glucagon solution through IP injection (the details of HCQ and AAV8 administration were given in Materials and Methods). Blood glucose levels were recorded at 0min (right before IP injection), 15min, 30min, 60min, 90min and 120min. Consistent with our *in vitro* results, the capabilities of glucose production under the presence of pyruvate, or under the stimulation of glucagon were significantly reduced in WT mice upon inhibition of autophagy, compared to their corresponding control groups (Figure 6A, C, E and G). To conclude, above *in vitro* and *in vivo* results demonstrated that

autophagy was necessary to maintain a proper function of HGP during starvation, and inhibition of autophagy significantly suppressed HGP.

Inhibition of autophagy reduces FoxO1 protein level

FoxO1 and CREB are two critical transcription factors controlling gluconeogenic genes expression (e.g., *pck1* and *g6pc*) in the liver. It has been demonstrated that the liver-specific FoxO1 knockout (L-FKO) mice, or mice with disrupted CREB activities, exhibit a significant impairment of gluconeogenesis[41, 44, 206, 217]. As our HGP results showed that inhibition of autophagy suppressed gluconeogenesis in WT mouse primary hepatocytes, we wanted to know whether those transcription factors were also affected. Notably, under the stimulation of glucagon, FoxO1-S273 phosphorylation and CREB-S133 phosphorylation would be elevated, which were critical for their nuclear localization and function as transcription factors[35, 39-41]. We detected the protein level of FoxO1 and CREB, and gluconeogenic enzymes in mouse primary hepatocytes with or without inhibition of autophagy, and found that the FoxO1 protein level was significantly reduced upon inhibition of autophagy induced by either CQ or siR-ATG7. Consistently, the protein level of PCK1 was also reduced (Figure 7). However, we did not observe any significant reduction of CREB and CREB-S133 under autophagy deficiency (Figure 7).

After knowing that the inhibition of autophagy could significantly reduce the FoxO1 protein amount in our *in vitro* model, we wanted to know if the reduction of FoxO1 could also be observed in our *in vivo* models. Indeed, we found that the protein amount of FoxO1 in the liver from WT mice was significantly reduced upon inhibition of autophagy induced by either HCQ or AAV8-shRNA-ATG7. Consistently, the protein level of PCK1 and

G6PC were also reduced (Figure 8A, B, F and G, WT panel). Above *in vitro* and *in vivo* results indicated that the FoxO1 signaling pathway, rather than CREB signaling pathway, was potentially the major pathway involved in autophagy-mediated HGP, and inhibition of autophagy remarkably reduced FoxO1 protein level.

Autophagy-mediated HGP is in FoxO1-dependent manner

By knowing the FoxO1 signaling pathway was involved in autophagy-mediated HGP, we wanted to know whether FoxO1 signaling pathway was the only major contributor in autophagy-mediated HGP. In order to address this question, we compared the effect of autophagy deficiency on HGP in L-FKO mice with WT mice. Similar to the *in vitro* and *in vivo* studies on WT primary hepatocytes and WT mice, we induced autophagy deficiency in L-FKO primary hepatocytes with either CQ or siRNA-ATG7, and in L-FKO mice with either HCQ or AAV8-shRNA-ATG7 (Figure 4B and Figure 8, L-FKO panel). Indeed, we found that in L-FKO mouse primary hepatocytes, the suppressive effect of the inhibition of autophagy on glucagon-induced HGP was significantly lower than that in WT mouse primary hepatocytes. In WT mouse hepatocytes, CQ treatment and siR-ATG7 treatment reduced the promotive effect of glucagon on HGP by 53.0% and 79.5%, respectively (Figure 5A and B, white bars). In comparison, in L-FKO mouse hepatocytes, CQ treatment and siR-ATG7 treatment only reduced the promotive effect of glucagon on HGP by 24.7% and 2.5%, respectively (Figure 5A and B, red bars). After checking the HGP results from L-FKO primary hepatocytes with or without glucogenic substrates, we confirmed that neither glycogenolysis nor gluconeogenesis could be significantly impaired by autophagy deficiency in L-FKO hepatocytes (Figure 5C and D). Meanwhile,

by comparing the *in vivo* results of the pyruvate tolerance test and the glucagon tolerance test from L-FKO mice with WT mice, we found that the inhibition of autophagy did not make any further suppression of glucose production in L-FKO mice under the presence of pyruvate, or under the stimulation of glucagon (Figure 6B, D, F and H). On top of that, we evaluated the protein levels of G6PC and PCK1 in our L-FKO mouse livers with or without autophagy deficiency, and noticed that autophagy deficiency did not further reduce the level of G6PC and PCK1 (Figure 8A, B, F and G). These western results were consistent with no significant change in pyruvate tolerance test and glucagon tolerance test in L-FKO mice with or without inhibition of autophagy. All above results demonstrated that autophagy regulated HGP mainly through FoxO1, and induction of HGP suppression through autophagy deficiency was in FoxO1-dependent manner.

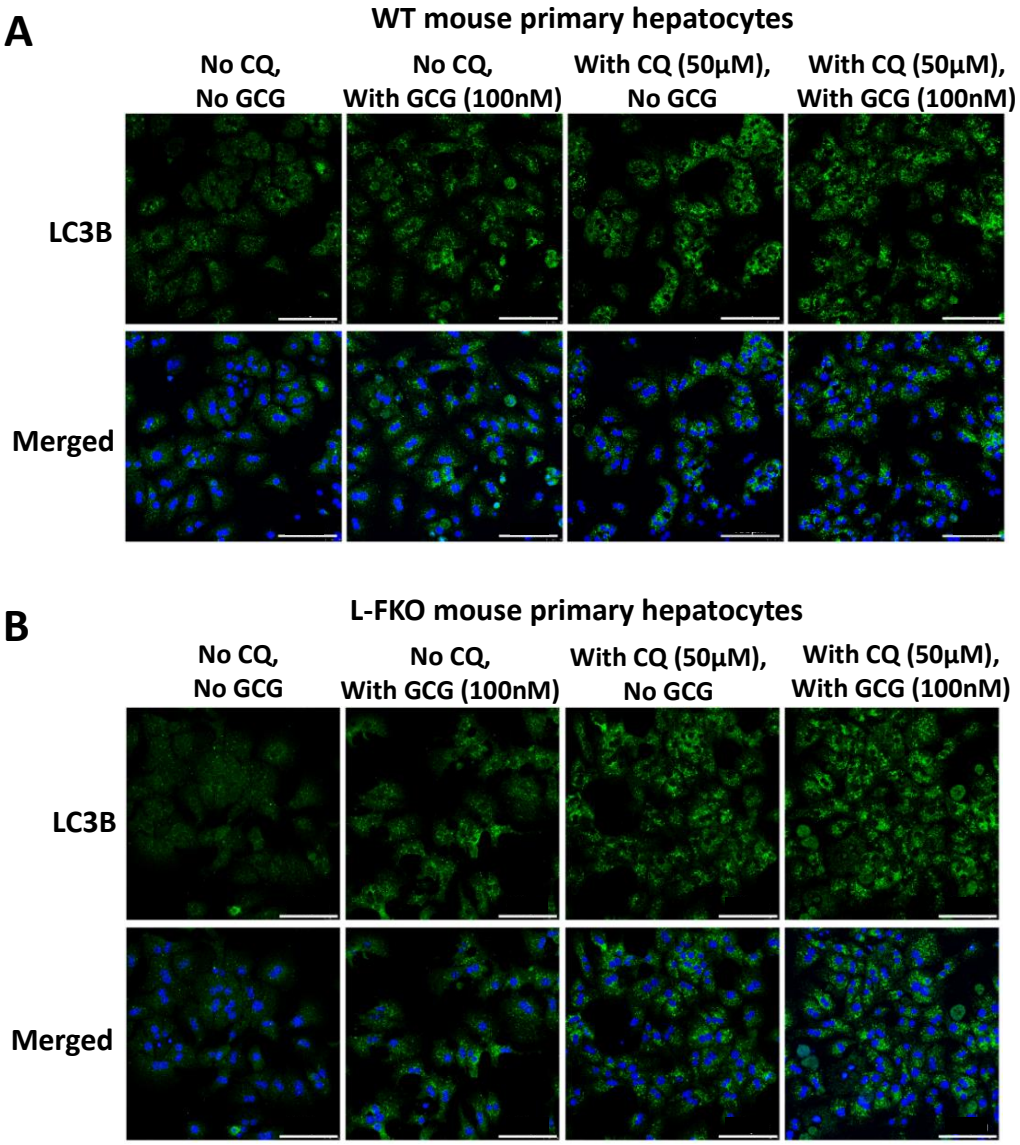

Figure 4. Inhibition of autophagy is induced by chloroquine in mouse primary hepatocytes.

Primary hepatocytes isolated from either WT (A) or L-FKO (B) mouse liver were cultured in the HGP buffer for 3 hours with or without chloroquine (CQ, 50µM) or glucagon (GCG, 100nM). Total intracellular LC3 using LC3B (D11) XP® rabbit mAb #3868 detected with anti-Rabbit Alexa Fluor® 488 conjugated secondary antibody #4412 (green) was imaged by the Leica SPE confocal microscope. Nuclei were labeled with DAPI #P36935 (blue) and merged with LC3 images. Scale bar = 100µm.

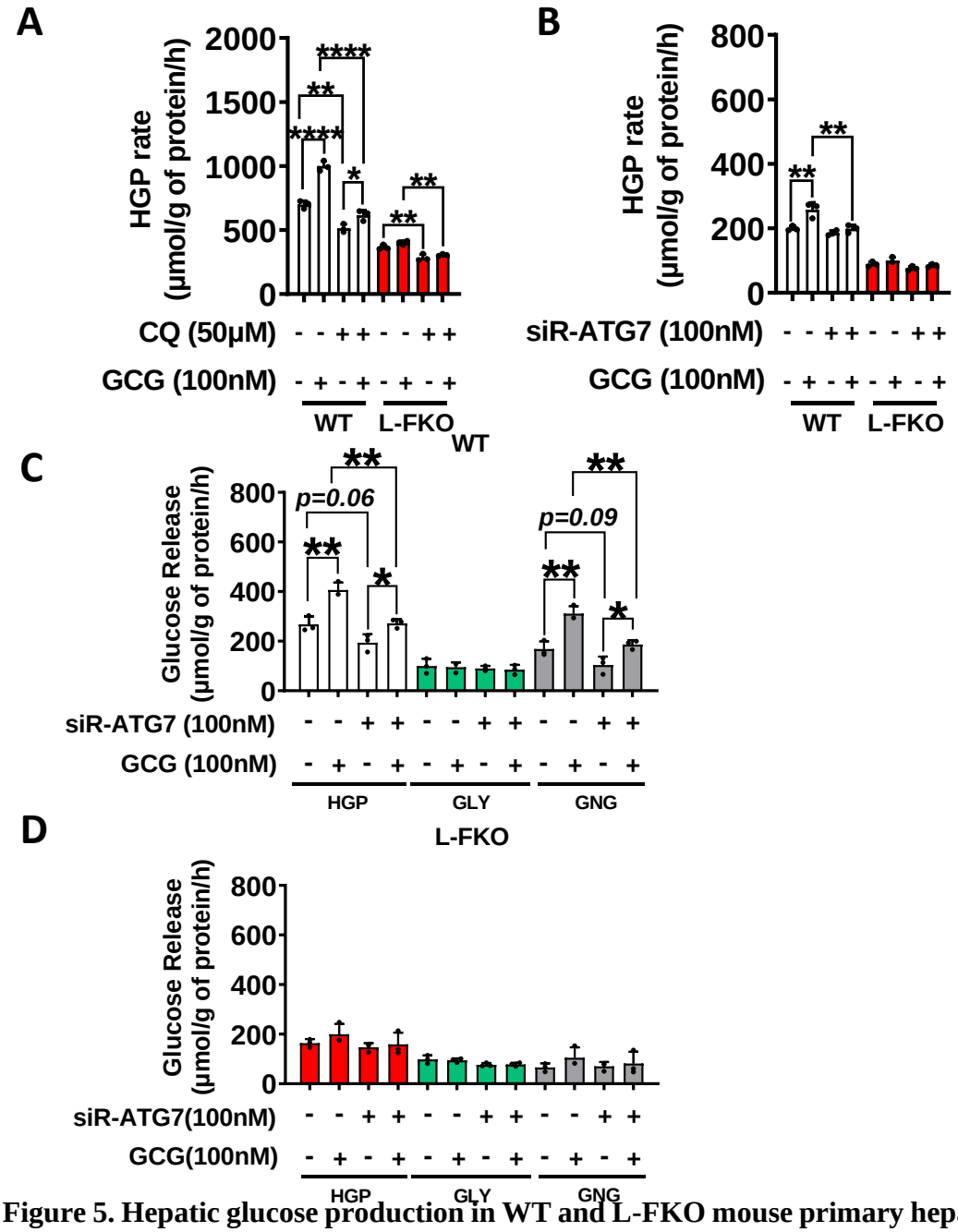

Figure 5. Hepatic glucose production in WT and L-FKO mouse primary hepatocytes with or without inhibition of autophagy *in vitro*.

Primary hepatocytes isolated from either WT or L-FKO mouse liver was cultured in the HGP buffer for 3 hours with or without inhibition of autophagy, under the treatment of CQ (50µM) (A) or siR-ATG7 (100nM) (B). Glucagon (GCG, 100nM) was used to stimulate HGP. To verify that the glycogenolysis was involved in the HGP of the WT (C) and L-FKO (D) hepatocytes, substrates (pyruvate and lactate) were removed prior to HGP assay (green bars). GLY, glycogenolysis, GNG, gluconeogenesis; HGP=GLY+GNG. Data is presented as mean±SEM. * p <0.05, ** p <0.01, *** p <0.005, ****p<0.001.

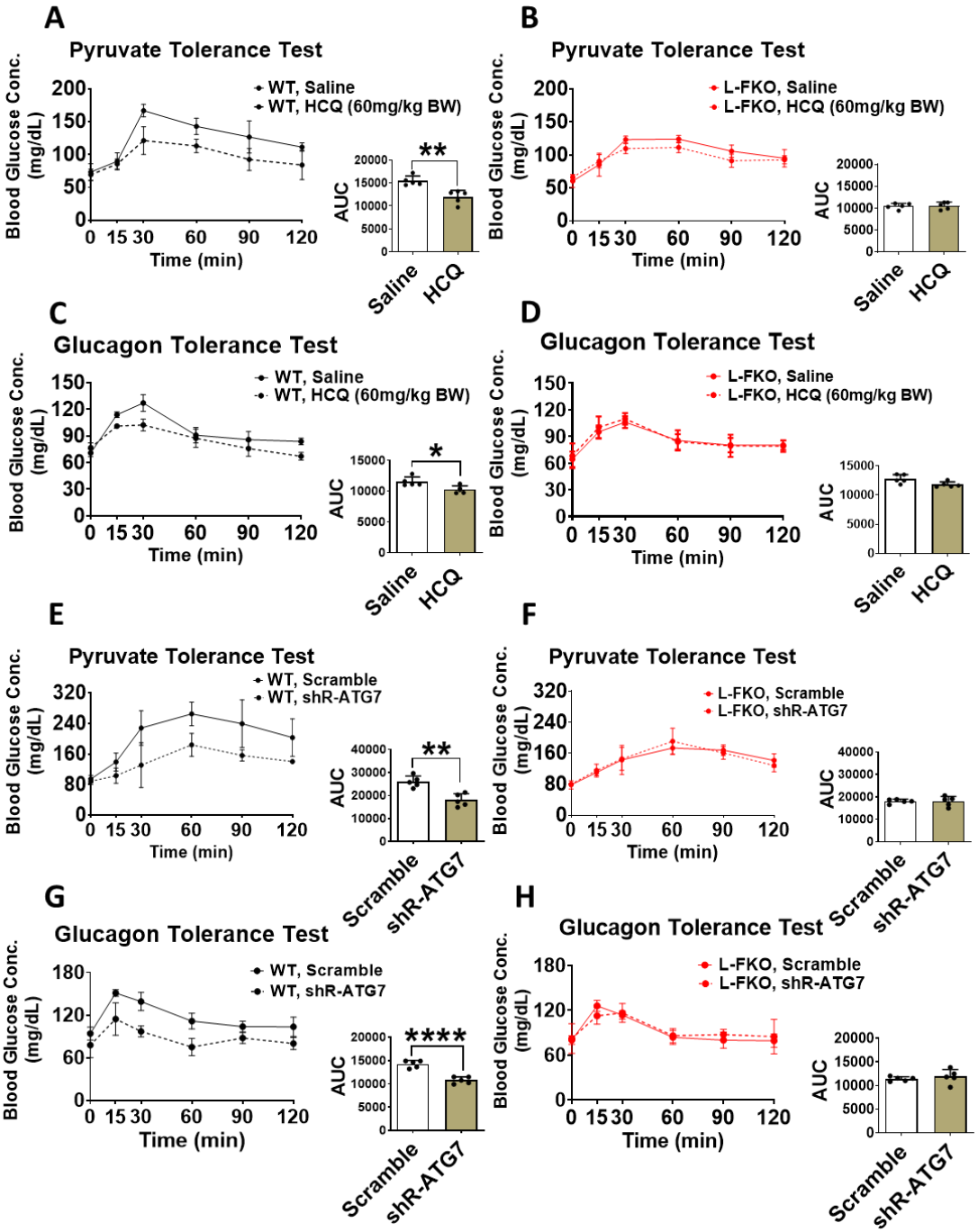

Figure 6. Gluconeogenesis in WT and L-FKO mice with or without inhibition of autophagy *in vivo*.

Pyruvate tolerance test and glucagon tolerance test were performed to evaluate the gluconeogenesis of both WT and FKO mice with or without inhibition of autophagy, under the treatment of HCQ or AAV8-shR-ATG7. n=5 (mice/group). Data is presented as mean±SD. * p <0.05, ** p <0.01. **** p <0.0001. AUC, area under curve.

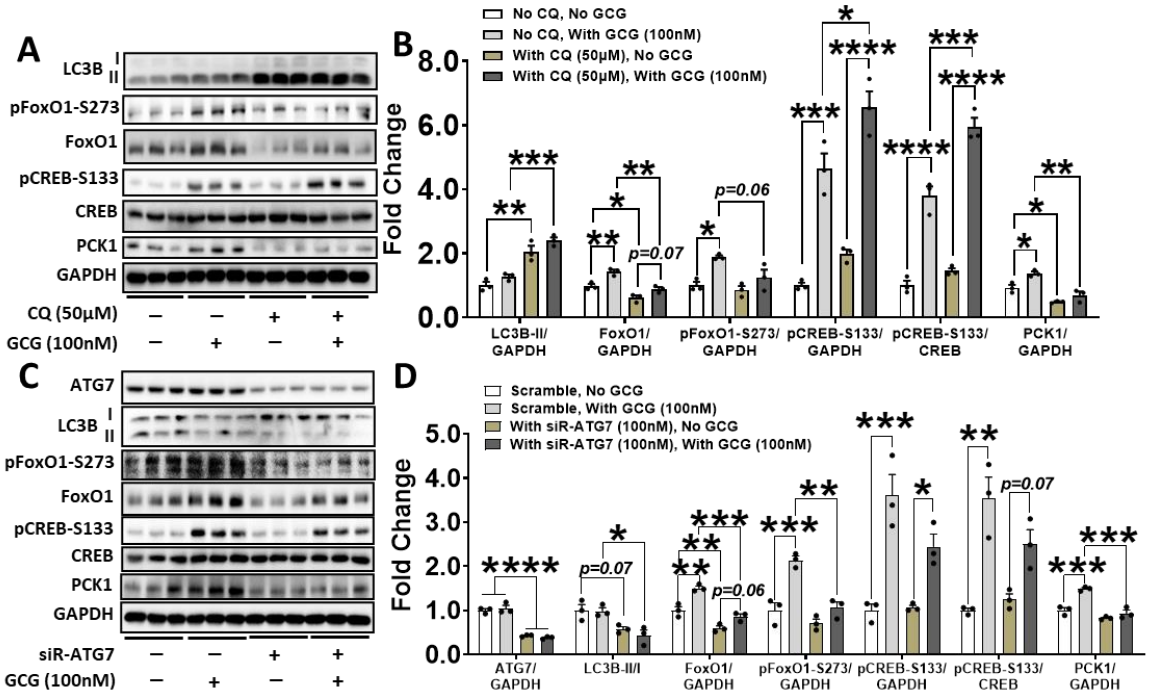

Figure 7. FoxO1 is significantly reduced upon inhibition of autophagy *in vitro*. Primary hepatocytes isolated from WT male mouse liver were cultured in HGP buffer for 3 hours with or without inhibition of autophagy, before protein collection. Target proteins were evaluated by western blot assay. Panel A is CQ treatment (50μM) study while panel C is siR-ATG7 treatment (100nM) study. Bands' intensities in panel A and panel C were quantified by ImageJ software (NIH, 1.8.0v) and given in penal B and D, respectively. Data was calculated as the relative fold change to the control group (i.e., the group without inhibition of autophagy and glucagon (GCG) treatment). Data was analyzed by two-way ANOVA coupled with post-test (Tukey's test) in GraphPad Prism software (Version 9.2.0) to check the statistical significance between groups, and presented as mean±SEM. *p<0.05, **p<0.01, ***p<0.005, ****p<0.0001.

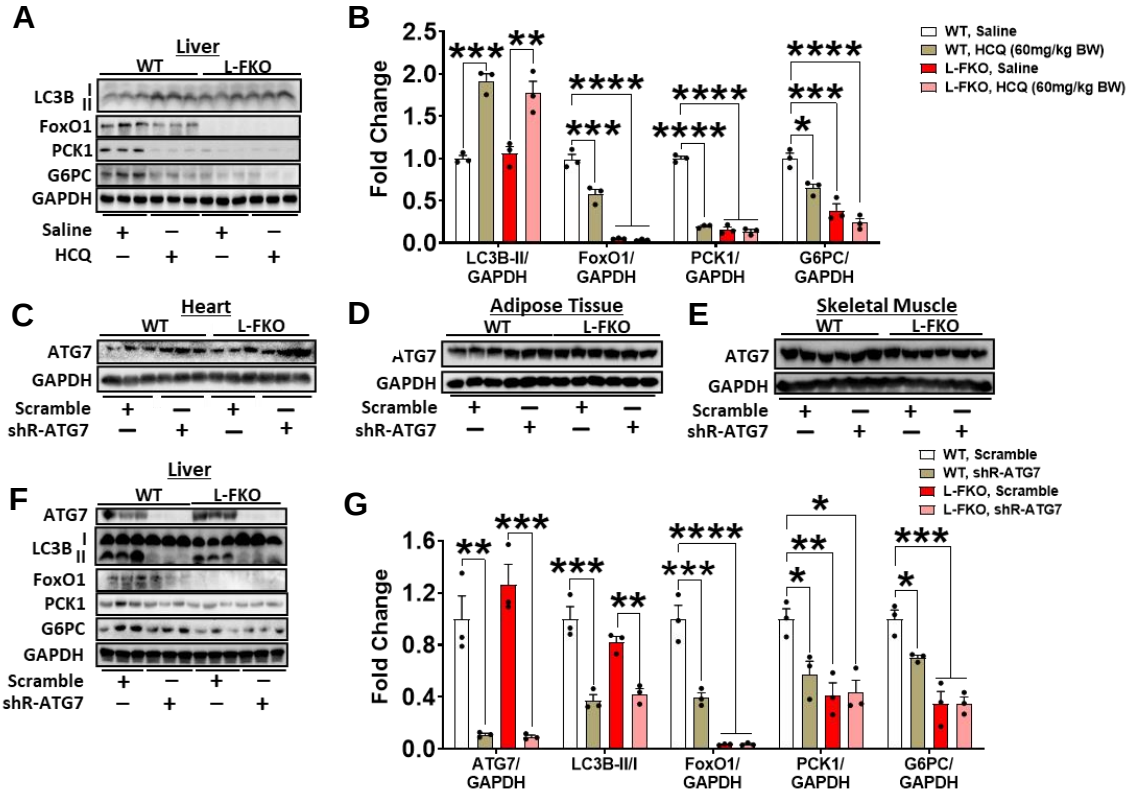

Figure 8. FoxO1 is significantly reduced upon inhibition of autophagy *in vivo*.
In HCQ treatment study (A and B), WT and L-FKO male mice received HCQ (60mg/kg BW) by IP injection after 16hr-fasting. Same volume of saline was used as control. Mice were sacrificed for tissue collection 4hr after HCQ injection. Target proteins in the liver tissues were evaluated by western blot assay. In AAV8-shRNA-ATG7 treatment study (C-G), WT and L-FKO male mice received AAV8-shRNA-ATG7 (10^{11} genome copies per mouse) by RO injection. Mice were sacrificed for tissue collection on the 17^{th} day after AAV8 injection. ATG7 protein amounts were measured in different tissues and organs (e.g., heart, adipose tissues, muscle, and the liver) to verify that ATG7 was liver-specifically knocked out (C-E). Target proteins in the liver were evaluated by western blot assay. Band intensities in panel A and panel F were quantified by ImageJ software (NIH, 1.8.0v) and given in penal B and G, respectively. Data was calculated as the relative fold change to the control group (i.e., the group without HCQ or shRNA-ATG7 treatment). Data was analyzed by two-way ANOVA coupled with post-test (Tukey's test) in GraphPad Prism software (Version 9.2.0) to check the statistical significance between groups, and presented as mean±SEM. * p<0.05, **p<0.01. ***p<0.005, ****p<0.0001.

Discussion

Autophagy is generally considered as a pro-survival catabolic activity because it promotes the turnover of carbon sources (e.g., glucose, fatty acids, and amino acids) which could be essential for energy balance and protein biosynthesis particularly under stress condition like starvation[134, 152, 164, 218]. Indeed, even under physiological conditions without too much stress, there is a basal level of autophagy which acts as a surveillant by timely delivering misfolded proteins or damaged organelles to lysosome for degradation, subsequently maintaining cellular homeostasis[130, 151, 219, 220]. Therefore, it is imperative to further investigate the specific contributions of autophagy involved in glucose homeostasis. In the present chapter, we applied a chemical approach (CQ or HCQ) or a genetic approach (siR-ATG7 or AAV8-shR-ATG7) to inhibit autophagy under starvation condition, aiming to evaluate the necessity of autophagy in HGP both *in vitro* and *in vivo*.

Consistent with previous reports[127, 132, 186], our results demonstrated that inhibition of autophagy significantly impaired the HGP *in vitro* and *in vivo*, indicating that a fully functioning autophagy was indispensable for glucose homeostasis under starvation. More importantly, our data shows that the impairment of HGP induced by inhibition of autophagy was due to impairment of gluconeogenesis (Figure 5C, Figure 6A, C, E and G) rather than glycogenolysis, which brought us to think about the role of transcription factors such as FoxO1 and CREB in the present study.

FoxO1, one member of forkhead box O-class subfamily of the forkhead transcription factors, has been reported to be a pivotal regulator in many important cellular activities including apoptosis[221-224], cell cycle[225-228], lipid metabolism[229-232], glucose metabolism[35,

[55, 185, 207, 233] depending on the treatments applied, and the type of target cells, tissues, and organs[43, 234, 235]. In particular, in the fasting state, it was recently reported that the FoxO1-S276 (equivalent to S273 in mouse FoxO1) phosphorylation could be promoted by glucagon-PKA signaling, followed by the prevention of nuclear exclusion which in turn promotes FoxO1-mediated gluconeogenic genes expression such as *pck1* and *g6pc*[35, 41, 42, 44]. Meanwhile, upon the stimulation of glucagon-PKA signaling, cAMP response element binding protein (CREB) recruits its transcriptional co-activator CBP and CRTC2 to form the CREB-CBP-CRTC2 complex in the nucleus, which can also promote gluconeogenic genes expression[39, 236]. Our results indicated that FoxO1, rather than CREB, was significantly affected by the inhibition of autophagy *in vitro* and *in vivo* (Figure 7 and Figure 8, WT panel). On top of that, by comparing the HGP results of WT hepatocytes to L-FKO hepatocytes, we found that the significant suppression of HGP induced by inhibition of autophagy could only be observed in WT hepatocytes, not in L-FKO hepatocytes. Consistently, the results of glucagon tolerance test and pyruvate tolerance test demonstrated that inhibition of autophagy could only significantly suppress HGP in WT mice, not in L-FKO mice. Although we could not completely rule out a possibility that there might be some other proteins/pathways participating in autophagy-mediated HGP, our data clearly emphasized that FoxO1 was the major participant due to the fact that no further suppression of HGP was found in L-FKO hepatocytes or mice upon inhibition of autophagy. In conclusion, we found that autophagy-mediated HGP was majorly in a FoxO1-dependent manner.

CHAPTER III

REDUCTION OF FOXO1 INDUCED BY AUTOPHAGY DEFICIENCY IS INDEPENDENT OF FOXO1 PHOSPHORYLATION, DEGRADATION AND TRANSCRIPTION

Introduction

In the fasted state, human glucagon secreted from pancreatic α cell interacts with glucagon receptor on the cell surface of hepatocytes, initiating an intracellular signaling cascade which subsequently promotes gluconeogenic genes expression[19, 36, 37, 237]. There are two major transcription factors responsible for glucagon signaling, cAMP response element-binding protein (CREB) and FoxO1[40, 208, 238, 239]. In CREB-mediated pathway, glucagon-activated PKA catalyzes the phosphorylation of CREB at S133, which in turn forms a complex with its transcription co-activator CBP and CRTC2 in the nucleus, followed by binding to the cAMP response element (CRE) in the promoter region of gluconeogenic genes such as *pck1* and *g6pc*[39, 103, 240]. Concurrently, glucagon-activated PKA catalyzes the phosphorylation of FoxO1 at S276 (equivalent to S273 in mouse FoxO1), leading to localization and stabilization of FoxO1 in the nucleus where FoxO1 binds to the insulin response element (IRE) in the promoter region of *pck1* and *g6pc* gene[35, 41]. In mammals, phosphoenolpyruvate carboxykinase (PCK) has two isoforms, PCK1 (mainly in the cytosol) and PCK2 (mainly in the mitochondria) which are encoded by *Pck1* and *Pck2* genes, respectively[212, 241, 242]. Although both PCK1 and PCK2 are controlling an important rate-limiting step of gluconeogenesis, which is catalyzing the formation of phosphoenolpyruvate (PEP) from oxaloacetate (OAA), PCK1 is the only

enzyme responsible for the hormonal stimulation (e.g., glucagon) in the liver[241, 243]. Meanwhile, glucose-6-phosphatase (G6Pase) has three different catalytic subunits (i.e., G6PC, G6PC2 and G6PC3) among which G6PC (encoded by *g6pc* gene) is the major subunit catalyzing the dephosphorylation of glucose-6-phosphate (the last step of gluconeogenesis) in the liver, generating glucose molecule[244-246].

On the other hand, in the fed state, human insulin secreted from pancreatic β cells interacts with insulin receptor on the surface of hepatocytes, which subsequently promotes AKT phosphorylation at T308 and S473[23, 49, 54]. Phosphorylated AKT catalyzes the phosphorylation of FoxO1 at S256 (equivalent to S253 in mouse FoxO1), leading to FoxO1 nuclear exclusion and ubiquitination in the cytosol[55, 233, 239]. Consequently, less FoxO1 is available in the nucleus, resulting in a decrease of *pck1* and *g6pc* genes expression, which in turn downregulates hepatic gluconeogenesis[55, 69].

According to our findings in the previous chapter, we hypothesized that the activity of FoxO1 in control of HGP was altered upon inhibition of autophagy. In the present chapter, we evaluated the protein and mRNA level of FoxO1, nuclear localization of FoxO1 and phosphorylation and degradation of FoxO1 with or without the inhibition of autophagy through our *in vitro* and *in vivo* models. We found that the protein level of FoxO1 in the cytosol and the nucleus was significantly reduced upon inhibition of autophagy, which was, however, independent of downregulation of FoxO1 mRNA, or FoxO1 phosphorylation and degradation.

Materials and methods

Ethics statement

Animal protocols were approved by the Institutional Animal Care and Use Committee (IACUC) at Texas A&M University. All mice were kept in laboratory animal resources and research facility (LARR), and housed in standard cages under 12hr-light/12hr-dark cycle with access to food and drinking water ad libitum as previously described[41, 44, 206]. Necessary procedures (e.g., performing euthanasia by means of isoflurane vaporizer) were conducted to minimize the discomfort, distress, and pain of the mice during the experiments.

Generation of genetically modified mice models

Liver-specific FoxO1-knockout (L-FKO) mice were generated by breeding floxed FoxO1 ($FoxO1^{fl/fl}$) mice with albumin-Cre mice as previously described[44, 207]. FoxO1-$S253^{A/A}$ knock-in (KI) mice, in which the endogenous FoxO1-S253 alleles were replaced by alanine (A) to prevent insulin-induced phosphorylation of FoxO1 at S253 (a loss-of-function mutation), were generated from heterozygous FoxO1-$S253^{A/+}$ parents as previously described[55]. FoxO1-$S273^{D/D}$ KI mice, in which the endogenous FoxO1-S273 alleles were replaced by aspartate (D) to mimic glucagon-induced phosphorylation of FoxO1 at S273 (a gain-of-function mutation), were generated by CRISPR/Cas9 approach as previously described[35, 41]. Neither significant defect on animal performance, nor liver damage was found in all these genetically modified mouse models, as previously reported[35, 41, 44, 55, 208]. The tail DNA of pup mice was genotyped by PCR and then

confirmed by DNA sequencing analysis, as previously described[35]. Eight to 12-week-old male mice were used for all our animal studies.

Animal treatment and tissue collection

HCQ and AAV8-shRNA-ATG7 were used to inhibit autophagy in WT and L-FKO mice. For HCQ treatment, an HCQ solution (60mg/kg BW) was administered via IP injection to 8- to 12-week-old male mice (5-6 mice each group) after overnight (16hr) fasting. The control group received the same volume of normal saline. Mice were sacrificed 4 hours after the HCQ injection for tissue collection, as previously reported[138, 140, 209, 210]. For AAV8-shRNA-ATG7 treatment, AAV8-shRNA-ATG7 (10^{11} genome copies/mouse) was administered via RO injection to 8- to 12-week-old male mice (5-6 mice each group). The control group received the same amount of AAV8-shRNA-scramble. Mice were sacrificed 17 days after the AAV8 injection for tissue collection, similar to our previous report[41].

Isolation of mouse primary hepatocytes and treatment

Mouse primary hepatocytes were isolated from 8- to 12-week-old male mouse liver and cultured in DMEM (containing 5.5 mM glucose) supplemented with 10% fetal bovine serum (FBS) as previously described[41, 44, 208]. When hepatocytes firmly attached on the bottom of coated culture plate, DMEM was replaced by the HGP buffer, proceeding to another 3hr-starvation prior to protein or RNA collection. For CQ treatment, a CQ solution (final concentration = 50 μM) was added in the corresponding treatment groups concurrently with replacement of the DMEM by the HGP buffer. A glucagon solution (final concentration = 100 nM) would be added in the corresponding treatment groups 30

min after CQ treatment. In siR-ATG7-treated groups, the transfection culture medium was replaced by the HGP buffer right after the transfection. A glucagon solution was added in the corresponding treatment groups at the same time. After a 3hr-incubation, hepatocytes were lysed by RIPA lysis buffer or TRIzol reagent (Cat# 15596018, ThermoFisher) for protein or RNA collection.

Extraction of nuclear and cytoplasmic proteins

To prepare the cell samples for extraction of nuclear and cytoplasmic proteins, mouse primary hepatocytes were first harvested by using trypsin-EDTA (0.25%) (Cat# 25200114, Thermofisher). Cells were then washed with PBS, followed by centrifugation at 500g, 3 min. After centrifugation, the supernatant was removed, and the remaining cell pellets proceeded to protein extraction with NE-PER™ Nuclear and Cytoplasmic Extraction Reagents (Cat# 78835, ThermoFisher) as previously described[35, 247].

Determination of protein concentration

For *in vitro* study, primary hepatocytes were lysed by the RIPA lysis buffer (MilliporeSigma) containing protease and phosphatase inhibitor cocktail (MilliporeSigma) and sodium orthovanadate (MilliporeSigma). For *in vivo* study, the liver, heart, or adipose tissue fragments (about 50 mg per tissue) were lysed by the RIPA lysis buffer containing a protease and phosphatase inhibitor cocktail and sodium orthovanadate, then proceeded to homogenization using the IKA T8 homogenizer (12-18V DC, 100W). Cell or tissue lysates were then centrifuged at 14000 rpm, 4°C for 15min, and the supernatant was collected. Protein concentration was determined by Pierce™ BCA Protein Assay Kit (ThermoFisher) following the manufacturer's instruction.

Protein immunoblotting

Western blotting was conducted as previously described[41, 44, 208]. In brief, protein samples were first normalized with Alfa Aesar™ laemmli SDS sample buffer (reducing, 6X) (Fisher Scientific) based on the concentration of protein samples, and denatured under 95.5°C for 10 min. Protein samples (25 – 40µg) were then resolved in a polyacrylamide gel (7.5-15%) by using a Mini-PROTEAN® Tetra Vertical Electrophoresis Cell (Bio-Rad), and electro-blotted onto the Amersham Hybond western blotting membranes (0.45µm PVDF) (VWR) by using Trans-Blot Turbo Transfer System (Bio-Rad). Membranes were incubated with primary antibodies (Table 2) in a 5% BSA solution (5% w/v in TBST) overnight at 4°C, followed by incubation with secondary antibodies (anti-rabbit IgG, HRP-linked, Cell Signaling Technology) in a 5% BSA solution on the second day. Clarity Western ECL Substrate (Bio-Rad) was used to react with HRP-linked secondary antibody to generate light signals which were captured by ChemiDoc™ Imaging System (Bio-Rad). The band intensity was quantified by ImageJ software (NIH, 1.8.0v) and expressed as a ratio to GAPDH (internal control). Antibody of human phosphor-FoxO1 (S276) (equivalent to S273 in mouse FoxO1) was generated as previously described[35].

Immunofluorescence staining

Mouse primary hepatocytes were cultured ($5*10^4$ cells/well) in the collagen coated Thermo Scientific™ Nunc™ Lab-Tek™ II Chamber Slide™ System (Fisher Scientific). The immunofluorescence assay was conducted following immunocytochemistry and immunofluorescence protocol (Abcam). In brief, after the experimental treatment, the

culture medium was discarded, followed by an addition of fixing reagent (100% methanol, pre-chilled at -20°C) and incubating at room temperature for 15 min. Fixed cells were then permeabilized by permeabilizing reagent (PBS with 0.2% TritonX-100) at room temperature for 15 min. After discarding the permeabilizing reagent, a blocking solution (PBS with 0.1% Tween-20, 1% BSA and 22.52 mg/ml glycine) was added to each well to block the cells at room temperature for an hour. After 1hr-blocking, cells were incubated with primary antibodies (Table 2) in an antibody dilution buffer (1% BSA w/v in PBS, with 0.1% Tween-20) overnight at 4°C. After overnight incubation with primary antibodies, cells were incubated with secondary antibodies (Alexa Fluor® 488 Conjugate) (Cell Signaling Technology) at room temperature for an hour (in the dark). Finally, cells were mounted by ProLong™ Gold Antifade Mountant with DAPI (Invitrogen) and covered with coverslip. Images were captured under SPE confocal microscopy (Leica Biosystems, Wetzlar, Germany).

Immunohistochemistry staining

After being fixed in formalin, the liver tissues were embedded in paraffin wax, then proceeded to tissue sectioning with 5 μm in thickness, by using HistoCore AUTOCUT - Automated Rotary Microtome (Leica Biosystems, Wetzlar, Germany). Tissue sections were air-dried for at least one hour, then put in 60°C oven for at least 30 min to melt the paraffin. The deparaffinization and rehydration procedures were conducted following below steps (Table 3).

Table 3. Steps of sections deparaffinization and rehydration.

Name of reagent (purity)	Times*Duration per time
Xylene (100%)	2*10min
Ethanol (100%)	2*5min
Ethanol (90%)	1*2min
Ethanol (70%)	1*2min
Running Tap Water	at least 5min

In order to break protein cross-links that mask antigens in formalin-fixed tissues, antigen retrieval procedures were conducted after rehydration procedures. In brief, rehydrated sections were placed in pre-heated coplin jar filled with antigen unmasking solution, citrate-based (Vector Laboratories, Cat#H-3300), then steamed for 25 min. Then tissue sections were cooled down at room temperature for at least 15 min prior to rinsing under running tap water. After antigen retrieval process, IHC staining was conducted according to the manufacturer's protocol of M.O.M.® (Mouse-on-Mouse) Elite® Immunodetection Kit, Peroxidase (Cat#PK-2200, Vector Laboratories) or VECTASTAIN® Elite ABC-HRP Kit, Peroxidase (Rabbit IgG) (PK-6101, Vector Laboratories). Nuclei were stained by hematoxylin. Images were captured under Aperio Slide Scanner (Leica Biosystems, Wetzlar, Germany).

RNA isolation from primary hepatocytes or tissue samples

For the *in vitro* study, mouse primary hepatocytes were lysed in the TRIzol reagent (ThermoFisher), then transferred to 1.7ml RNAse-free centrifugal tubes. For the *in vivo* study, liver tissue fragments were lysed in the TRIzol reagent, followed by homogenization using IKA T8 homogenizer (12-18V DC, 100W). Tissue lysates were then centrifuged at 14000 rpm, 4℃ for 15 min. The supernatants were collected in new 1.7ml RNAse-free centrifugal tubes. Two hundred microliters of chloroform (Cat# 97064-

680, VWR) per 1ml of TRIzol reagent was added to the above cell or tissue lysates. Samples then proceeded to gentle mixing, followed by 3min-standing still prior to centrifugation at 12000g, 4°C for 15min. After centrifugation, the upper aqueous phase of samples was transferred to a fresh tube, mixing with same volume of 80% ethanol then undergoing vortex. After vortex, 700µl of liquid mixture was transferred to the EconoSpin® RNA Mini Spin Column (Cat# NC0772081, Fisher Scientific) followed by centrifugation at 8000g, 4°C for 60sec. Isopropyl ethanol (500µl) was added into the spin column, then proceeded to 10min-incubation at room temperature. The mixture was centrifuged at 8000g, 4°C for 60sec again to discard the isopropyl ethanol (RNA extracts were trapped in the RNA-binding membrane of columns). Two repeating washing steps by adding 80% ethanol and centrifugation at 8000g, 4°C for 60sec were then conducted to these columns. After washing steps, columns were centrifuged once again at 12000g, 4°C for 3min to completely remove the leftover ethanol. Finally, 30µl of UltraPure™ DNase/RNase-Free distilled water (Cat# 10977015, ThermoFisher) was added into the column to redissolve the RNA. Total RNA extracts were quantified by NanoDrop 2000/2000c Spectrophotometer (ThermoFisher).

Real-time reverse transcription quantitative polymerase chain reaction (RT-qPCR)

RNA templates (1000ng) were reverse transcribed to their corresponding complementary DNAs (cDNA) with iScript™ Reverse Transcription Supermix (Bio-Rad) following manufacturer's instructions. cDNA was mixed with primers (Table 4) and SsoAdvanced Universal SYBR® Green Supermix (Cat# 1725274, Bio-Rad), then proceeded to real-time PCR in CFX384 Touch™ Real-Time PCR Detection System (Cat#

1855485, Bio-Rad). Cyclophilin was used as an internal control. RT-qPCR assay was conducted in triplicate for each biological replicate. Relative gene expression level was calculated by using the 2(-Delta Delta C(T)) method[248].

Statistical analysis

All data was presented as mean ± standard error of the mean (SEM), unless otherwise stated. One-way ANOVA (with Dunnett's T3 test) was used to compare the means of more than two treatment groups if there is one independent variables (e.g., CQ time-course study) among groups. Two-way ANOVA (coupled with post-test, Tukey's test) was used to compare the means of more than two treatment groups if there are two independent variables (e.g., treatments) among the groups. $p<0.05$ was considered as statistically significant. *denotes $p<0.05$; **denotes $p<0.01$; ***denotes $p<0.005$; ****denotes $p<0.0001$. Statistical analysis was performed in GraphPad Prism software (Version 9.2.0).

Table 4. Primers for RT-qPCR.

Name	Sequence (5'-3')		Reference
Acc1	Forward	CCTCCGTCAGCTCAGATACA	41
	Reverse	TTTACTAGGTGCAAGCCAGACA	
Atf4	Forward	CCTAGGTCTCTTAGATGACTATCTGGAGG	249
	Reverse	CCAGGTCATCCATTCGAAACAGAGCATCG	
Atg7	Forward	AGTTGAGCGGCGACAGCATTA	NCBI Ref Seq: NM_001253717.2
	Reverse	GTTCTTACCAGCCTCACTGTCA	
Cd36	Forward	GATGACGTGGCAAAGAACAG	41
	Reverse	TCCTCGGGGTCCTGAGTTAT	
Cpt1a	Forward	GCCGATCATGGTTAACAGCAACT	41, 208
	Reverse	AGACCTTGAAGTAACGGCCTC	
Cyclophilin	Forward	CTAAAGCATACAGGTCCTGGCATCTTG	41, 207
	Reverse	TGCCATCCAGCCATTCAGTCTTG	
FoxO1	Forward	AGATGAGTGCCCTGGGCAGC	41, 207, 208
	Reverse	GATGGACTCCATGTCACAGT	
G6pc	Forward	CATTGTGGCTTCCTTGGTCC	41, 207, 208
	Reverse	GGCAGTATGGGATAAGACTG	
Gsr	Forward	CCACGGCTATGCAACATTCG	41
	Reverse	AATCAGGATGTGTGGAGCGG	
Map1LC3b	Forward	GGGACCCTAACCCCATAGGA	NCBI Ref Seq: NM_001364358.1
	Reverse	CTATAATCACCCGCCTGCCC	
Pck1	Forward	CCATCGGCTACATCCCTAAG	41, 207, 208
	Reverse	GACCTGGTCCTCCAGATACC	
Prdx3	Forward	CCGTTTGGTAAAGGCGTTCC	41
	Reverse	GGCTTGATCGTAGGGGACTC	
Prdx5	Forward	TCGTCGGCTGAAAAGGTTCT	41
	Reverse	ATCTGGCTCCACGTTCAGTG	
Scd1	Forward	CTGTACGGGATCATACTGGTTC	41
	Reverse	GCCGTGCCTTGTAAGTTCTG	
Slc7a5/Lat1	Forward	CTTCGGCTCTGTCAATGGGT	250
	Reverse	TTCACCTTGATGGGACGCTC	
Sod2	Forward	AAGGTCGCTTACAGATTGCTGC	41
	Reverse	AGCGGAATAAGGCCTGTTGTTC	
Srebp1c	Forward	GGAGCCATGGATTGCACATT	41
	Reverse	GGCCCGGGAAGTCACTGT	

Results

Inhibition of autophagy significantly suppresses nuclear localization of FoxO1

Since FoxO1 is a transcription factor which is required to localize in the nucleus in order to regulate the target genes expression[35, 44, 239], and we observed that the total protein amount of FoxO1 was significantly reduced upon the inhibition of autophagy (Figure 7 and Figure 8), we wanted to know that whether the reduction of total FoxO1 protein amount would be associated with a reduction of the nuclear localization of FoxO1. To address this question, we extracted the cytosolic and nuclear proteins from mouse primary hepatocytes with or without inhibition of autophagy, then evaluated the FoxO1 protein amount inside and outside the nucleus. In addition, as the nuclear localization of FoxO1 is tightly related to FoxO1-S253 and FoxO1-S273 phosphorylation, we would also like to evaluate the FoxO1 phosphorylation at both sites under autophagy deficiency. Our western blot results showed that upon the inhibition of autophagy, both cytosolic and nuclear protein amount of total FoxO1 were significantly reduced. Meanwhile, we found that there was no significant increase of FoxO1-S253 inside or outside the nucleus. In contrast, we found that the FoxO1-S253 protein amount was significantly reduced in the cytosol. Nevertheless, we did observe a slight decrease of FoxO1-S273 in the nucleus (Figure 9A and B). Then we evaluated the distribution of FoxO1 protein in the primary hepatocytes by immunofluorescence assay. Consistently, the confocal microscopy showed that a significant less amount of FoxO1 was observed in the nucleus in mouse primary hepatocytes upon inhibition of autophagy (Figure 9 C). In addition, immunohistochemical analysis of FoxO1 protein on the mouse liver tissues showed that the FoxO1 protein level

was significantly reduced in the nucleus under the AAV8-shR-ATG7 treatment (Figure 10 A-D). Our data demonstrated that without a proper functioning autophagy, both the total protein amount and nuclear localization of FoxO1 were significantly downregulated, which could possibly explain why FoxO1-mediated gluconeogenic pathway was impaired afterwards.

Reduction of FoxO1 protein induced by inhibition of autophagy is independent of FoxO1 phosphorylation and degradation

We wanted to further investigate the possible mechanisms causing the reduction of FoxO1 protein level upon inhibition of autophagy. It has been well-reported that the stability and nuclear localization of FoxO1 are highly associated with the phosphorylation of FoxO1. Phosphorylation of human FoxO1 at S256 (equivalent to S253 in mouse FoxO1), which is usually triggered by insulin-stimulated AKT signaling, promotes the nuclear exclusion of FoxO1, followed by ubiquitination and degradation of FoxO1 in the cytoplasm[55]. In contrast, phosphorylation of human FoxO1 at S276 (equivalent to S273 in mouse FoxO1), which is usually triggered by glucagon → PKA signaling, promotes the nuclear localization of FoxO1, thereby increasing the stability of FoxO1[35]. In Figure 9, although we did not observe an increase of FoxO1-S253 phosphorylation, we did observe a decrease of FoxO1-S273, which brought attention to the fact that we need to further investigate the behavior of FoxO1 phosphorylation upon inhibition of autophagy. Under these circumstances, we isolated mouse primary hepatocytes from WT, FoxO1-S253$^{A/A}$ KI mouse, or FoxO1-S273$^{D/D}$ KI mouse livers, then evaluated the FoxO1 protein level in these three types of hepatocytes under different time points (i.e., 0.5hr, 1hr, 2hr, 3hr) with

treatment of CQ. In FoxO1-S253$^{A/A}$ hepatocytes, FoxO1-S253 alleles are replaced by alanine (A), which in turn prevent the phosphorylation of FoxO1 at S253, thereby suppressing FoxO1 nuclear exclusion and ubiquitination. Meanwhile, in FoxO1-S273$^{D/D}$ hepatocytes, FoxO1-S273 alleles are replaced by aspartate (D) which mimic the phosphorylation of FoxO1 at S273, thereby stabilizing FoxO1 in the nucleus and allowing FoxO1 to proceed with transcriptional regulation. Our results showed that neither FoxO1-S253$^{A/A}$, nor FoxO1-S273$^{D/D}$ was able to prevent the reduction of FoxO1 protein amount after 3 hours of inhibition of autophagy (Figure 11 A-F), although the reduction rate of FoxO1 protein level within these 3 hours of CQ treatment was sightly delayed in FoxO1-S253$^{A/A}$ and FoxO1-S273$^{D/D}$ primary hepatocytes in comparison to WT hepatocytes (Figure 11B, D and F). On top of that, since the phosphorylation of FoxO1 at S253 was mainly triggered by AKT after AKT was phosphorylated at S473 and activated[251-254], we checked the protein level of total AKT and AKT-S473 phosphorylation. Indeed, we did not observe any upregulation of AKT phosphorylation at S473 in all three types of hepatocytes upon inhibition of autophagy (Figure 11 A, C and E). Above results suggested that inhibition of autophagy did not promote FoxO1-S253 phosphorylation, or inhibit FoxO1-S273 phosphorylation. The decrease of FoxO1-S273 observed in the nucleus (Figure 9A) was probably due to decrease of total FoxO1 protein amount.

Since alteration of FoxO1 phosphorylation sites failed to prevent FoxO1 from reduction upon autophagy deficiency, we decided to use MG132, a well-known proteasome inhibitor to directly block the degradation of ubiquitin-conjugated proteins in mouse primary hepatocytes[255-257]. We pre-treated the primary hepatocytes with MG132

(10μM) for 30min prior to CQ treatment, then collected the proteins after 3 hours. Interestingly, the reduction of FoxO1 induced by autophagy deficiency persisted even under the treatment of MG132 (Figure 12 A and B). This piece of evidence indicated that reduction of FoxO1 level was unlikely due to promotion of FoxO1 protein degradation under autophagy deficiency.

To conclude, all the above evidence suggested that the FoxO1 phosphorylation and degradation were not the major mechanisms to cause the reduction of FoxO1 protein level upon inhibition of autophagy.

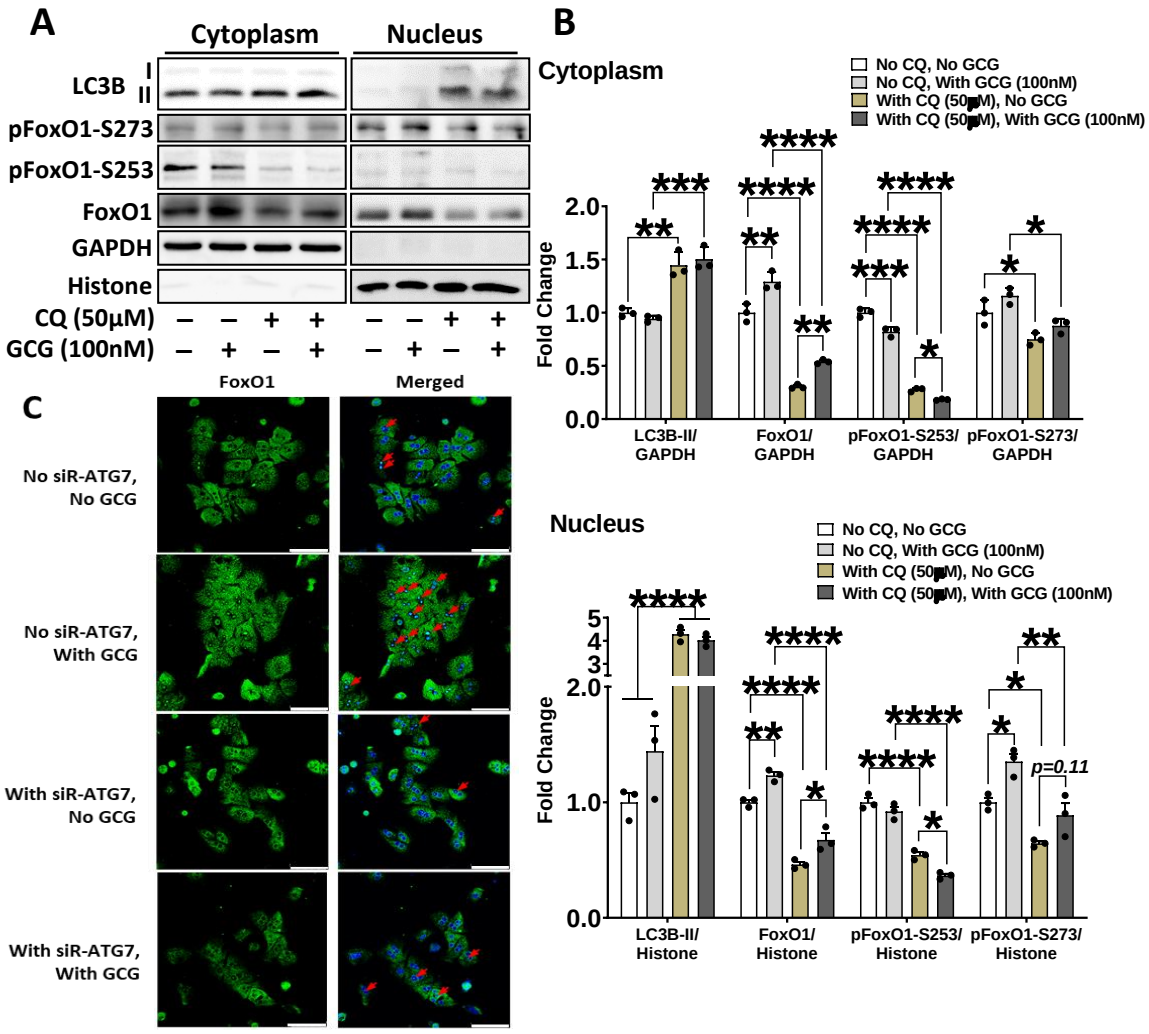

Figure 9. Nuclear localization of FoxO1 is significantly suppressed upon inhibition of autophagy.

Primary hepatocytes isolated from WT male mouse liver were cultured in HGP buffer for 3hr with or without inhibition of autophagy (CQ treatment, 50μM). Nuclear and cytoplasmic proteins were extracted separately, and the target proteins were evaluated by western blot assay (A). Representative protein blot images were given in panel A, and the bands' intensities (from three independent repeated experiments) in the cytoplasm or the nucleus were quantified by ImageJ software (NIH, 1.8.0v) and given in penal B. Distribution of FoxO1 (green) with or without inhibition of autophagy (siR-ATG7 treatment, 100nM) in mouse primary hepatocytes was imaged by Leica SPE confocal microscope. Nuclei were labeled with DAPI (blue) and merged with FoxO1 images (C). Red arrows indicated the nuclear localization of FoxO1. Data was calculated as the relative fold change to the control group (i.e., the group without inhibition of autophagy and glucagon (GCG) treatment). Data was analyzed by two-way ANOVA coupled with post-test (Tukey's test) and presented as mean±SEM. *p<0.05, **p<0.01. ***p<0.005., ****p<0.0001. Scale bar = 75μm.

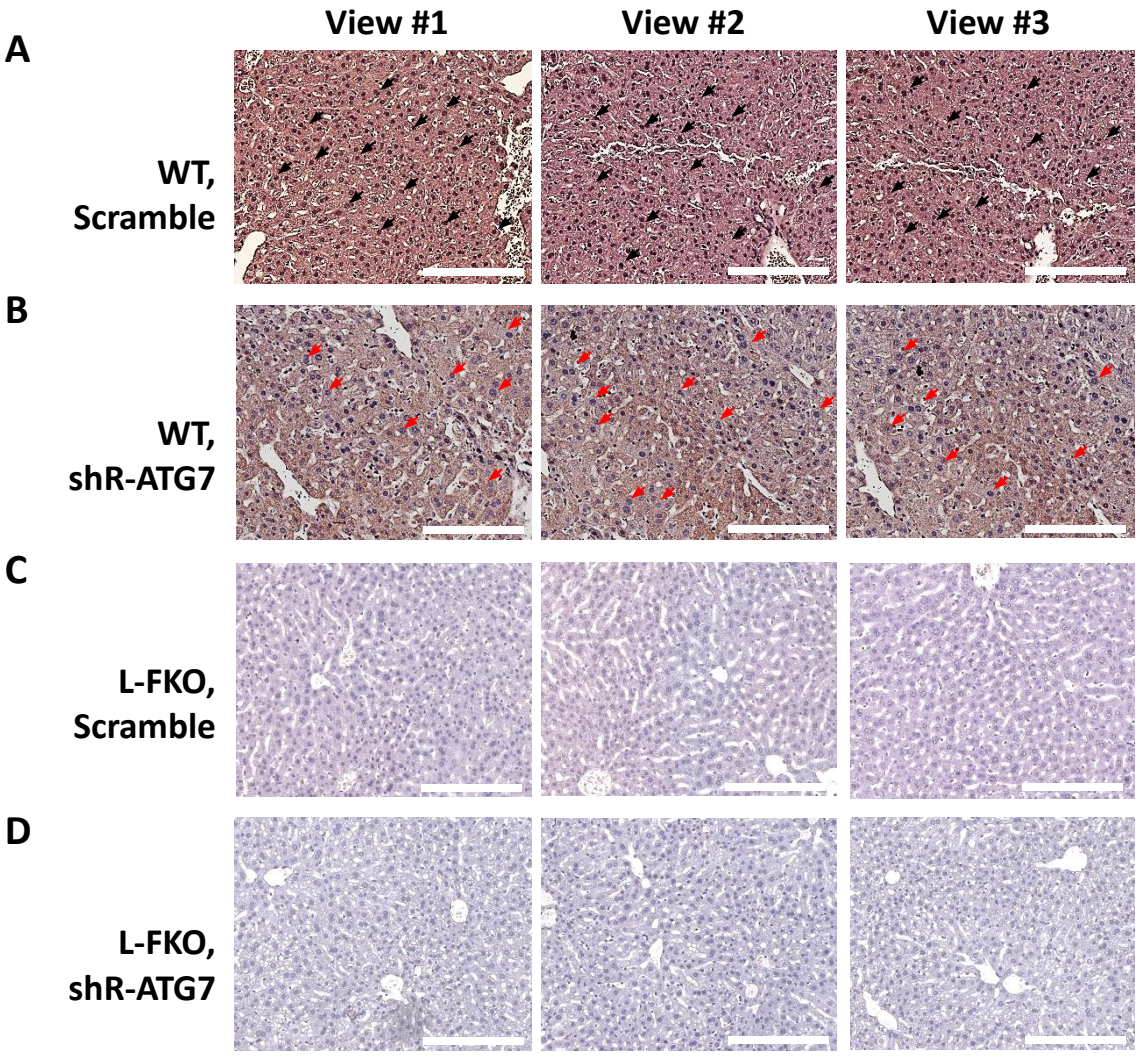

Figure 10. Immunohistochemical analysis of FoxO1 protein in the WT & L-FKO mouse liver tissues, with or without inhibition of autophagy.
WT or L-FKO male mouse livers were fixed in formalin, then embedded in paraffin wax prior to sectioning with Automated Rotary Microtome. Immunohistochemistry staining was performed following the manufacturer's protocols. FoxO1 protein was stained in brown color while the nucleus was stained in blue color. Three representative views (view #1, #2 and #3) from different liver tissue sections under corresponding treatment groups were provided (A-D). Black arrows indicated the localization of FoxO1. Red arrows indicated the lack of nuclear localization of FoxO1. Scale bar = 200 μm.

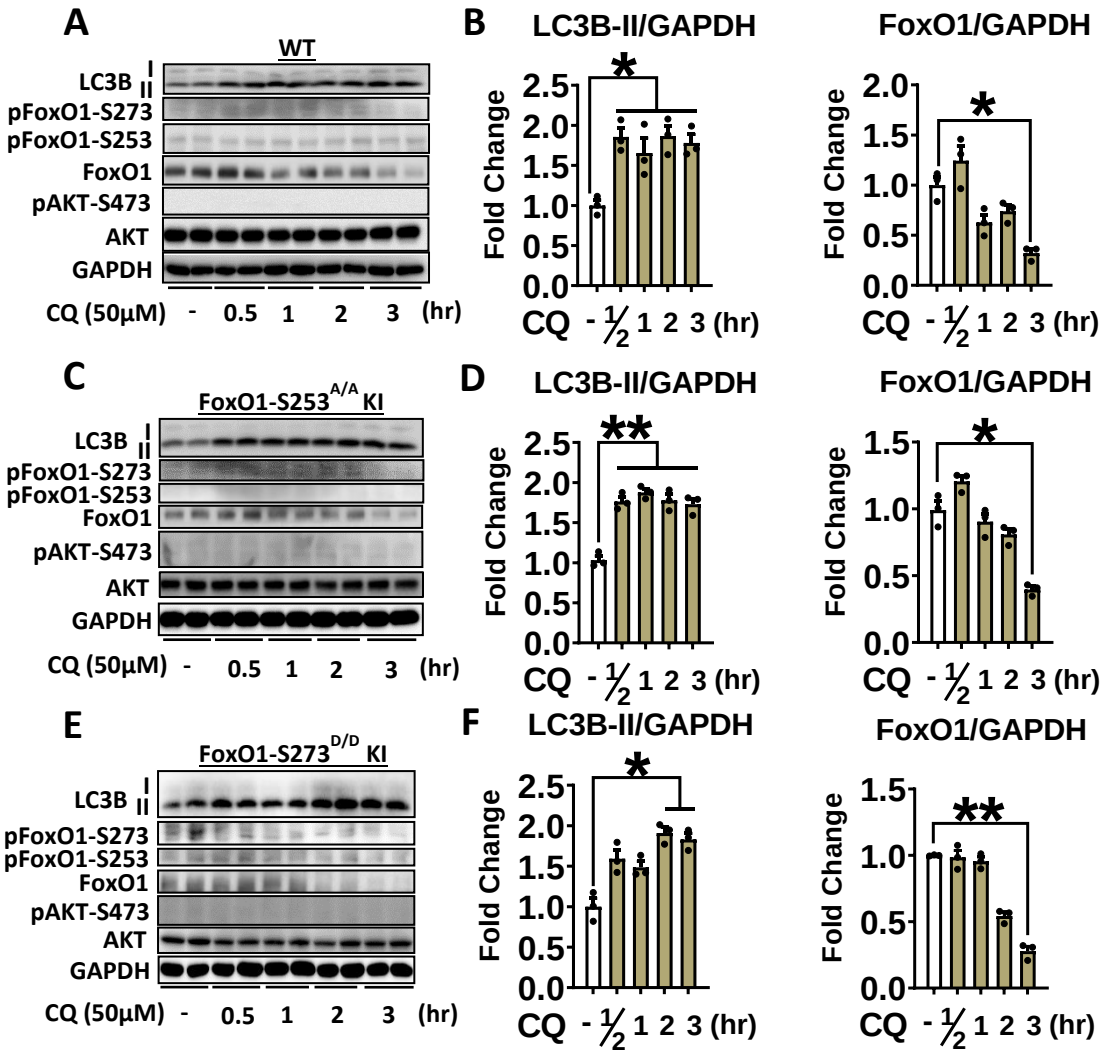

Figure 11. Reduction of FoxO1 protein induced by inhibition of autophagy persists in FoxO1-S273$^{D/D}$ KI and FoxO1-S253$^{A/A}$ KI mouse primary hepatocytes.

Primary hepatocytes isolated from WT (A), FoxO1-S253$^{A/A}$ KI (C) and FoxO1-S273$^{D/D}$ KI (E) male mouse livers were cultured in HGP buffer for 3hr. CQ (50μM) treatment time was indicated in the figures. After 3hr, proteins of hepatocytes were collected, and the target proteins were evaluated by western blotting assay. Representative protein blot images of corresponding genotype were given in panel A, C and E, respectively. Bands' intensities (from three independent repeated experiments) were quantified by ImageJ software (NIH, 1.8.0v) and given in penal B, D and F. Data was calculated as the relative fold change to the control group (i.e., the group without CQ treatment). Data was analyzed by one-way ANOVA coupled with post-test (Dunnett's T3 test) in GraphPad Prism software (Version 9.2.0) to check the statistical significance between groups, and presented as mean±SEM. *p<0.05, **p<0.01.

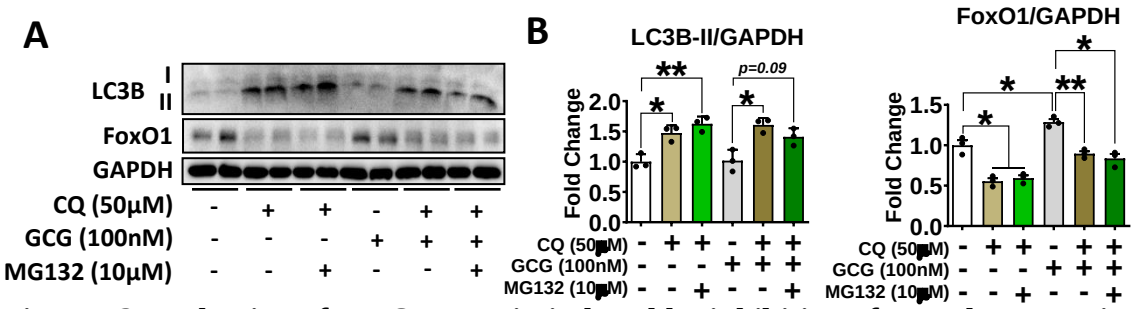

Figure 12. Reduction of FoxO1 protein induced by inhibition of autophagy persists under the treatment of MG132.

Primary hepatocytes isolated from WT male mouse liver were cultured in HGP buffer. In MG132-treated groups, MG132 (10μM) treatment was conducted 30min before CQ treatment. Proteins were collected 4hr after MG132 treatment, and target proteins were evaluated by western blot assay. Representative protein blot images were given in panel A. Bands' intensities (from three independent repeated experiments) were quantified by ImageJ software (NIH, 1.8.0v) and given in penal B. Data was calculated as the relative to the control group (i.e., the group without MG132, CQ, and GCG treatment). Data was analyzed by one-way ANOVA coupled with post-test (Dunnett's T3 test) in GraphPad Prism software (Version 9.2.0) to check the statistical significance between groups, and presented as mean±SEM. *p<0.05, **p<0.01.

Reduction of FoxO1 protein upon inhibition of autophagy is independent of regulation of FoxO1 mRNA level

It was recently reported that autophagy deficiency in the liver induced by ablation of ATG7 impaired the fatty acids and triglyceride genes expression through accumulation of nuclear receptor co-repressor 1 (NCoR1) [258, 259]. Therefore, we hypothesized that the decrease of FoxO1 may also be related to downregulation of FoxO1 gene expression through unknown mechanisms. To verify this hypothesis, we extracted the mRNA from mouse primary hepatocytes with or without inhibition of autophagy induced by either CQ or siRNA-ATG7, then evaluated the mRNA levels of target genes, including *foxo1*, *pck1* and *g6pc*. However, according to our RT-qPCR results, although the mRNA levels of *pck1* and *g6pc* were significantly reduced upon inhibition of autophagy in comparison to the control group, which was consistent with our HGP (Figure 5) and western blot results

(Figure 7), we did not observe any significant decrease of the FoxO1 mRNA level (Figure 13 A and B). Consistent with our *in vitro* results, the FoxO1 mRNA level in our WT mouse livers treated with AAV8-shR-ATG7 was similar to WT mouse livers with AAV8-shR-scramble treatment (Figure 13 C). Nevertheless, we did observe that the mRNA levels of *pck1* and *g6pc* in WT mouse livers upon autophagy deficiency were significantly reduced, although the reduction rate was not as striking as we could observe from *in vitro* study. In addition, the mRNA levels of *pck1* and *g6pc* in WT mouse livers with autophagy deficiency were similar to L-FKO mouse livers, which could be one of the reasons to explain why the capability of glucose production under the presence of glucagon or pyruvate in WT mice with autophagy deficiency was similar to L-FKO mice (Figure 6). Again, we did not observe any effect of autophagy deficiency on *pck1* and *g6pc* mRNA levels in L-FKO mouse livers, which was another piece of evidence suggesting that autophagy-mediated HGP was largely in a FoxO1-dependent manner. To conclude, our RT-qPCR data demonstrated that the reduction of FoxO1 upon the inhibition of autophagy was independent of downregulation of FoxO1 mRNA level.

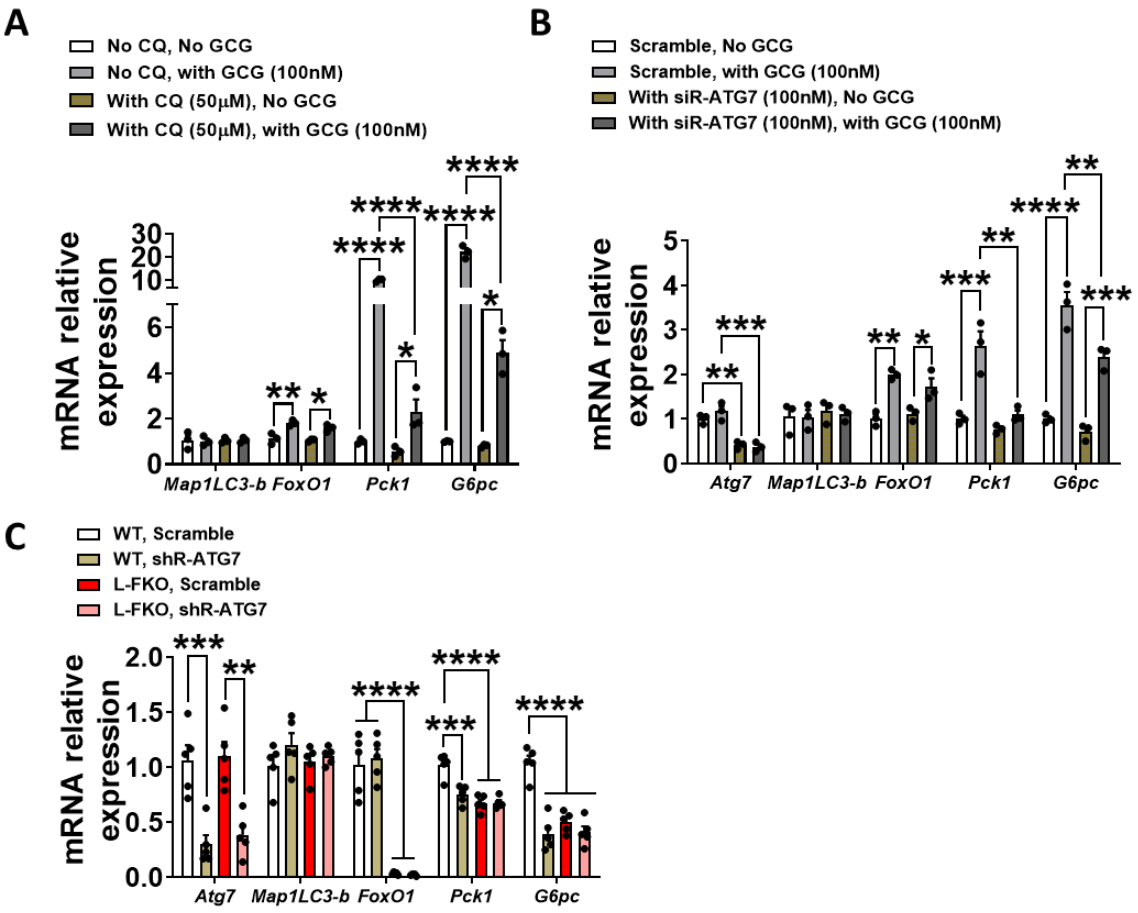

Figure 13. Reduction of FoxO1 protein induced by inhibition of autophagy is independent of regulation of FoxO1 in mRNA level.

Primary hepatocytes isolated from WT male mouse liver were cultured in HGP buffer for 3hr with or without CQ (A) or siR-ATG7 treatment (B), followed by mRNA extraction then RT-qPCR analysis. Seventeen days after AAV8-shRNA RO injection, mice (n=5 per group) were sacrificed, and the livers were collected. mRNA in WT and L-FKO mice liver tissues were extracted with TRIzol reagents and evaluated by RT-qPCR (C). Primer sequences were given in Materials and Methods. mRNA level of cyclophilin was used as the internal control. Data was calculated as the relative expression to their corresponding control groups. Data was analyzed by two-way ANOVA coupled with post-test (Tukey's test) in GraphPad Prism software (Version 9.2.0) to check the statistical significance between groups, and presented as mean±SEM. *p<0.05, **p<0.01, ***p<0.005, ****p<0.0001

Discussion

FoxO1-mediated gluconeogenic signaling is playing an essential role on the HGP particularly during starvation. Upon binding with the IRE in the promoter region of *pck1* and *g6pc*, FoxO1 significantly upregulates the gene expression of *pck1* and *g6pc*, which in turn favors the catalytic reactions involved in two rate-limiting steps of gluconeogenesis: converting oxaloacetate to phosphoenolpyruvate and converting glucose-6-phosphate into glucose molecule, thereby promoting glucose production in hepatocytes[36, 52, 233]. There are several mechanisms having been demonstrated to affect FoxO1 activity. First, phosphorylation of FoxO1 at S253 triggered by AKT signaling causes a redistribution of the FoxO1 from the nucleus, leading to FoxO1 ubiquitination and degradation in the cytoplasm, thereby preventing FoxO1 from activating its target genes[260, 261]. AKT catalyzes the phosphorylation of FoxO1 at three different sites, T24, S253 and S316. However, only S253 is the principal phosphorylation site responsible for the insulin effects on HGP[262, 263]. To figure out whether the reduction of FoxO1 upon the inhibition of autophagy was related to increase of FoxO1 phosphorylation at S253, we checked the amount of FoxO1, pFoxO1-S253 in both nucleus and cytoplasm (Figure 9 and Figure 10), then evaluated the change of FoxO1 in FoxO1-S253$^{A/A}$ KI mice upon inhibition of autophagy (Figure 11 C and D). Our results clearly showed that the phosphorylation of FoxO1 at S253 was not increased, and autophagy deficiency-induced reduction of FoxO1 level persisted even in FoxO1-S253$^{A/A}$ KI mouse primary hepatocytes in which FoxO1 was more stable than WT due to prevention of FoxO1-S253 phosphorylation. Consistently, we did not observe any upregulation of pAKT-S473

phosphorylation upon inhibition of autophagy. All the above evidence suggested that the reduction of FoxO1 upon inhibition of autophagy was independent of promotion of FoxO1-S253 phosphorylation.

Second, phosphorylation of FoxO1 at S273 triggered by PKA signaling stabilizes FoxO1 in the nucleus, preventing FoxO1 from ubiquitination and degradation in the cytoplasm[35, 41]. In fact, phosphorylation of FoxO1 at S273 could be a potential mechanism for insulin resistance at the FoxO1 level[35]. In order to investigate whether the FoxO1-S273 phosphorylation induced by glucagon was impaired upon inhibition of autophagy, we checked the pFoxO1-S273 amount in both nucleus and cytoplasm (Figure 7 and Figure 9), and evaluated the change of FoxO1 in FoxO1-S273$^{D/D}$ KI mice upon inhibition of autophagy (Figure 10, Figure 11 E and F). Our data suggested that FoxO1-S273 phosphorylation induced by glucagon was barely affected by autophagy deficiency, and autophagy deficiency-induced reduction of FoxO1 level persisted even in FoxO1-S273$^{D/D}$ KI mouse primary hepatocytes in which FoxO1 was supposed to be more stable than WT due to mimicking of FoxO1-S273 phosphorylation, indicating that the reduction of FoxO1 upon inhibition of autophagy was independent of the impairment of FoxO1-S273 phosphorylation.

Third, the ubiquitination and degradation of FoxO1 potentially cause the reduction of total FoxO1 protein level. Although FoxO1-S253 phosphorylation was not promoted based on our results, we wanted to further rule out the possibility that ubiquitination and degradation of FoxO1 was contributing to the reduction of FoxO1 level upon inhibition of autophagy. It has been reported that one of the autophagy target substrates, CRY1 could

interact with FoxO1, then promote FoxO1 ubiquitination and degradation. Therefore, the inhibition of autophagy can potentially improve the stability of CRY1, leading to reduction of FoxO1[185, 186]. However, our data showed that reduction of FoxO1 persisted even under the treatment of proteasome inhibitor MG132 (Figure 12 A and B), suggesting that there was an alternative mechanism causing reduction of FoxO1 level upon inhibition of autophagy in our case.

Fourth, regulation of FoxO1 gene expression affects FoxO1 protein level. For instance, it has been reported that in the patients with nonalcoholic fatty liver disease (NAFLD), high hepatic oxidative stress significantly upregulated the gene expression of FoxO1, leading to dysregulation of hepatic glucose output and insulin resistance[264, 265]. Therefore, we wanted to figure out whether downregulation of FoxO1 transcription was involved in the reduction of FoxO1 level induced by autophagy deficiency. Based on our RT-qPCR results, the mRNA levels of *pck1* and *g6pc* were significantly reduced upon inhibition of autophagy, which could be a consequence of the reduction of FoxO1 protein (Figure 13). However, the mRNA level of FoxO1 was not affected by autophagy deficiency, suggesting that the reduction of FoxO1 protein level upon inhibition of autophagy was unlikely due to the suppression of gene transcription of FoxO1.

In conclusion, in the present chapter, we investigated several potential mechanisms which could possibly participate in the reduction of FoxO1 protein amount upon inhibition of autophagy. Our results clearly indicated that FoxO1 phosphorylation, FoxO1 degradation and downregulation of FoxO1 gene transcription were not the major mechanisms explaining the decrease of FoxO1 level induced by autophagy deficiency.

CHAPTER IV

THE ALTERATION OF CELLULAR AMINO ACID POOLS INDUCED BY INHIBITION OF AUTOPHAGY AFFECTS FOXO1 PROTEIN AMOUNT AND ACTIVITIES

Introduction

In general, there are two typical physiological significances of autophagy under starvation conditions. First, autophagy is one of the important mechanisms supporting the protein turnover. For instance, it has been demonstrated that autophagy accounts for about one-third of mitochondrial protein turnover in the study of autophagy-deficient ATG7 mutant fruit fly and ATG7-/ATG5-deficient human fibroblasts[266]. Consistently, Komatsu et al. discovered that the reduction of protein and organelles induced by starvation was largely impaired in ATG7-deficent mouse liver[267], suggesting an indispensable role of autophagy in protein turnover during fasting. Second, autophagy is an essential mechanism in the maintenance of cellular amino acid pools during starvation. It is well-recognized that in the end stage of autophagy, amino acids derived from lysosomal degradation are released from the lysosome to the cytoplasm. These autophagy-derived amino acids will participate in new protein synthesis and/or energy metabolism afterwards[168, 268]. On top of that, Onodera and Ohsumi reported that during nitrogen starvation, the contents of cellular free amino acid, total protein synthesis and the synthesis of certain proteins which were supposed to be highly expressed upon starvation were significantly suppressed in ATG7-deficnent yeast in comparison to wild type groups[269]. Later, Chen et al. proposed a detailed mechanism of the general amino acid control

(GAAC) under starvation in which autophagy is involved[166]. In brief, under starvation (i.e., serum and glutamine starvation in the study of Chen et al.), the activity of mTOR is suppressed, which in turn leads to autophagy activation. Concurrently, a typical transcriptional factor, activating transcription factor 4 (ATF4) is in an active state, subsequently promoting the gene expression of LAT1/SLC7A5 which is a large neutral amino acid transporter (AAT) responsible for uptake of essential amino acids such as leucine, isoleucine, valine, phenylalanine, tyrosine, tryptophan, methionine, and histidine[166, 270, 271]. In cancer cell lines, inhibition of autophagy has shown a significant upregulation of ATF4-AAT axis, which is believed to compensate the shortage of cellular amino acid content due to inhibition of autophagy in cancer cells[272]. However, there is still limited evidence to show the association between the autophagy-mediated amino acid pools and FoxO1-mediated HGP under starvation.

Since our data in the previous chapter showed that reduction of FoxO1 induced by the inhibition of autophagy was unlikely due to FoxO1 phosphorylation, FoxO1 degradation and FoxO1 transcription, we decided to evaluate the amino acid pools under inhibition of autophagy *in vitro* and *in vivo*, and tried to find a potential relationship between autophagy-mediated amino acid pools and FoxO1 protein level, thereby explaining the role of autophagy in the regulation of HGP under starvation. Our data demonstrated that the inhibition of autophagy significantly altered the cellular amino acid pools in primary hepatocytes and in the liver. Addition of amino acids which were found to be significantly reduced upon inhibition of autophagy, remarkably restored the FoxO1 protein amount as well as the capability of HGP even under autophagy deficiency. On top

of that, the addition of protein synthesis inhibitor CHX significantly suppressed the amino acids supplementation-induced restoration of FoxO1 protein and HGP. In addition, we evaluated mRNA level of genes related to lipogenesis, fatty acid oxidation and redox regulation with or without inhibition of autophagy in WT and L-FKO mouse primary hepatocytes, and found that the autophagy-mediated FoxO1 activities could probably be extended to several other essential metabolic activities beyond glucose homeostasis. Our results highlight the importance of autophagy-FoxO1 axis in the maintenance of cellular homeostasis during fasting.

Materials and methods

Ethics statement

Animal protocols were approved by the Institutional Animal Care and Use Committee (IACUC) at Texas A&M University. All mice were kept in the laboratory animal resources and research facility (LARR), and housed in standard cages under 12hr-light/12hr-dark cycle with access to food and drinking water ad libitum as previously described[41, 44, 206]. Necessary procedures (e.g., performing euthanasia by means of isoflurane vaporizer) were conducted to minimize the discomfort, distress, and pain of the mice during the experiments.

Animal treatment and tissue collection

HCQ and AAV8-shRNA-ATG7 were used to inhibit autophagy in WT and L-FKO mice. For HCQ treatment, HCQ solution (60mg/kg BW) was administered via IP injection to 8- to 12-week-old male mice (5-6 mice each group) after overnight (16hr) fasting. The control group received the same volume of normal saline. Mice were sacrificed 4 hours after the HCQ injection for tissue collection. For AAV8-shRNA-ATG7 treatment, AAV8-shRNA-ATG7 (10^{11} genome copies/mouse) was administered via RO injection to 8- to 12-week-old male mice (5-6 mice each group). The control group received the same amount of AAV8-shRNA-scramble. Mice were sacrificed 17days after the AAV8 injection for tissue collection.

Isolation of mouse primary hepatocytes and treatment

Mouse primary hepatocytes were isolated from 8- to 12-week-old male mice liver and cultured in DMEM (containing 5.5mM glucose) supplemented with 2% fetal bovine

serum (FBS) as previously described[41, 44, 208]. When hepatocytes firmly attached on the bottom of a collage-coated culture plate, DMEM was replaced by HGP buffer, proceeding to another 3 hours starvation prior to protein collection or RNA extraction. For CQ treatment, CQ solution (final concentration=50μM) was added in the corresponding treatment groups concurrently with replacement of DMEM by the HGP buffer. Glucagon solution (final concentration=100nM) would be added in the corresponding treatment groups 30 min after the CQ treatment. For amino acid treatment, different concentrations (0μM, 40μM, 80μM, 160μM and 320μM) of mixed solution of amino acids, including alanine, leucine, valine, glycine, glutamine, isoleucine, glutamate, and phenylalanine were freshly prepared before the experiment, then added to corresponding wells concurrently with glucagon treatment. In siR-ATG7-treated groups, a transfection culture medium was replaced by HGP buffer right after the siR-ATG7 (100nM) transfection. Glucagon solution was added in the corresponding treatment groups at the same time. After 3 hours incubation, hepatocytes were lysed by the RIPA lysis buffer (supplemented with protease and phosphatase inhibitor cocktail and sodium orthovanadate) or TRIzol reagent for protein collection or RNA extraction.

Determination of protein concentration

For *in vitro* study, primary hepatocytes were lysed by the RIPA lysis buffer (MilliporeSigma) containing protease and phosphatase inhibitor cocktail (MilliporeSigma) and sodium orthovanadate (MilliporeSigma). For *in vivo* study, liver tissue fragments (about 50 mg) were lysed by RIPA lysis buffer containing protease and phosphatase inhibitor cocktail and sodium orthovanadate, then proceeded to

homogenization using IKA T8 homogenizer (12-18V DC, 100W). Cell or tissue lysates were then centrifuged at 14000rpm, 4°C for 15min, and the supernatant was collected. Protein concentration was determined by using Pierce™ BCA Protein Assay Kit (ThermoFisher) following the manufacturer's instruction.

Preparation of samples for amino acid determination by HPLC

To prepare samples from primary hepatocytes, $HClO_4$ (1.5 M, 0.5 ml) (Cat# BDH4550, VWR) was added in each well, followed by a transfer of lysate to 15ml-contrifuge tube. K_2CO_3 (2.0 M, 250µl) was then added to the tube, following by addition of HPLC-grade H_2O (2.25 ml) (Cat# JT4218, VWR). The mixture was centrifuged at 600g for 10min, and the supernatant was collected. To prepare samples from the liver tissues, 100mg of the liver tissue fragments was weighed and placed in homogenizer. Tissue samples were homogenized with 1 ml of 1.5 M $HClO_4$. Homogenates was transferred to a 15ml-centrifuge tube. Then HPLC-grade H_2O (1 ml) was used to rinse the homogenizer and transferred into above tube. K_2CO_3 (2.0 M, 500 µl) was then added into the tube. This mixture was centrifuged at 2000 rpm for 5 min and the supernatant was collected. Amino acids were measured using HPLC (Waters, Milford, MA, USA) as previously described[273].

Protein immunoblotting

Western blotting was conducted as previously described[41, 44, 208]. In brief, protein samples were first normalized with Alfa Aesar™ laemmli SDS sample buffer (reducing, 6X) (Fisher Scientific) based on the concentration of protein samples, and denatured under 95.5°C for 10 min. Protein samples (25-40µg) were then resolved in a polyacrylamide gel (7.5-15%) by using Mini-PROTEAN® Tetra Vertical Electrophoresis Cell (Bio-Rad), and

electro-blotted onto the Amersham Hybond western blotting membranes, (0.45μm PVDF) (VWR) by using Trans-Blot Turbo Transfer System (Bio-Rad). Membranes were incubated with primary antibodies (Table 2) in 5% BSA solution (5% w/v in TBST) overnight at 4°C, followed by incubation with secondary antibodies (anti-rabbit IgG, HRP-linked, Cell Signaling Technology) in 5% BSA solution on the second day. Clarity Western ECL Substrate (Bio-Rad) was used to react with HRP-linked secondary antibody to generate light signal which was captured by ChemiDoc™ Imaging System (Bio-Rad). The band intensity was quantified by the ImageJ software (NIH, 1.8.0v) and expressed as a ratio to GAPDH (internal control).

Real-time reverse transcription quantitative polymerase chain reaction (RT-qPCR)

RNA templates (1000ng) extracted by TRIzol reagent were reverse transcribed to their corresponding complementary DNAs (cDNA) with iScript™ Reverse Transcription Supermix (Bio-Rad) following the manufacturer's instruction. cDNA was mixed with primers (Table 3) and SsoAdvanced Universal SYBR® Green Supermix (Bio-Rad), then proceeded to real-time PCR in CFX384 Touch™ Real-Time PCR Detection System (Bio-Rad) following the manufacturer's instruction. Cyclophilin was used as an internal control. RT-qPCR assay was conducted in duplicate or triplicate for each biological replicate. Relative gene expression level was calculated by using 2(-Delta Delta C(T)) method[248].

Statistical analysis

Data was presented as mean ± standard error of the mean (SEM), unless otherwise stated. Student t-test (with Welch's correction) was used to compare the means of two treatment groups. One-way ANOVA (with Dunnett's T3 test) was used to compare the means of more than two treatment groups if there is one independent variables (e.g., AAs dose-response study) among the groups. Two-way ANOVA (coupled with post-test, Tukey's test) was used to compare the means of more than two treatment groups if there are two independent variables (e.g., treatments) among the groups. $p<0.05$ was considered as statistically significant. *denotes $p<0.05$; **denotes $p<0.01$; ***denotes $p<0.005$; ****denotes $p<0.0001$. Statistical analysis was performed in GraphPad Prism software (Version 9.2.0).

Results

Inhibition of autophagy significantly alters hepatic amino acid pools

Since the reduction of FoxO1 under inhibition of autophagy is independent of FoxO1 phosphorylation, FoxO1 ubiquitination and degradation, and regulation of FoxO1 mRNA level, we proceeded to hypothesize that the reduction of FoxO1 could potentially be associated with the restriction of protein synthesis caused by inhibition of autophagy. The activity of autophagy has been reported to be tightly related to the regulation of cellular amino acid pools particularly under starvation conditions[268, 269], and amino acids are the building blocks for protein synthesis, which could be really limited during fasting. We evaluated the cellular amino acid pools with or without inhibition of autophagy in mouse primary hepatocytes. According to the HPLC results, we found that the cellular contents of amino acid in mouse primary hepatocytes were substantially altered upon inhibition of autophagy, in comparison to the group without CQ or siR-ATG7 treatment. Notably, not the entire amino acid profile was significantly altered by autophagy deficiency. In CQ-treated mouse primary hepatocytes, the cellular concentrations of alanine, aspartate, glutamate, glutamine, glycine, histidine, isoleucine, leucine, lysine, methionine, phenylalanine, serine, tryptophan, tyrosine, and valine decreased significantly, while the concentrations of arginine, asparagine, taurine, and threonine stayed broadly the same compared to the control groups (Table 6 and Figure 14 A). Similarly, comparing with primary hepatocytes without siRNA-ATG7 transfection, in primary hepatocytes transfected with siRNA-ATG7, the concentration of alanine, asparagine, glutamate, glutamine, glycine, histidine, isoleucine, leucine, ornithine, phenylalanine, threonine,

tryptophan, tyrosine, and valine was remarkably reduced, while the rest of the amino acids was not significantly affected (Table 6 and Figure 14 B). In addition, we found that the concentration of amino acids, for example, alanine, showed a significant reduction in glucagon-treated group. It is probably because of the glucagon-induced gluconeogenesis in which alanine were one of the main substrates.

Addition of amino acids successfully restores FoxO1 protein amount and HGP

Next, we wanted to verify the association between the cellular amino acid pools, FoxO1 protein levels, and the HGP, which we believe could be a potential mechanism to explain the phenotypes that we observed in Chapter II. First, we selected the amino acids which showed a significant reduction in concentration under autophagy deficiency. They were alanine (ALA), leucine (LEU), valine (VAL), glycine (GLY), glutamine (GLN), isoleucine (ILE), glutamate (GLU) and phenylalanine (PHE). Then we took the range of concentrations for these amino acids in cell culture medium (CCM) as a reference (Table 5)[274, 275], to prepare a gradient of concentrations for our amino acids (AAs) mixture (i.e., 0μM, 40μM, 80μM, 160μM, 320μM). We used these AAs mixtures to treat the freshly isolated mouse primary hepatocytes which were cultured in HGP buffer with or without CQ and glucagon co-treatment for 3 hours, followed by HGP determination and protein collection.

Table 5. Selected amino acid content in cell culture media (CCM).

Amino acids	Minimum concentration in CCM (μM) [274, 275]	Maximum concentration in CCM (μM) [274, 275]	Concentration in DMEM (Sigma, Cat#D6046) (μM)
Alanine (ALA)	101.021	3569.424	-
Leucine (LEU)	381.185	4269.269	800.488
Valine (VAL)	170.720	3755.836	802.383
Glycine (GLY)	106.567	4395.897	399.627
Glutamine (GLN)	-	-	3996.168
Isoleucine (ILE)	381.185	3484.028	800.488
Glutamate (GLU)	74.764	4363.488	-
Phenylalanine (PHE)	90.805	1894.788	399.540

As we expected, our HGP assay results showed that the addition of AAs mixture successfully restored the capability of glucose production in mouse primary hepatocytes under inhibition of autophagy (Figure 15 A). Consistently, our western blotting results showed that the FoxO1 protein levels were also gradually restored upon the addition of different concentration of AAs mixture (Figure 15 B and C). These results indicated that by supplementing the amino acids which were significantly reduced under the inhibition of autophagy, FoxO1-mediated HGP could be recovered. On top of that, we wanted to verify that the restoration of FoxO1 and HGP triggered by amino acid supplementation was mainly due to restoration of FoxO1 protein synthesis. We used protein synthesis inhibitor cycloheximide (CHX), which is able to block the elongation phase of eukaryotic translation[276-278], to treat the primary hepatocytes, along with the addition of amino acid

mixture under the inhibition of autophagy. The results showed that the amino acid supplementation-induced restoration of HGP capability were largely abolished by CHX (Figure 16 A). Consistently, the restoration of the FoxO1 protein level induced by amino acid supplementation was significantly reduced under CHX treatment (Figure 16B and C). This piece of evidence indicated that alteration of amino acid pools caused by autophagy deficiency could significantly inhibit the protein synthesis of FoxO1, which in turn impair the capability of HGP during starvation.

Table 6. Cellular amino acid pools in WT mouse primary hepatocytes with or without the treatment of CQ and/or glucagon.

μmol/ g of protein	No CQ		With CQ (50μM)	
	No GCG	With GCG (100nM)	No GCG	With GCG (100nM)
ALA	21.49±3.10	13.73±1.12*[a]	13.72±3.29*[a]	7.03±0.93*[b]
ARG	0.53±0.25	0.51±0.06	0.97±0.25	0.66±0.26
ASN	0.33±0.03	0.19±0.03	0.36±0.05	0.32±0.14
ASP	0.70±0.17	0.58±0.04	0.55±0.11	0.18±0.05**[b]
beta-ALA	0.28±0.13	0.21±0.02	0.28±0.02	0.20±0.07
CIT	0.10±0.02	0.06±0.01	0.13±0.03	0.06±0.01
GLU	4.17±0.36	2.56±0.26**[a]	2.41±0.49**[a]	1.35±0.24*[b]
GLN	3.90±0.44	2.87±0.40*[a]	1.11±0.18****[a]	0.96±0.39***[b]
GLY	4.16±0.76	3.91±0.72	3.06±0.34	1.99±0.35**[b]
HIS	1.09±0.15	1.09±0.28	0.34±0.05**[a]	0.19±0.01***[b]
ILE	3.64±0.45	3.04±0.34	0.82±0.19****[a]	0.46±0.08****[b]
LEU	5.29±0.82	4.57±0.44	2.63±0.89**[a]	1.71±0.21**[b]
LYS	2.26±0.11	1.79±0.13	1.41±0.33**[a]	0.94±0.25**[b]
MET	0.39±0.04	0.33±0.03	0.05±0.01****[a]	0.04±0.02****[b]
ORN	3.35±0.28	2.35±0.47	2.47±0.71	1.37±0.31
PHE	2.15±0.30	1.77±0.20	0.39±0.10****[a]	0.22±0.01****[b]
SER	0.90±0.11	0.58±0.06	0.58±0.13	0.67±0.31
TAU	0.74±0.12	0.62±0.06	0.95±0.2	0.73±0.28
THR	0.45±0.05	0.26±0.03	0.35±0.09	0.28±0.10
TRP	0.82±0.12	0.70±0.09	0.19±0.04****[a]	0.13±0.02***[b]
TYR	1.54±0.07	1.36±0.20	0.74±0.24**[a]	0.65±0.02**[b]
VAL	5.89±0.76	4.62±0.30*[a]	2.18±0.51****[a]	1.63±0.15***[b]

Note: ALA, Alanine; ARG, Arginine; ASN, Asparagine; ASP, Aspartate; beta-ALA, beta-alanine; CIT, Citrulline; GLU, Glutamate; GLN, Glutamine; GLY, Glycine; HIS, Histidine; ILE, Isoleucine; LEU, Leucine; LYS, Lysine; MET, Methionine; ORN, Ornithine; PHE, Phenylalanine; SER, Serine; TAU, Taurine; THR, Threonine; TRP, Tryptophan; TYR, Tyrosine; VAL, Valine; CQ, Chloroquine; GCG, Glucagon;
Data was analyzed by two-way ANOVA coupled with post-test (Tukey's test) in GraphPad Prism software (Version 9.2.0) to check the statistical significance between groups, and presented as mean±SD.

[a] *p<0.05, **p<0.01, ***p<0.005, ****p<0.0001 vs. group without CQ, without GCG.

[b] *p<0.05, **p<0.01, ***p<0.005, ****p<0.0001 vs. group without CQ, with GCG.

Table 7. Cellular amino acid pools WT mouse primary hepatocytes with or without the treatment of siR-ATG7 and/or glucagon.

μmol/ g of protein	Scramble		With siR-ATG7 (100nM)	
	No GCG	With GCG (100nM)	No GCG	With GCG (100nM)
ALA	28.45±2.08	19.69±2.35**[a]	12.20±0.25****[a]	11.59±2.80**[b]
ARG	0.58±0.05	0.40±0.08	0.56±0.08	0.52±0.13
ASN	0.81±0.07	0.56±0.08*[a]	0.52±0.06*[a]	0.47±0.12
ASP	0.51±0.04	0.43±0.09	0.41±0.06	0.44±0.11
beta-ALA	0.39±0.03	0.28±0.08	0.26±0.02*[a]	0.46±0.02*[b]
CIT	0.13±0.04	0.07±0.02	0.10±0.03	0.08±0.02
GLU	3.10±0.20	2.25±0.31*[a]	2.01±0.19**[a]	1.86±0.42
GLN	4.83±0.43	3.94±0.40*[a]	1.02±0.06****[a]	0.96±0.21****[b]
GLY	6.75±0.54	4.94±0.51*[a]	4.00±0.13**[a]	4.43±0.88
HIS	1.78±0.20	1.66±0.17	0.39±0.09****[a]	0.35±0.05****[b]
ILE	4.69±0.41	4.26±0.48	0.66±0.10****[a]	0.61±0.24****[b]
LEU	9.71±0.89	8.50±0.80	4.47±0.07***[a]	5.51±1.25*[b]
LYS	2.46±0.35	2.51±0.21	2.24±0.14	2.37±0.59
MET	0.72±0.04	0.73±0.24	0.54±0.13	0.61±0.19
ORN	3.38±0.14	2.51±0.32	2.33±0.06	3.69±2.78
PHE	2.82±0.18	2.48±0.28	0.40±0.03****[a]	0.38±0.07****[b]
SER	1.21±0.34	0.87±0.24	0.70±0.08	0.62±0.14
TAU	0.60±0.05	0.53±0.07	0.67±0.05	0.72±0.20
THR	0.86±0.41	0.49±0.10	0.30±0.02*[a]	0.29±0.05
TRP	1.79±0.18	1.59±0.12	1.01±0.17**[a]	1.11±0.24
TYR	2.01±0.17	1.96±0.18	0.78±0.09****[a]	0.82±0.09****[b]
VAL	8.53±0.53	7.74±0.65	3.58±0.10****[a]	4.08±0.87***[b]

Note: ALA, Alanine; ARG, Arginine; ASN, Asparagine; ASP, Aspartate; beta-ALA, beta-alanine; CIT, Citrulline; GLU, Glutamate; GLN, Glutamine; GLY, Glycine; HIS, Histidine; ILE, Isoleucine; LEU, Leucine; LYS, Lysine; MET, Methionine; ORN, Ornithine; PHE, Phenylalanine; SER, Serine; TAU, Taurine; THR, Threonine; TRP, Tryptophan; TYR, Tyrosine; VAL, Valine; Scramble, siRNA-scramble; siR-ATG7, siRNA-ATG7; GCG, Glucagon

Data was analyzed by two-way ANOVA coupled with post-test (Tukey's test) in GraphPad Prism software (Version 9.2.0) to check the statistical significance between groups, and presented as mean±SD.

[a] *p<0.05, **p<0.01, ***p<0.005, ****p<0.0001 vs. group with scramble, without GCG.

[b] *p<0.05, **p<0.01, ***p<0.005, ****p<0.0001 vs. group with scramble and with GCG.

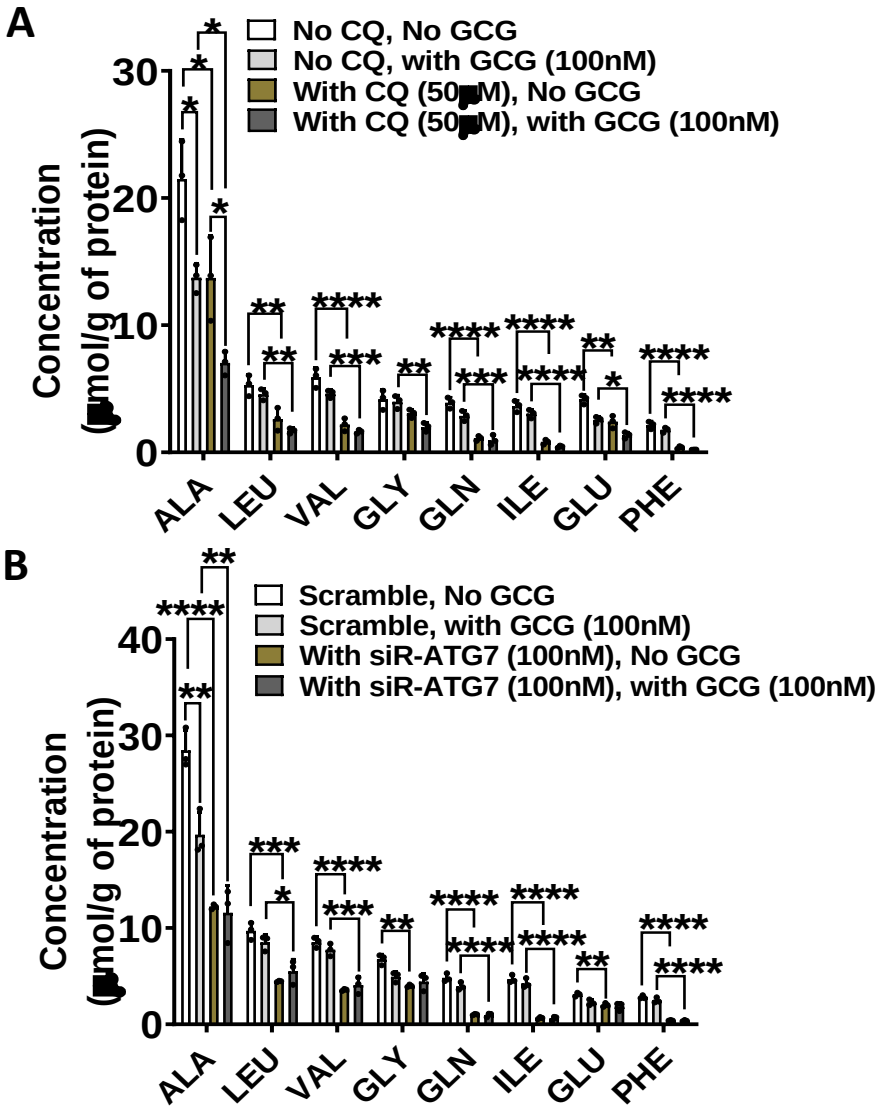

Figure 14. Amino acid pools in mouse primary hepatocytes are significantly altered under inhibition of autophagy .

Primary hepatocytes (n=3 per group) isolated from WT male mouse liver were cultured in HGP buffer for 3hr with or without treatment of CQ (A) or siR-ATG7 (B). Preparation of hepatocyte lysates for amino acid determination by HPLC method was described in the Materials and method. Alanine (ALA), leucine (LEU), valine (VAL), glycine (GLY), glutamine (GLN), isoleucine (ILE), glutamate (GLU) and phenylalanine (PHE) were the top eight amino acids affected by inhibition of autophagy. Full amino acids profiles were given in Table 6 and 7. Data was analyzed by two-way ANOVA coupled with post-test (Tukey's test) to check the statistical significance between groups, and presented as mean±SD. *p<0.05, **p<0.01, ***p<0.005, ****p<0.0001.

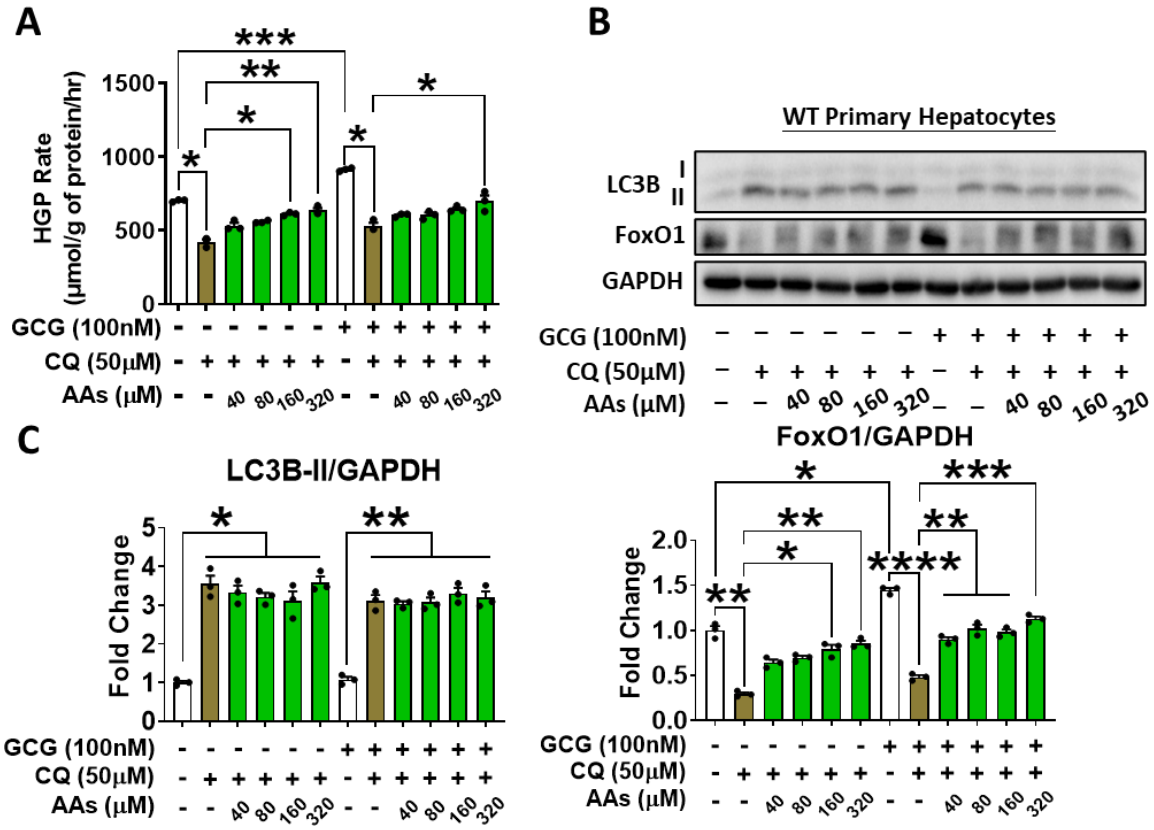

Figure 15. Addition of amino acids restores FoxO1 protein amount and HGP.
Primary hepatocytes isolated from WT male mouse liver were cultured in HGP buffer with or without CQ (50μM) treatment and GCG (100nM) treatment. In amino acids (AAs)-treated groups, a mixture of eight amino acids solution, including alanine (ALA), leucine (LEU), valine (VAL), glycine (GLY), glutamine (GLN), isoleucine (ILE), glutamate (GLU) and phenylalanine (PHE) was added in HGP buffer in the beginning of the 3h incubation. The concentration gradients of each amino acids were indicated in the figure. HGP per hour of each treatment group was measured after 3hr-incubation (A). Protein amounts were evaluated by western blotting assay. Representative protein blot images were given in panel B. Bands' intensities (from three independent repeated experiments) were quantified by ImageJ software (NIH, 1.8.0v) and given in penal C. Data was calculated as the relative to the control group (i.e., the group without CQ, GCG, and AAs treatment). Data was analyzed by one-way ANOVA coupled with post-test (Dunnett's T3 test) in GraphPad Prism software (Version 9.2.0) to check the statistical significance between groups, and presented as mean±SEM. *p<0.05, **p<0.01, ***p<0.005, ****p<0.0001

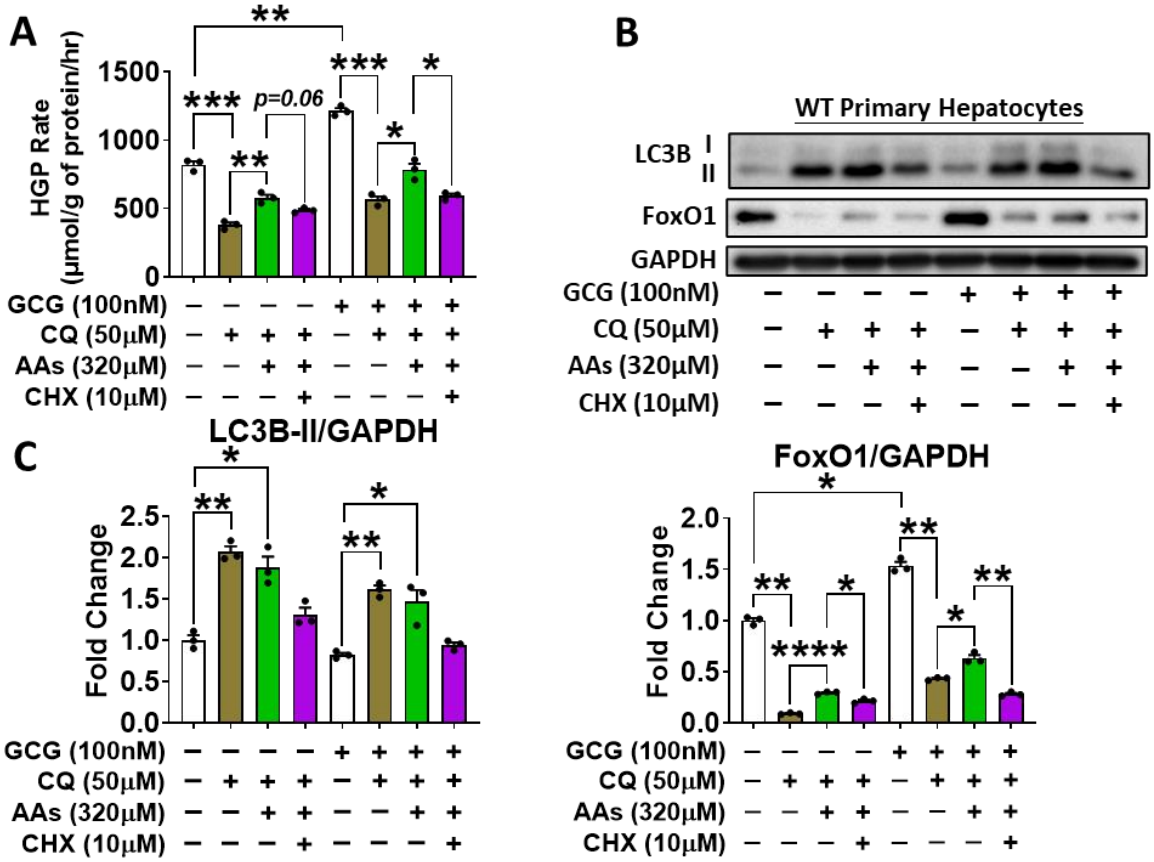

Figure 16. Addition of protein synthesis inhibitor decreases the AAs supplementation-induced restoration of FoxO1 protein amount and HGP.
Primary hepatocytes isolated from WT male mouse liver were cultured in HGP buffer with or without CQ (50μM) treatment and GCG (100nM) treatment. In amino acids (Aas)-treated groups, a mixture of eight amino acids solution (320μM per AA), including alanine (ALA), leucine (LEU), valine (VAL), glycine (GLY), glutamine (GLN), isoleucine (ILE), glutamate (GLU) and phenylalanine (PHE) was added in HGP buffer in the beginning of 3h-incubation. In CHX-treated groups, cycloheximide (CHX, 10μM, dissolved in DMSO) was added in HGP buffer along with Aas mixture. HGP per hour of each treatment group was measured after 3hr-incubation (A). Protein amounts were evaluated by western blotting assay. Representative protein blot images were given in panel B. Bands' intensities (from three independent repeated experiments) were quantified by ImageJ software (NIH, 1.8.0v) and given in penal C. Data was calculated as the relative to the control group (i.e., the group without CQ, GCG, and Aas treatment). Data was analyzed by one-way ANOVA coupled with post-test (Dunnett's T3 test) in GraphPad Prism software (Version 9.2.0) to check the statistical significance between groups, and presented as mean±SEM. *p<0.05, **p<0.01, ***p<0.005, ****p<0.0001.

Autophagy deficiency in the liver alters hepatic amino acid pools, and potentially promotes ATF4-LAT1 pathway

On the other hand, our *in vivo* liver amino acid profiles showed that the autophagy deficiency induced by AAV8-shRNA-ATG7 altered the amino acid pools in the liver, although the alteration was relatively mild in comparison to our *in vitro* results. Particularly, the concentrations of alanine, citrulline, glutamine, glycine, isoleucine, leucine, and valine showed significant reduction in the WT mouse livers under the treatment of AAV8-shRNA-ATG7, compared to WT mouse livers with AAV8-shRNA-scramble treatment. Notably, in L-FKO mouse livers, we could barely observe an effect of autophagy deficiency on amino acid pools, and the amino acids profiles were similar to WT mouse livers without autophagy deficiency (Table 8 and Figure 17 A). This is probably because the FoxO1 protein synthesis and gluconeogenesis are so low in L-FKO mouse livers that the demand of autophagy-derived amino acids is insignificant.

Considering that the general amino acid control (GAAC) under starvation requires the activation of transcription factor ATF4 (encoded by gene *Atf4*), which in turn upregulates the expression of amino acids transporter including LAT1 (encoded by gene *Slc7a5*)[166, 279, 280], we wanted to know if we could observe an activation of ATF4-LAT1 pathway in our WT and L-FKO mouse livers with autophagy deficiency. Indeed, the mRNA and protein levels of ATF4 and LAT1 were significantly increased in WT mouse livers upon autophagy deficiency (Figure 17 B-D). Interestingly, in L-FKO mouse livers, the expression of ATF4 and LAT1 didn't change after AAV8-shRNA-ATG7 treatment, and was similar to WT mouse livers treated with AAV8-shRNA-ATG7 (Figure 17 B-D).

Table 8. The amino acid pools of WT and L-FKO mouse livers with or without the treatment of AAV8-shR-ATG7.

μmol/ g of protein	WT		L-FKO	
	Scramble	shR-ATG7	Scramble	shR-ATG7
ALA	5.09±0.23	4.19±0.38**[a]	4.45±0.87	5.35±0.76
ARG	0.24±0.08	0.31±0.11	0.27±0.09	0.45±0.23
ASN	0.55±0.12	0.58±0.06	0.59±0.14	0.63±0.15
ASP	0.44±0.10	0.43±0.02	0.58±0.18	0.56±0.13
beta-ALA	0.23±0.02	0.24±0.04	0.31±0.04	0.26±0.05
CIT	0.02±0.01	0.03±0.01	0.03±0.01	0.02±0.01
GLU	1.80±0.19	1.43±0.44	1.85±0.45	1.71±0.45
GLN	5.40±0.46	3.65±0.25***[a]	4.37±0.56	5.35±0.52*[b]
GLY	4.31±0.34	3.61±0.12**[a]	3.98±0.48	3.90±0.35
HIS	0.55±0.10	0.52±0.08	0.58±0.10	0.57±0.09
ILE	0.36±0.01	0.32±0.03*[a]	0.37±0.06	0.41±0.06
LEU	0.94±0.06	0.80±0.05**[a]	0.89±0.12	0.92±0.13
LYS	0.98±0.12	1.08±0.08	1.06±0.18	1.16±0.11
MET	0.54±0.05	0.55±0.06	0.54±0.04	0.52±0.05
ORN	0.50±0.08	0.54±0.06	0.55±0.12	0.54±0.27
PHE	0.35±0.06	0.35±0.04	0.34±0.04	0.35±0.07
SER	0.89±0.19	0.86±0.11	0.95±0.19	0.85±0.19
TAU	18.22±4.64	18.14±4.00	18.56±2.36	16.95±2.64
THR	0.60±0.11	0.57±0.03	0.69±0.15	0.67±0.12
TRP	0.12±0.01	0.15±0.01*[a]	0.13±0.01	0.14±0.02
TYR	0.40±0.05	0.42±0.05	0.44±0.07	0.47±0.09
VAL	0.62±0.02	0.55±0.07	0.67±0.11	0.71±0.11

Note: ALA, Alanine; ARG, Arginine; ASN, Asparagine; ASP, Aspartate; beta-ALA, beta-alanine; CIT, Citrulline; GLU, Glutamate; GLN, Glutamine; GLY, Glycine; HIS, Histidine; ILE, Isoleucine; LEU, Leucine; LYS, Lysine; MET, Methionine; ORN, Ornithine; PHE, Phenylalanine; SER, Serine; TAU, Taurine; THR, Threonine; TRP, Tryptophan; TYR, Tyrosine; VAL, Valine; siR-ATG7, Scramble, AAV8-shRNA-scramble; shR-ATG7, AAV8-shRNA-ATG7 (10^{11} genome copies/mouse).

Data (n=5) was analyzed by student t-test (with Welch's correction) in GraphPad Prism software (Version 9.2.0) to check the statistical significance between groups in WT or L-FKO mice, and presented as mean±SD.

[a] *p<0.05, **p<0.01, ***p<0.005 vs. WT group with scramble

[b] *p<0.05 vs. L-FKO group with scramble.

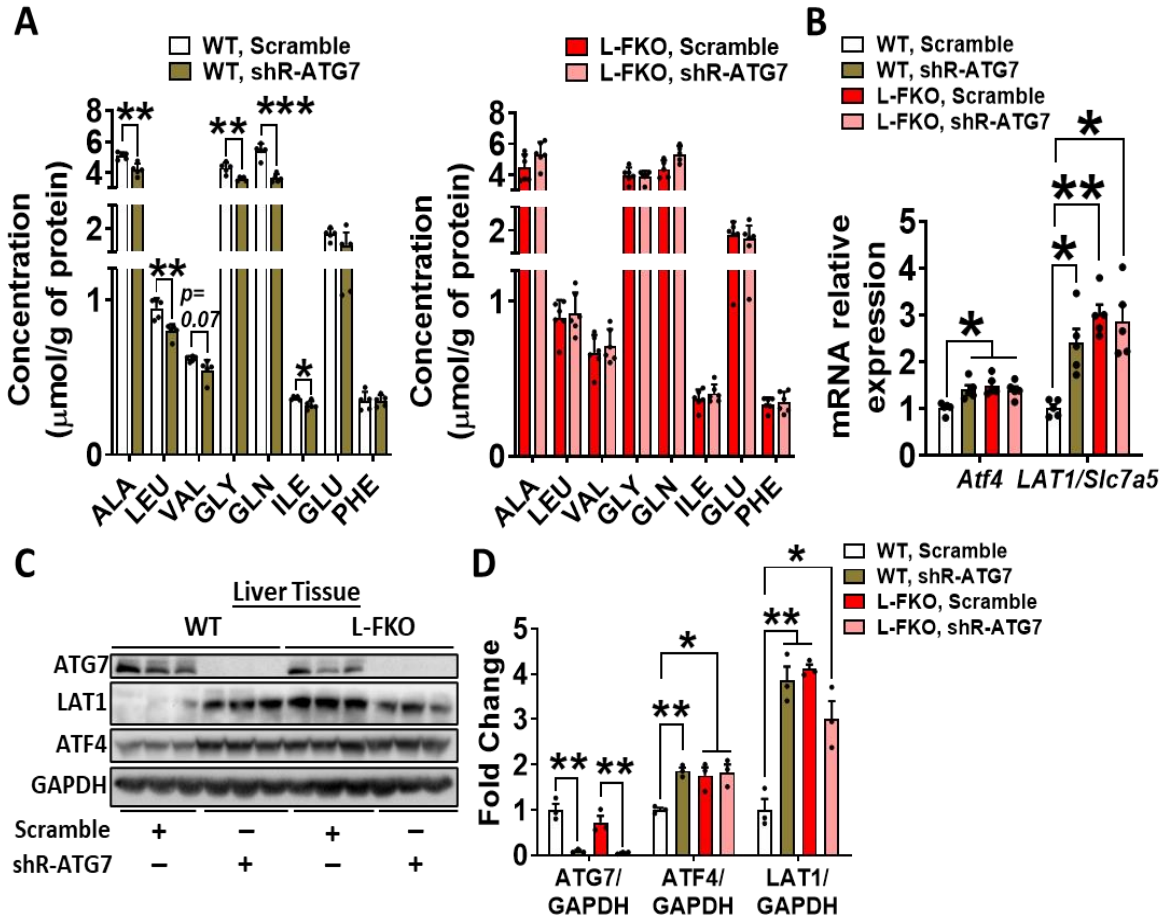

Figure 17. Amino acid profiles are altered in WT mouse livers, coupled with promotion of amino acids transportation upon inhibition of autophagy.

WT and L-FKO male mice (n=5 per group) received AAV8-shRNA-scramble or AAV8-shRNA-ATG7 (10^{11} genome copies per mouse) by RO injection. Mice were sacrificed for tissue collection on the 17th day after AAV8 injection. Preparation of the liver tissue lysates for amino acid determination by HPLC method was described in the Materials and method. Alanine (ALA), leucine (LEU), valine (VAL), glycine (GLY), glutamine (GLN), isoleucine (ILE), glutamate (GLU) and phenylalanine (PHE) were the top eight amino acids affected by inhibition of autophagy *in vitro*, and shown here for comparison (A). Data was analyzed by student t-test (with Welch's correction) to check the statistical significance between groups, and presented as mean±SD. **p*<0.05, ***p*<0.01, ****p*<0.005. Full amino acids profiles of mouse liver were given in Table 8. mRNA and protein levels of LAT1 and ATF4 were evaluated by RT-qPCR (B) and western blot assay (C). Representative protein blot images were given in panel B. Bands' intensities (from three independent repeated experiments) were quantified by ImageJ software (NIH, 1.8.0v) and given in penal D. Data was analyzed by two-way ANOVA coupled with post-test (Tukey's test) to check the statistical significance between groups, and presented as mean±SEM. **p*<0.05, ***p*<0.01.

The effect of autophagy in control of FoxO1 protein amount potentially contribute to lipid metabolism or redox regulation under starvation conditions

In addition to glucose metabolism, there are several other important intracellular activities requiring the participation of FoxO1, including lipogenesis[229, 230, 264], fatty acid oxidation[41, 208, 232, 264] and redox regulation[222, 225, 264, 265]. It has been reported that in FoxO1 transgenic mice, lipogenesis-related genes were significantly downregulated by about 70%[251], while in liver-specific insulin receptor and FoxO1 double knockout mice, genes related to fatty acid transportation and oxidation were significantly suppressed[281]. Besides that, FoxO1 demonstrated a protective effect against oxidative stress involved in fatty liver diseases by upregulating the expression anti-oxidant genes[264, 282-284].

Since we demonstrated that FoxO1 activity could be mediated by autophagy, we were interested to know if the lipid metabolism and redox regulation-related genes that were mediated by FoxO1 could also be affected by autophagy deficiency. Indeed, under the inhibition of autophagy, the lipogenesis-related genes, such as *Srebp1c*, *Scd1*, *Acc1* were significantly upregulated, while the fatty acid oxidation-related genes and redox regulation-related genes, such as *Cd36*, *Cpt1a*, *Sod1*, *Gsr*, and *Prdx3* were significantly downregulated. Notably, all these phenomena were barely observed in L-FKO hepatocytes (Figure 18 A and B), indicating that the alteration of these gene expression induced by inhibition of autophagy was largely in FoxO1-dependent manner. To conclude, this piece of evidence highlighted the importance of autophagy-FoxO1 axis in regulation of cellular homeostasis during starvation.

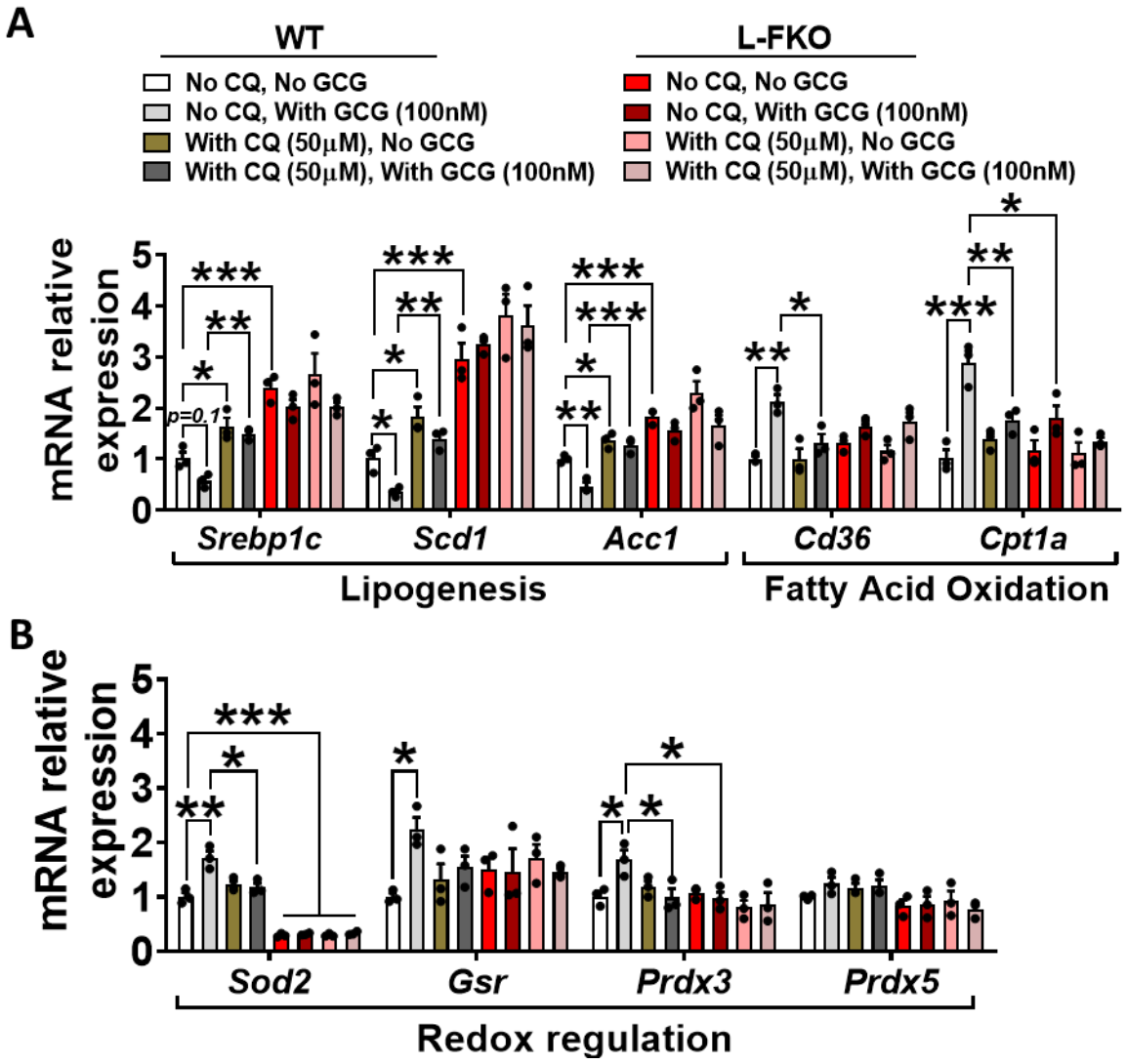

Figure 18. The effect of autophagy deficiency on FoxO1 protein level could potentially influence lipid metabolism and redox regulation in the hepatocytes.
Primary hepatocytes isolated from WT and L-FKO male mouse liver were cultured in HGP buffer for 3hr with or without CQ (50μM) treatment and GCG (100nM) treatment, followed by mRNA extraction. Genes related to lipid metabolism (A) and redox regulation (B) were evaluated by RT-qPCR. Data was calculated as the relative to the control group (i.e., the group without CQ and GCG treatment). Data was analyzed by two-way ANOVA coupled with post-test (Tukey's test) in GraphPad Prism software (Version 9.2.0) to check the statistical significance between groups, and presented as mean±SEM. *p<0.05, **p<0.01, ***p<0.005

Discussion

The necessity of autophagy in the maintenance of cellular amino acid pools during starvation has been demonstrated in the past decades. However, there is limited evidence showing the physiological impact of cellular amino acid pools alteration caused by autophagy deficiency in the hepatocytes. Nearly two decades ago, Onodera and Ohsumi demonstrated that in yeasts with autophagy deficiency (ATG7-mutant), nitrogen starvation-induced proteins, such as arginosuccinate synthetase (Arg1p) and heat shock protein of 26kDa (Hsp26p) were largely reduced comparing with WT cells. On top of that, such reduction of protein level was mostly due to a post-transcriptional defect, rather than downregulation of the mRNA level. Although both WT and ATG7-mutant cells showed a dramatically reduction in protein synthesis in the first 3 hours of nitrogen starvation (which was consistent with the reduction of cellular amino acids contents in their study), only WT cells restored the rate of protein synthesis after 3 hours (which was also consistent with the restoration of cellular amino acid level after 3 hours in their study). Notably, when starved ATG7-deficient cells were pre-incubated in a medium containing an excess of free amino acids, those cells exhibited a similar rate of protein synthesis in comparison to WT cells[269].

Later, another study focusing on autophagic substrate p62/SQSTM1 further highlighted the importance of autophagy-derived amino acids during starvation. Apart from LC3, p62/SQSTM1 is another commonly used indicator of autophagic degradation. Basically, when autophagy is upregulated, the amount of cellular p62/SQSTM1 will be reduced due to the promotion of autolysosomal degradation. However, Sahani et al.

reported that at least in HepG2 and mouse embryonic fibroblasts (MEFs), although the amount of p62 decreased in the first 2 hours of starvation (by using starvation medium lacking amino acids and serum), a restoration of p62 could be observed when they prolonged the starvation to 4 hours. If MEFs were cultured in a starvation medium containing autophagy inhibitor CQ, the restoration of p62 during prolonged starvation was no longer observable. Consistent with Onodera and Ohsumi's findings, exogenously added amino acids successfully compensated the inhibitory effect of CQ on p62/SQSTM1 protein synthesis during prolonged starvation[165]. Considering the level of p62 did not always inversely associate with autophagic degradation, we only used LC3 as the main indicator of autophagy activity in the present study.

In the present chapter, we discovered that the amino acid pools were significantly altered in hepatocytes upon autophagy deficiency. Alteration of cellular amino acid pools potentially dysregulated the process of protein synthesis of FoxO1 which was considered to be highly expressed during starvation for HGP. In addition, the activation of the ATF4-LAT1 pathway in WT mouse liver with autophagy deficiency, and in L-FKO mouse liver have three interesting implications for future study. First, inhibition of autophagy not only alters the amino acid pools in the liver, but also potentially activates ATF4-LAT1 pathway which could support the hepatic amino acids uptake from environment. Nonetheless, in our case, such activation of ATF4-LAT1 pathway is not sufficient to compensate the shortage of intracellular amino acid pools under inhibition of autophagy; Second, in L-FKO mouse livers, since FoxO1-mediated gluconeogenesis was almost shut down, amino acids were unable to contribute to FoxO1 protein synthesis or gluconeogenesis, which

may make the autophagy-derived amino acids less significant. Last, there might be a negative correlation between the activity of FoxO1 and ATF4-LAT1 pathway, suggesting that FoxO1 is participating in the regulation of amino acid uptake in hepatocytes.

In summary, the present study highlighted an indispensable role of autophagy in the regulation of HGP, which was to sustain the protein level of FoxO1 by maintaining the cellular amino acid pools during starvation. In addition to glucose homeostasis, an intact autophagy activity during starvation could probably be essential for many other FoxO1-mediated cellular metabolic pathways in the hepatocytes, such as lipogenesis, fatty acid oxidation, and redox regulation.

CHAPTER V

SUMMARY

Insulin resistance is usually coupled with an abnormal upregulation of HGP, eventually contributing to the development of type 2 diabetes. Therefore, understanding the mechanisms regulating the HGP could be a key for the development of therapeutic strategies to treat insulin resistance and type 2 diabetes in the future. Under starvation conditions, glucagon released from pancreatic α cells signals the liver to upregulate the HGP. Meanwhile, autophagy, which is a natural catabolic mechanism, can also be upregulated during starvation or under the stimulation of glucagon, indicating that autophagy could potentially participate in the regulation of HGP. In addition, FoxO1 is an essential transcription factor regulating the expression of gluconeogenic genes such as *pck1* and *g6pc*, which inspires us to investigate the potential relationship between autophagy and FoxO1 regarding the regulation of HGP.

The first part of this study aimed to investigate the importance of autophagy to the HGP during starvation. We found that the HGP in WT mouse primary hepatocytes was significantly suppressed upon the inhibition of autophagy induced by CQ or siR-ATG7 treatment. Moreover, the HGP results showed that the reduction of glucose production from gluconeogenesis, rather than glycogenolysis, was the main cause of the reduction of HGP upon autophagy deficiency, indicating that FoxO1 or CREB-mediated signaling was the potential target. Consistently, the capability of glucose production in WT mice under the stimulation of glucagon, or under the presence of pyruvate, was significantly reduced upon the treatment of HCQ or AAV8-shR-ATG7. After checking the protein level of

FoxO1 and CREB upon inhibition of autophagy, we confirmed that only FoxO1, but not CREB, was significantly reduced by autophagy deficiency. In order to verify that autophagy deficiency-induced FoxO1 protein reduction was the main cause for the suppression of HGP in our case, we checked the effect of inhibition of autophagy in L-FKO mouse primary hepatocytes or in L-FKO mice. The results showed that in L-FKO mouse primary hepatocytes or L-FKO mice, inhibition of autophagy failed to further suppress the HGP. Collectively, this chapter suggested that a fully functioning autophagy is necessary for the HGP during fasting, and the suppression of HGP induced by autophagy deficiency is potentially in a FoxO1-dependent manner.

The second part of this study aimed to identify the effects of autophagy deficiency on FoxO1. Since the inhibition of autophagy cannot further reduce the HGP in L-FKO hepatocytes or mice, we hypothesized that autophagy deficiency suppressed the HGP by impairing FoxO1 activities. Indeed, the protein level of FoxO1, as well as PCK1 and G6PC showed a significant reduction upon inhibition of autophagy. Then we investigated the potential underlying mechanisms for the reduction of FoxO1 through several directions. First, we checked the FoxO1-S253 phosphorylation under autophagy deficiency, because FoxO1-S253 phosphorylation promotes FoxO1 nuclear exclusion, followed by FoxO1 ubiquitination and degradation in the cytoplasm. Although we found that the FoxO1 nuclear localization was reduced upon autophagy deficiency, we did not find any upregulation of FoxO1 phosphorylation at S253. In addition, even in the primary hepatocytes of FoxO1-S253$^{A/A}$ KI mice, the reduction of FoxO1 protein level induced by inhibition of autophagy persisted. We then checked whether the glucagon-induced FoxO1-

S273 phosphorylation was impaired upon the inhibition of autophagy, because FoxO1-S273 phosphorylation stabilizes FoxO1 in the nucleus, which prevents FoxO1 from ubiquitination and degradation in the cytoplasm. However, we found that FoxO1-S273 phosphorylation did not exhibit any significant impairment upon autophagy deficiency. Likewise, in the primary hepatocytes of FoxO1-S273$^{D/D}$ KI mice, the reduction of FoxO1 protein level persisted under the inhibition of autophagy. On top of that, the autophagy deficiency-induced reduction of FoxO1 could not be prevented by the proteasome inhibitor MG132, indicating that FoxO1 degradation was not the major mechanism. Last but not least, we found that under autophagy deficiency, although the mRNA levels of *pck1* and *g6pc* were significantly reduced, the mRNA level of *FoxO1* kept unchanged, suggesting that the reduction of FoxO1 was unlikely due to a transcriptional defect. Collectively, this chapter demonstrated that the inhibition of autophagy significantly reduced nuclear localization of FoxO1. Furthermore, our results ruled out the possibility that the reduction of FoxO1 protein upon the inhibition of autophagy was due to FoxO1 phosphorylation, FoxO1 degradation, or downregulation of FoxO1 mRNA level.

Considering that autophagy is important for protein turnover and maintenance of cellular amino acid pools under starvation, the third part of this study aimed to investigate the relationship between autophagy-mediated amino acid pools and FoxO1 activities. Indeed, the cellular amino acid pools were significantly altered upon the inhibition of autophagy in WT hepatocytes. Particularly, alanine, leucine, valine, glycine, glutamine, isoleucine, glutamate and phenylalanine were the top eight amino acids reduced by the inhibition of autophagy *in vitro*. By supplying exogenous amino acids to WT hepatocytes,

we successfully restored the protein level of FoxO1 and HGP even under the inhibition of autophagy. Furthermore, such amino acid supplementation-induced FoxO1 and HGP restoration could be largely suppressed by protein synthesis inhibitor CHX, indicating that autophagy-mediated amino acid pools were essential for FoxO1 protein synthesis, particularly during starvation. In addition, the alteration of gene expression related to lipid metabolism, redox regulation, and amino acid uptake under the inhibition of autophagy in the WT, but not in the L-FKO hepatocytes further highlighted the importance of autophagy-mediated FoxO1 activities in the cellular homeostasis from different aspects.

In summary, in the present study, we successfully unveil an important role of autophagy involved in the glucose homeostasis, which is to maintain the hepatic amino acid pools under starvation, subsequently supporting the protein level and activity of FoxO1 in control of the HGP (Figure 19). By clarifying the autophagy-mediated FoxO1 activity, this study provides a great supporting evidence for the previous study which demonstrated that the liver-specific ATG7 knockout mice were protected from HFD-induced obesity and insulin resistance[279]. However, the deficiency of lipophagy (autophagy selectively targets lipid droplets) was claimed to be observed during aging process, which could possibly contribute to hepatic lipid accumulation and metabolic syndromes[126]. Under these circumstances, we must admit that the roles of autophagy in the maintenance of hepatic homeostasis are very complicated. It is impossible to simply define that the autophagy is good or bad for diabetic patients. In order to develop the most appropriate therapeutic strategies in the patients with autophagy abnormality-related

insulin resistance, it is necessary to identify the specific pathological conditions in which the autophagy is involved.

Nevertheless, in the clinical aspect, the present study has two implications: First, a therapeutic strategy/medication which has an inhibitory effect on autophagy (e.g., HCQ treatment) could be potentially beneficial for the patients with insulin resistance or type 2 diabetes; Second, when a therapeutic strategy/medication is reported to have an inhibitory effect on autophagy, the patients who receive this therapeutic strategy/medication need to be aware of hypoglycemia as a potential side effect. In the nutritional aspect, foods rich in amino acids that are significantly affected upon autophagy deficiency shown in the present study could be a potential dietary intervention for the individuals who are considered as a high-risk group with blood glucose dysregulation, such as elderly people.

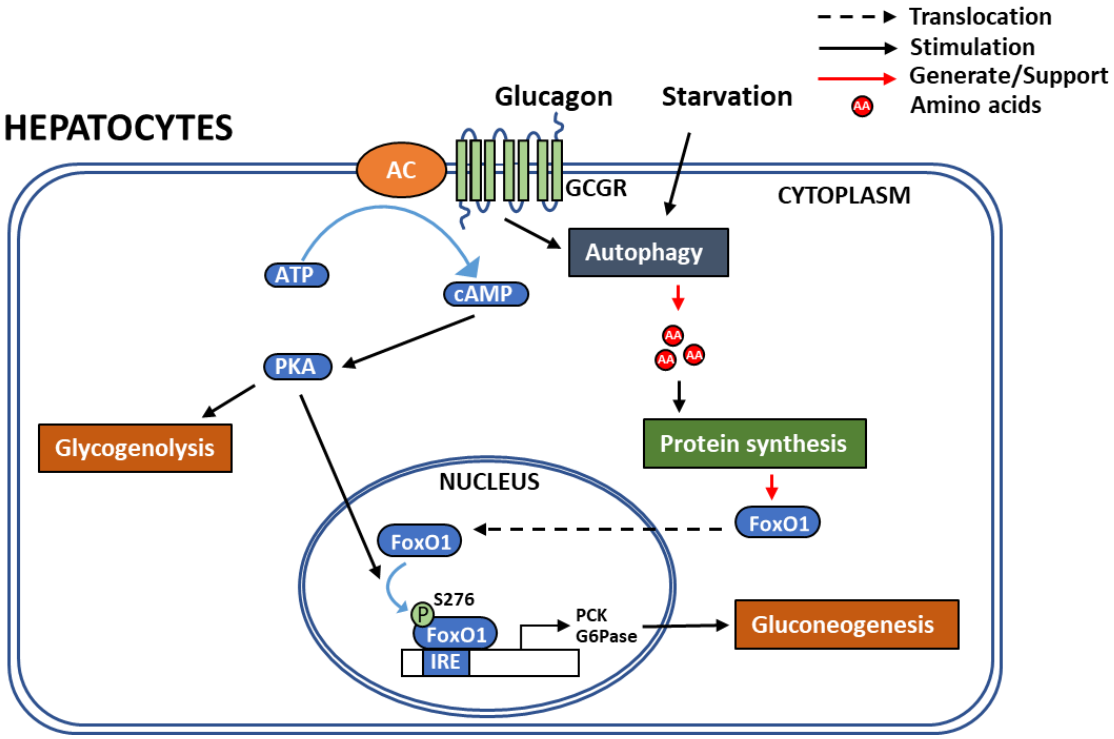

Figure 19. A diagram illustrates the role of autophagy in control of the HGP under starvation.

Upon starvation (and glucagon stimulation), the activity of autophagy is upregulated, which actively participates in protein turnover and amino acid recycling to maintain the cellular amino acid pools in the hepatocytes. FoxO1, a critical transcription factor controlling gluconeogenic gene expression, is phosphorylated at S276 (equivalent to S273 in mouse FoxO1) then stabilized in the nucleus under glucagon signaling during starvation. Notably, a sufficient FoxO1 protein synthesis requires autophagy-derived amino acids as the building blocks, which is essential for the upregulation of HGP during starvation. AC, adenylate cyclase; GCGR, G-protein coupled glucagon receptor; PKA, cAMP-dependent protein kinase; FoxO1, forkhead box protein O1; IRE, insulin response element; PCK, phosphoenolpyruvate carboxykinase; G6Pase, glucose 6-phosphatase; AA, amino acids

REFERENCES

1. Sanz París, A. [Diabetes and nutrition]. *Nutr. Hosp.* **15 Suppl 1**, 58-68 (2000).
2. Genuth, S.M., Palmer, J.P. & Nathan, D.M. Classification and Diagnosis of Diabetes, in *Diabetes in America*. (eds. rd *et al.*) (National Institute of Diabetes and Digestive and Kidney Diseases (US), Bethesda (MD); 2018).
3. Schwerin, D.L. & Svancarek, B. EMS Diabetic Protocols For Treat and Release, in *StatPearls* (StatPearls Publishing Copyright © 2021, StatPearls Publishing LLC., Treasure Island (FL); 2021).
4. Mohseni, S. Neurologic damage in hypoglycemia. *Handb. Clin. Neurol.* **126**, 513-532 (2014).
5. Hershey, T., Lillie, R., Sadler, M. & White, N.H. Severe hypoglycemia and long-term spatial memory in children with type 1 diabetes mellitus: A retrospective study. *J. Int. Neuropsychol. Soc.* **9**, 740-750 (2003).
6. Ben-Ami, H., Nagachandran, P., Mendelson, A. & Edoute, Y. Drug-induced hypoglycemic coma in 102 diabetic patients. *Arch. Intern. Med.* **159**, 281-284 (1999).
7. Guo, X. *et al.* Glycolysis in the control of blood glucose homeostasis. *Acta Pharmaceutica Sinica B* **2**, 358-367 (2012).
8. D'Alessandro, A., Gevi, F. & Zolla, L. Red blood cell metabolism under prolonged anaerobic storage. *Mol. Biosyst.* **9**, 1196-1209 (2013).

9. Ghashghaeinia, M., Köberle, M., Mrowietz, U. & Bernhardt, I. Proliferating tumor cells mimick glucose metabolism of mature human erythrocytes. *Cell Cycle* **18**, 1316-1334 (2019).

10. Kugler, W. & Lakomek, M. Glucose-6-phosphate isomerase deficiency. *Baillieres Best Pract. Res. Clin. Haematol.* **13**, 89-101 (2000).

11. Siems, W.G., Sommerburg, O. & Grune, T. Erythrocyte free radical and energy metabolism. *Clin. Nephrol.* **53**, S9-17 (2000).

12. Ebertowska, A., Ludkiewicz, B., Klejbor, I., Melka, N. & Moryś, J. Pyruvate dehydrogenase deficiency: morphological and metabolic effects, creation of animal model to search for curative treatment. *Folia Morphol. (Warsz.)* **79**, 191-197 (2020).

13. Szutowicz, A., Bielarczyk, H., Jankowska-Kulawy, A., Pawełczyk, T. & Ronowska, A. Acetyl-CoA the key factor for survival or death of cholinergic neurons in course of neurodegenerative diseases. *Neurochem. Res.* **38**, 1523-1542 (2013).

14. Hargreaves, M. & Spriet, L.L. Skeletal muscle energy metabolism during exercise. *Nat Metab* **2**, 817-828 (2020).

15. Sahlin, K., Tonkonogi, M. & Söderlund, K. Energy supply and muscle fatigue in humans. *Acta Physiol. Scand.* **162**, 261-266 (1998).

16. Deary, I.J., Sommerfield, A.J., McAulay, V. & Frier, B.M. Moderate hypoglycaemia obliterates working memory in humans with and without insulin

treated diabetes. *Journal of neurology, neurosurgery, and psychiatry* **74**, 278-279 (2003).

17. Runge, S. *et al.* Three distinct epitopes on the extracellular face of the glucagon receptor determine specificity for the glucagon amino terminus. *J. Biol. Chem.* **278**, 28005-28010 (2003).
18. Tran, C.D., Beddard, G.S. & Osborne, A.D. Secondary structure and dynamics of glucagon in solution. *Biochim. Biophys. Acta* **709**, 256-264 (1982).
19. Campbell, J.E. & Drucker, D.J. Islet α cells and glucagon--critical regulators of energy homeostasis. *Nat. Rev. Endocrinol.* **11**, 329-338 (2015).
20. Aronoff, S.L., Berkowitz, K., Shreiner, B. & Want, L. Glucose Metabolism and Regulation: Beyond Insulin and Glucagon. *Diabetes Spectr.* **17**, 183 (2004).
21. Briant, L., Salehi, A., Vergari, E., Zhang, Q. & Rorsman, P. Glucagon secretion from pancreatic α-cells. *Ups. J. Med. Sci.* **121**, 113-119 (2016).
22. Wilcox, G. Insulin and insulin resistance. *The Clinical biochemist. Reviews* **26**, 19-39 (2005).
23. Boucher, J., Kleinridders, A. & Kahn, C.R. Insulin receptor signaling in normal and insulin-resistant states. *Cold Spring Harb. Perspect. Biol.* **6**, a009191 (2014).
24. Yang, Z. & Klionsky, D.J. Mammalian autophagy: core molecular machinery and signaling regulation. *Curr. Opin. Cell Biol.* **22**, 124-131 (2010).
25. Singh, R. & Cuervo, A.M. Autophagy in the cellular energetic balance. *Cell Metab.* **13**, 495-504 (2011).

26. Schworer, C.M. & Mortimore, G.E. Glucagon-induced autophagy and proteolysis in rat liver: mediation by selective deprivation of intracellular amino acids. *Proc. Natl. Acad. Sci. U. S. A.* **76**, 3169-3173 (1979).

27. Ruan, H.B. *et al.* Calcium-dependent O-GlcNAc signaling drives liver autophagy in adaptation to starvation. *Genes Dev.* **31**, 1655-1665 (2017).

28. Tian, X. *et al.* A Voltage-Gated Calcium Channel Regulates Lysosomal Fusion with Endosomes and Autophagosomes and Is Required for Neuronal Homeostasis. *PLoS Biol.* **13**, e1002103 (2015).

29. Høyer-Hansen, M. *et al.* Control of Macroautophagy by Calcium, Calmodulin-Dependent Kinase Kinase-β, and Bcl-2. *Mol. Cell* **25**, 193-205 (2007).

30. Shen, J.Z., Wu, G. & Guo, S. Amino Acids in Autophagy: Regulation and Function. *Adv. Exp. Med. Biol.* **1332**, 51-66 (2021).

31. Aromataris, E.C., Roberts, M.L., Barritt, G.J. & Rychkov, G.Y. Glucagon activates Ca2+ and Cl- channels in rat hepatocytes. *J. Physiol.* **573**, 611-625 (2006).

32. Houslay, M.D., Morris, N.J., Savage, A., Marker, A. & Bushfield, M. Regulation of hepatocyte adenylate cyclase by amylin and CGRP: a single receptor displaying apparent negative cooperatively towards CGRP and simple saturation kinetics for amylin, a requirement for phosphodiesterase inhibition to observe elevated hepatocyte cyclic AMP levels and the phosphorylation of Gi-2. *J. Cell. Biochem.* **55 Suppl**, 66-82 (1994).

33. Shpakov, A.O. & Derkach, K.V. [Adenylyl Cyclase Signaling System in the Liver and Pancreas Innorm and in Diabetic Pathology]. *Ross. Fiziol. Zh. Im. I. M. Sechenova* **102**, 1030-1050 (2016).

34. Grinde, B. & Ichihara, A. Effects of prostaglandins and divalent cations on cAMP production in isolated rat hepatocytes. *Exp. Cell Res.* **148**, 163-172 (1983).

35. Wu, Y. *et al.* Novel Mechanism of Foxo1 Phosphorylation in Glucagon Signaling in Control of Glucose Homeostasis. *Diabetes* **67**, 2167-2182 (2018).

36. Paredes-Flores, M.A. & Mohiuddin, S.S. Biochemistry, Glycogenolysis, in *StatPearls* (StatPearls Publishing Copyright © 2021, StatPearls Publishing LLC., Treasure Island (FL); 2021).

37. Klover, P.J. & Mooney, R.A. Hepatocytes: critical for glucose homeostasis. *Int. J. Biochem. Cell Biol.* **36**, 753-758 (2004).

38. Rui, L. Energy metabolism in the liver. *Compr Physiol* **4**, 177-197 (2014).

39. Koo, S.-H. *et al.* The CREB coactivator TORC2 is a key regulator of fasting glucose metabolism. *Nature* **437**, 1109-1114 (2005).

40. Sun, X. *et al.* Glucagon-CREB/CRTC2 signaling cascade regulates hepatic BMAL1 protein. *The Journal of biological chemistry* **290**, 2189-2197 (2015).

41. Liao, W. *et al.* Heme Oxygenase-1 Regulates Ferrous Iron and Foxo1 in Control of Hepatic Gluconeogenesis. *Diabetes* **70**, 696-709 (2021).

42. Gross, D.N., van den Heuvel, A.P.J. & Birnbaum, M.J. The role of FoxO in the regulation of metabolism. *Oncogene* **27**, 2320-2336 (2008).

43. Lu, H. & Huang, H. FOXO1: a potential target for human diseases. *Curr. Drug Targets* **12**, 1235-1244 (2011).

44. Yan, H. *et al.* Estrogen Improves Insulin Sensitivity and Suppresses Gluconeogenesis via the Transcription Factor Foxo1. *Diabetes* **68**, 291-304 (2019).

45. Samuel, V.T. & Shulman, G.I. The pathogenesis of insulin resistance: integrating signaling pathways and substrate flux. *J. Clin. Invest.* **126**, 12-22 (2016).

46. De Meyts, P. The Insulin Receptor and Its Signal Transduction Network, in *Endotext*. (eds. K.R. Feingold *et al.*) (MDText.com, Inc. Copyright © 2000-2021, MDText.com, Inc., South Dartmouth (MA); 2000).

47. Mardilovich, K., Pankratz, S.L. & Shaw, L.M. Expression and function of the insulin receptor substrate proteins in cancer. *Cell Communication and Signaling* **7**, 14 (2009).

48. Guo, S. *et al.* The Irs1 branch of the insulin signaling cascade plays a dominant role in hepatic nutrient homeostasis. *Mol. Cell. Biol.* **29**, 5070-5083 (2009).

49. Rabiee, A., Krüger, M., Ardenkjær-Larsen, J., Kahn, C.R. & Emanuelli, B. Distinct signalling properties of insulin receptor substrate (IRS)-1 and IRS-2 in mediating insulin/IGF-1 action. *Cell. Signal.* **47**, 1-15 (2018).

50. Dong, X.C. *et al.* Inactivation of hepatic Foxo1 by insulin signaling is required for adaptive nutrient homeostasis and endocrine growth regulation. *Cell Metab.* **8**, 65-76 (2008).

51. Porta, C., Paglino, C. & Mosca, A. Targeting PI3K/Akt/mTOR Signaling in Cancer. *Front. Oncol.* **4**, 64-64 (2014).

52. Haeusler, R.A., McGraw, T.E. & Accili, D. Biochemical and cellular properties of insulin receptor signalling. *Nature Reviews Molecular Cell Biology* **19**, 31-44 (2018).

53. Lee, J.Y., Chiu, Y.H., Asara, J. & Cantley, L.C. Inhibition of PI3K binding to activators by serine phosphorylation of PI3K regulatory subunit p85alpha Src homology-2 domains. *Proc. Natl. Acad. Sci. U. S. A.* **108**, 14157-14162 (2011).

54. Świderska, E. *et al.* Role of PI3K/AKT Pathway in Insulin-Mediated Glucose Uptake, in *Blood Glucose Levels* (2020).

55. Zhang, K. *et al.* Phosphorylation of Forkhead Protein FoxO1 at S253 Regulates Glucose Homeostasis in Mice. *Endocrinology* **160**, 1333-1347 (2019).

56. Biggs, W.H., Meisenhelder, J., Hunter, T., Cavenee, W.K. & Arden, K.C. Protein kinase B/Akt-mediated phosphorylation promotes nuclear exclusion of the winged helix transcription factor FKHR1. *Proceedings of the National Academy of Sciences* **96**, 7421 (1999).

57. Beurel, E., Grieco, S.F. & Jope, R.S. Glycogen synthase kinase-3 (GSK3): Regulation, actions, and diseases. *Pharmacol. Ther.* **148**, 114-131 (2015).

58. DeFronzo, R.A. Pathogenesis of Type 2 Diabetes Mellitus, in *Diabetes Epidemiology, Genetics, Pathogenesis, Diagnosis, Prevention, and Treatment*. (eds. E. Bonora & R.A. DeFronzo) 181-253 (Springer International Publishing, Cham; 2018).

59. Saeedi, P. *et al.* Global and regional diabetes prevalence estimates for 2019 and projections for 2030 and 2045: Results from the International Diabetes Federation Diabetes Atlas, 9(th) edition. *Diabetes Res. Clin. Pract.* **157**, 107843 (2019).

60. Hieronymus, L. & Griffin, S. Role of Amylin in Type 1 and Type 2 Diabetes. *Diabetes Educ.* **41**, 47s-56s (2015).

61. Powers, A.C. Type 1 diabetes mellitus: much progress, many opportunities. *J. Clin. Invest.* **131** (2021).

62. Carré, A. & Mallone, R. Making Insulin and Staying Out of Autoimmune Trouble: The Beta-Cell Conundrum. *Front. Immunol.* **12**, 639682 (2021).

63. Banarer, S., McGregor, V.P. & Cryer, P.E. Intraislet hyperinsulinemia prevents the glucagon response to hypoglycemia despite an intact autonomic response. *Diabetes* **51**, 958-965 (2002).

64. Morran, M.P., Vonberg, A., Khadra, A. & Pietropaolo, M. Immunogenetics of type 1 diabetes mellitus. *Mol. Aspects Med.* **42**, 42-60 (2015).

65. Noble, J.A. & Valdes, A.M. Genetics of the HLA region in the prediction of type 1 diabetes. *Curr. Diab. Rep.* **11**, 533-542 (2011).

66. Chen, Y.-L. *et al.* Climates on incidence of childhood type 1 diabetes mellitus in 72 countries. *Sci. Rep.* **7**, 12810-12810 (2017).

67. Snell-Bergeon, J.K. *et al.* Early childhood infections and the risk of islet autoimmunity: the Diabetes Autoimmunity Study in the Young (DAISY). *Diabetes Care* **35**, 2553-2558 (2012).

68. Monaghan, M., Helgeson, V. & Wiebe, D. Type 1 diabetes in young adulthood. *Curr. Diabetes Rev.* **11**, 239-250 (2015).

69. Janež, A. *et al.* Insulin Therapy in Adults with Type 1 Diabetes Mellitus: a Narrative Review. *Diabetes therapy : research, treatment and education of diabetes and related disorders* **11**, 387-409 (2020).

70. Varanauskiene, E., Varanauskaite, I. & Ceponis, J. [An update on multiple insulin injection therapy in type 1 and 2 diabetes]. *Medicina (Kaunas)* **42**, 770-779 (2006).

71. Misso, M.L., Egberts, K.J., Page, M., O'Connor, D. & Shaw, J. Continuous subcutaneous insulin infusion (CSII) versus multiple insulin injections for type 1 diabetes mellitus. *Cochrane Database Syst. Rev.*, Cd005103 (2010).

72. Serbis, A., Giapros, V., Kotanidou, E.P., Galli-Tsinopoulou, A. & Siomou, E. Diagnosis, treatment and prevention of type 2 diabetes mellitus in children and adolescents. *World J. Diabetes* **12**, 344-365 (2021).

73. Songer, T. *et al.* Examining the economic costs related to lifestyle and pharmacological interventions in youth with Type 2 diabetes. *Expert Rev. Pharmacoecon. Outcomes Res.* **6**, 315-324 (2006).

74. Cavaghan, M.K., Ehrmann, D.A. & Polonsky, K.S. Interactions between insulin resistance and insulin secretion in the development of glucose intolerance. *The Journal of clinical investigation* **106**, 329-333 (2000).

75. Petersen, K.F. *et al.* Mitochondrial Dysfunction in the Elderly: Possible Role in Insulin Resistance. *Science* **300**, 1140 (2003).

76. Taylor, R. Insulin Resistance and Type 2 Diabetes. *Diabetes* **61**, 778 (2012).

77. Krssak, M. *et al.* Intramyocellular lipid concentrations are correlated with insulin sensitivity in humans: a 1H NMR spectroscopy study. *Diabetologia* **42**, 113-116 (1999).

78. Sinha, R. *et al.* Assessment of skeletal muscle triglyceride content by (1)H nuclear magnetic resonance spectroscopy in lean and obese adolescents: relationships to insulin sensitivity, total body fat, and central adiposity. *Diabetes* **51**, 1022-1027 (2002).

79. Gassaway, B.M. *et al.* PKCε contributes to lipid-induced insulin resistance through cross talk with p70S6K and through previously unknown regulators of insulin signaling. *Proceedings of the National Academy of Sciences* **115**, E8996 (2018).

80. Nawaratne, R. *et al.* Regulation of insulin receptor substrate 1 pleckstrin homology domain by protein kinase C: role of serine 24 phosphorylation. *Molecular endocrinology (Baltimore, Md.)* **20**, 1838-1852 (2006).

81. Copps, K.D. & White, M.F. Regulation of insulin sensitivity by serine/threonine phosphorylation of insulin receptor substrate proteins IRS1 and IRS2. *Diabetologia* **55**, 2565-2582 (2012).

82. Guillausseau, P.J. *et al.* Abnormalities in insulin secretion in type 2 diabetes mellitus. *Diabetes Metab.* **34 Suppl 2**, S43-48 (2008).

83. Cantley, J. & Ashcroft, F.M. Q&A: insulin secretion and type 2 diabetes: why do β-cells fail? *BMC Biol.* **13**, 33-33 (2015).

84. Kahn, B.B. Type 2 Diabetes: When Insulin Secretion Fails to Compensate for Insulin Resistance. *Cell* **92**, 593-596 (1998).

85. Thomas, D.D., Corkey, B.E., Istfan, N.W. & Apovian, C.M. Hyperinsulinemia: An Early Indicator of Metabolic Dysfunction. *Journal of the Endocrine Society* **3**, 1727-1747 (2019).

86. Ferrannini, E. *et al.* beta-Cell function in subjects spanning the range from normal glucose tolerance to overt diabetes: a new analysis. *J. Clin. Endocrinol. Metab.* **90**, 493-500 (2005).

87. Ferrannini, E. *et al.* Insulin resistance and hypersecretion in obesity. European Group for the Study of Insulin Resistance (EGIR). *The Journal of clinical investigation* **100**, 1166-1173 (1997).

88. Jacobson, D.A. & Philipson, L.H. Action potentials and insulin secretion: new insights into the role of Kv channels. *Diabetes Obes. Metab.* **9 Suppl 2**, 89-98 (2007).

89. Sarmiento, B.E., Santos Menezes, L.F. & Schwartz, E.F. Insulin Release Mechanism Modulated by Toxins Isolated from Animal Venoms: From Basic Research to Drug Development Prospects. *Molecules* **24** (2019).

90. Skelin Klemen, M., Dolenšek, J., Slak Rupnik, M. & Stožer, A. The triggering pathway to insulin secretion: Functional similarities and differences between the human and the mouse β cells and their translational relevance. *Islets* **9**, 109-139 (2017).

91. Orci, L., Malaisse-Lagae, F., Ravazzola, M., Amherdt, M. & Renold, A.E. Exocytosis-Endocytosis Coupling in the Pancreatic Beta Cell. *Science* **181**, 561 (1973).

92. Cho, J.-H., Kim, J.-W., Shin, J.-A., Shin, J. & Yoon, K.-H. β-cell mass in people with type 2 diabetes. *Journal of diabetes investigation* **2**, 6-17 (2011).

93. Hanley, S.C. *et al.* {beta}-Cell mass dynamics and islet cell plasticity in human type 2 diabetes. *Endocrinology* **151**, 1462-1472 (2010).

94. Ahrén, B. Type 2 diabetes, insulin secretion and beta-cell mass. *Curr. Mol. Med.* **5**, 275-286 (2005).

95. Matveyenko, A.V. & Butler, P.C. Relationship between beta-cell mass and diabetes onset. *Diabetes Obes. Metab.* **10 Suppl 4**, 23-31 (2008).

96. Lupi, R. & Del Prato, S. Beta-cell apoptosis in type 2 diabetes: quantitative and functional consequences. *Diabetes Metab.* **34 Suppl 2**, S56-64 (2008).

97. Del Guerra, S. *et al.* Gliclazide protects human islet beta-cells from apoptosis induced by intermittent high glucose. *Diabetes Metab. Res. Rev.* **23**, 234-238 (2007).

98. Sakuraba, H. *et al.* Reduced beta-cell mass and expression of oxidative stress-related DNA damage in the islet of Japanese Type II diabetic patients. *Diabetologia* **45**, 85-96 (2002).

99. Ježek, P., Jabůrek, M. & Plecitá-Hlavatá, L. Contribution of Oxidative Stress and Impaired Biogenesis of Pancreatic β-Cells to Type 2 Diabetes. *Antioxidants & redox signaling* **31**, 722-751 (2019).

100. Kugelberg, E. Diabetes: Macrophages mediate β-cell loss in T2DM. *Nat. Rev. Endocrinol.* **9**, 626 (2013).

101. Bridges, H.R., Jones, A.J.Y., Pollak, M.N. & Hirst, J. Effects of metformin and other biguanides on oxidative phosphorylation in mitochondria. *The Biochemical journal* **462**, 475-487 (2014).

102. Mannucci, E. *et al.* Effect of Metformin on Glucagon-Like Peptide 1 (GLP-1) and Leptin Levels in Obese Nondiabetic Subjects. *Diabetes Care* **24**, 489 (2001).

103. He, L. *et al.* Metformin and insulin suppress hepatic gluconeogenesis through phosphorylation of CREB binding protein. *Cell* **137**, 635-646 (2009).

104. Doyle, M.E. & Egan, J.M. Mechanisms of action of glucagon-like peptide 1 in the pancreas. *Pharmacol. Ther.* **113**, 546-593 (2007).

105. Gilbert, M.P. & Pratley, R.E. GLP-1 Analogs and DPP-4 Inhibitors in Type 2 Diabetes Therapy: Review of Head-to-Head Clinical Trials. *Front. Endocrinol. (Lausanne)* **11**, 178-178 (2020).

106. Lilao-Garzón, J., Valverde-Tercedor, C., Muñoz-Descalzo, S., Brito-Casillas, Y. & Wägner, A.M. In Vivo and In Vitro Models of Diabetes: A Focus on Pregnancy. *Adv. Exp. Med. Biol.* **1307**, 553-576 (2021).

107. Cooper, D.B. & Yang, L. Pregnancy And Exercise, in *StatPearls* (StatPearls Publishing Copyright © 2021, StatPearls Publishing LLC., Treasure Island (FL); 2021).

108. Armistead, B. *et al.* Placental Regulation of Energy Homeostasis During Human Pregnancy. *Endocrinology* **161** (2020).

109. Bell, A.W. & Bauman, D.E. Adaptations of glucose metabolism during pregnancy and lactation. *J. Mammary Gland Biol. Neoplasia* **2**, 265-278 (1997).

110. Baumann, M.U., Deborde, S. & Illsley, N.P. Placental glucose transfer and fetal growth. *Endocrine* **19**, 13-22 (2002).

111. Knopp, R.H., Montes, A., Childs, M., Li, J.R. & Mabuchi, H. Metabolic adjustments in normal and diabetic pregnancy. *Clin. Obstet. Gynecol.* **24**, 21-49 (1981).

112. Campbell, D.M., Sutherland, H.W. & Pearson, D.W. Maternal glucose response to a standardized test meal throughout pregnancy and postnatally. *Am. J. Obstet. Gynecol.* **171**, 143-146 (1994).

113. Kelly, A.C., Powell, T.L. & Jansson, T. Placental function in maternal obesity. *Clin. Sci. (Lond.)* **134**, 961-984 (2020).

114. Kumar, P. & Magon, N. Hormones in pregnancy. *Niger. Med. J.* **53**, 179-183 (2012).

115. Goyvaerts, L. *et al.* Prolactin receptors and placental lactogen drive male mouse pancreatic islets to pregnancy-related mRNA changes. *PLoS One* **10**, e0121868 (2015).

116. Homko, C., Sivan, E., Chen, X., Reece, E.A. & Boden, G. Insulin secretion during and after pregnancy in patients with gestational diabetes mellitus. *J. Clin. Endocrinol. Metab.* **86**, 568-573 (2001).

117. Sonagra, A.D., Biradar, S.M., K, D. & Murthy D S, J. Normal pregnancy- a state of insulin resistance. *Journal of clinical and diagnostic research : JCDR* **8**, CC01-CC03 (2014).

118. Catalano, P.M., Huston, L., Amini, S.B. & Kalhan, S.C. Longitudinal changes in glucose metabolism during pregnancy in obese women with normal glucose tolerance and gestational diabetes mellitus. *Am. J. Obstet. Gynecol.* **180**, 903-916 (1999).

119. Chu, A.H.Y. & Godfrey, K.M. Gestational Diabetes Mellitus and Developmental Programming. *Ann. Nutr. Metab.* **76 Suppl 3**, 4-15 (2020).

120. Juan, J. & Yang, H. Prevalence, Prevention, and Lifestyle Intervention of Gestational Diabetes Mellitus in China. *Int. J. Environ. Res. Public Health* **17** (2020).

121. Lende, M. & Rijhsinghani, A. Gestational Diabetes: Overview with Emphasis on Medical Management. *Int. J. Environ. Res. Public Health* **17** (2020).

122. Berghella, V. & Saccone, G. Exercise in pregnancy! *Am. J. Obstet. Gynecol.* **216**, 335-337 (2017).

123. Brawerman, G.M. & Dolinsky, V.W. Therapies for gestational diabetes and their implications for maternal and offspring health: Evidence from human and animal studies. *Pharmacol. Res.* **130**, 52-73 (2018).

124. Landon, M.B. *et al.* A multicenter, randomized trial of treatment for mild gestational diabetes. *N. Engl. J. Med.* **361**, 1339-1348 (2009).

125. Amin, M., Suksomboon, N., Poolsup, N. & Malik, O. Comparison of glyburide with metformin in treating gestational diabetes mellitus: a systematic review and meta-analysis. *Clin. Drug Investig.* **35**, 343-351 (2015).

126. Singh, R. *et al.* Autophagy regulates lipid metabolism. *Nature* **458**, 1131-1135 (2009).

127. Moruno, F., Pérez-Jiménez, E. & Knecht, E. Regulation of autophagy by glucose in Mammalian cells. *Cells* **1**, 372-395 (2012).

128. Ghislat, G., Patron, M., Rizzuto, R. & Knecht, E. Withdrawal of Essential Amino Acids Increases Autophagy by a Pathway Involving Ca2+/Calmodulin-dependent Kinase Kinase-β (CaMKK-β). **287**, 38625-38636 (2012).

129. Hayat, M.A. Chapter 1 - Overview of Autophagy, in *Autophagy: Cancer, Other Pathologies, Inflammation, Immunity, Infection, and Aging*. (ed. M.A. Hayat) 3-73 (Academic Press, 2016).

130. Hayat, M.A. Chapter 1 - Introduction to Autophagy: Cancer, Other Pathologies, Inflammation, Immunity, Infection and Aging, Volumes 1–4, in *Autophagy: Cancer, Other Pathologies, Inflammation, Immunity, Infection, and Aging*. (ed. M.A. Hayat) 1-32 (Academic Press, Amsterdam; 2014).

131. Yang, Z. & Klionsky, D.J. Eaten alive: a history of macroautophagy. *Nat. Cell Biol.* **12**, 814-822 (2010).

132. Karsli-Uzunbas, G. *et al.* Autophagy is required for glucose homeostasis and lung tumor maintenance. *Cancer Discov.* **4**, 914-927 (2014).

133. Cagnol, S. & Chambard, J.-C. ERK and cell death: Mechanisms of ERK-induced cell death – apoptosis, autophagy and senescence. *The FEBS Journal* **277**, 2-21 (2010).

134. Das, C.K., Mandal, M. & Kögel, D. Pro-survival autophagy and cancer cell resistance to therapy. *Cancer Metastasis Rev.* **37**, 749-766 (2018).

135. Zhang, Y., Zhang, L., Gao, J. & Wen, L. Pro-Death or Pro-Survival: Contrasting Paradigms on Nanomaterial-Induced Autophagy and Exploitations for Cancer Therapy. *Acc. Chem. Res.* **52**, 3164-3176 (2019).

136. Mortimore, G.E. & Reeta Pösö, A. The lysosomal pathway of intracellular proteolysis in liver: Regulation by amino acids. *Adv. Enzyme Regul.* **25**, 257-276 (1986).

137. Yim, W.W. & Mizushima, N. Lysosome biology in autophagy. *Cell Discov* **6**, 6 (2020).

138. Mauthe, M. *et al.* Chloroquine inhibits autophagic flux by decreasing autophagosome-lysosome fusion. *Autophagy* **14**, 1435-1455 (2018).

139. Wang, Z. *et al.* The Vici Syndrome Protein EPG5 Is a Rab7 Effector that Determines the Fusion Specificity of Autophagosomes with Late Endosomes/Lysosomes. *Mol. Cell* **63**, 781-795 (2016).

140. Haspel, J. *et al.* Characterization of macroautophagic flux in vivo using a leupeptin-based assay. *Autophagy* **7**, 629-642 (2011).

141. Mizushima, N., Yoshimori, T. & Ohsumi, Y. The Role of Atg Proteins in Autophagosome Formation. *Annu. Rev. Cell. Dev. Biol.* **27**, 107-132 (2011).

142. Schuck, S. Microautophagy - distinct molecular mechanisms handle cargoes of many sizes. *J. Cell Sci.* **133** (2020).

143. Sahu, R. *et al.* Microautophagy of cytosolic proteins by late endosomes. *Dev. Cell* **20**, 131-139 (2011).

144. Schuck, S., Gallagher, C.M. & Walter, P. ER-phagy mediates selective degradation of endoplasmic reticulum independently of the core autophagy machinery. *J. Cell Sci.* **127**, 4078-4088 (2014).

145. Liu, X.M. *et al.* ESCRTs Cooperate with a Selective Autophagy Receptor to Mediate Vacuolar Targeting of Soluble Cargos. *Mol. Cell* **59**, 1035-1042 (2015).

146. Dash, S., Aydin, Y. & Moroz, K. Chaperone-Mediated Autophagy in the Liver: Good or Bad? *Cells* **8** (2019).

147. Liao, Z. *et al.* Dysfunction of chaperone-mediated autophagy in human diseases. *Mol. Cell. Biochem.* **476**, 1439-1454 (2021).

148. Schneider, J.L., Suh, Y. & Cuervo, A.M. Deficient chaperone-mediated autophagy in liver leads to metabolic dysregulation. *Cell Metab.* **20**, 417-432 (2014).

149. Cuervo, A.M., Knecht, E., Terlecky, S.R. & Dice, J.F. Activation of a selective pathway of lysosomal proteolysis in rat liver by prolonged starvation. *Am. J. Physiol.* **269**, C1200-1208 (1995).

150. Yu, L., Chen, Y. & Tooze, S.A. Autophagy pathway: Cellular and molecular mechanisms. *Autophagy* **14**, 207-215 (2018).

151. Hansen, M., Rubinsztein, D.C. & Walker, D.W. Autophagy as a promoter of longevity: insights from model organisms. *Nature Reviews Molecular Cell Biology* **19**, 579-593 (2018).

152. Yonekawa, T. & Thorburn, A. Autophagy and cell death. *Essays Biochem.* **55**, 105-117 (2013).

153. Lee, E.J. & Tournier, C. The requirement of uncoordinated 51-like kinase 1 (ULK1) and ULK2 in the regulation of autophagy. *Autophagy* **7**, 689-695 (2011).

154. McAlpine, F., Williamson, L.E., Tooze, S.A. & Chan, E.Y. Regulation of nutrient-sensitive autophagy by uncoordinated 51-like kinases 1 and 2. *Autophagy* **9**, 361-373 (2013).

155. Kanazawa, T. *et al.* Amino acids and insulin control autophagic proteolysis through different signaling pathways in relation to mTOR in isolated rat hepatocytes. *J. Biol. Chem.* **279**, 8452-8459 (2004).

156. Chotechuang, N. *et al.* Down-regulation of the ubiquitin-proteasome proteolysis system by amino acids and insulin involves the adenosine monophosphate-activated protein kinase and mammalian target of rapamycin pathways in rat hepatocytes. *Amino Acids* **41**, 457-468 (2011).

157. Meley, D. *et al.* AMP-activated protein kinase and the regulation of autophagic proteolysis. *J. Biol. Chem.* **281**, 34870-34879 (2006).

158. Xu, Z.X. *et al.* A plant triterpenoid, avicin D, induces autophagy by activation of AMP-activated protein kinase. *Cell Death Differ.* **14**, 1948-1957 (2007).

159. Orsi, A. *et al.* Dynamic and transient interactions of Atg9 with autophagosomes, but not membrane integration, are required for autophagy. *Mol. Biol. Cell* **23**, 1860-1873 (2012).

160. Walker, S., Chandra, P., Manifava, M., Axe, E. & Ktistakis, N.T. Making autophagosomes: localized synthesis of phosphatidylinositol 3-phosphate holds the clue. *Autophagy* **4**, 1093-1096 (2008).

161. Baba, M., Takeshige, K., Baba, N. & Ohsumi, Y. Ultrastructural analysis of the autophagic process in yeast: detection of autophagosomes and their characterization. *J. Cell Biol.* **124**, 903-913 (1994).

162. Mizushima, N. *et al.* A protein conjugation system essential for autophagy. *Nature* **395**, 395-398 (1998).

163. Kabeya, Y. *et al.* LC3, a mammalian homologue of yeast Apg8p, is localized in autophagosome membranes after processing. *EMBO J.* **19**, 5720-5728 (2000).

164. Galluzzi, L. *et al.* Molecular definitions of autophagy and related processes. *The EMBO Journal* **36**, 1811 (2017).

165. Sahani, M.H., Itakura, E. & Mizushima, N. Expression of the autophagy substrate SQSTM1/p62 is restored during prolonged starvation depending on transcriptional upregulation and autophagy-derived amino acids. *Autophagy* **10**, 431-441 (2014).

166. Chen, R. *et al.* The general amino acid control pathway regulates mTOR and autophagy during serum/glutamine starvation. *The Journal of cell biology* **206**, 173-182 (2014).

167. Tato, I., Bartrons, R., Ventura, F. & Rosa, J.L. Amino Acids Activate Mammalian Target of Rapamycin Complex 2 (mTORC2) via PI3K/Akt Signaling. *J. Biol. Chem.* **286**, 6128-6142 (2011).

168. Angcajas, A.B. *et al.* Diversity of amino acid signaling pathways on autophagy regulation: A novel pathway for arginine. *Biochem. Biophys. Res. Commun.* **446**, 8-14 (2014).

169. Ghislat, G. & Knecht, E. Chapter 3 - Regulation of Autophagy by Amino Acid Starvation Involving Ca2+, in *Autophagy: Cancer, Other Pathologies, Inflammation, Immunity, Infection, and Aging*. (ed. M.A. Hayat) 69-79 (Academic Press, Amsterdam; 2015).

170. Ogier-Denis, E., Pattingre, S., El Benna, J. & Codogno, P. Erk1/2-dependent Phosphorylation of Gα-interacting Protein Stimulates Its GTPase Accelerating Activity and Autophagy in Human Colon Cancer Cells. *J. Biol. Chem.* **275**, 39090-39095 (2000).

171. Martinez-Lopez, N., Athonvarangkul, D., Mishall, P., Sahu, S. & Singh, R. Autophagy proteins regulate ERK phosphorylation. *Nature Communications* **4**, 2799 (2013).

172. Corcelle, E. *et al.* Control of the Autophagy Maturation Step by the MAPK ERK and p38: Lessons from Environmental Carcinogens. *Autophagy* **3**, 57-59 (2007).

173. Wang, J. *et al.* A Non-canonical MEK/ERK Signaling Pathway Regulates Autophagy via Regulating Beclin 1. *J. Biol. Chem.* **284**, 21412-21424 (2009).

174. Shaker, J.L. & Deftos, L. Calcium and Phosphate Homeostasis, in *Endotext*. (eds. K.R. Feingold *et al.*) (MDText.com, Inc. Copyright © 2000-2021, MDText.com, Inc., South Dartmouth (MA); 2000).

175. Macrez, N. & Mironneau, J. Ca2+ Release in Muscle Cells, in *Calcium: The Molecular Basis of Calcium Action in Biology and Medicine*. (eds. R. Pochet, R. Donato, J. Haiech, C. Heizmann & V. Gerke) 9-25 (Springer Netherlands, Dordrecht; 2000).

176. Marsh, S.J., Wanaverbecq, N., Selyanko, A.A. & Brown, D.A. Calcium Signalling in Neurons Exemplified by Rat Sympathetic Ganglion Cells, in *Calcium: The Molecular Basis of Calcium Action in Biology and Medicine*. (eds. R. Pochet, R. Donato, J. Haiech, C. Heizmann & V. Gerke) 27-44 (Springer Netherlands, Dordrecht; 2000).

177. Tordjmann, T., Clair, C., Claret, M. & Combettes, L. Intercellular Calcium Signaling in "Non-Excitable" Cells, in *Calcium: The Molecular Basis of Calcium Action in Biology and Medicine*. (eds. R. Pochet, R. Donato, J. Haiech, C. Heizmann & V. Gerke) 95-108 (Springer Netherlands, Dordrecht; 2000).

178. Kiselyov, K., Yamaguchi, S., Lyons, C.W. & Muallem, S. Aberrant Ca2+ handling in lysosomal storage disorders. *Cell Calcium* **47**, 103-111 (2010).

179. Shen, Y. & Czaja, M.J. A Novel Mechanism of Starvation-Stimulated Hepatic Autophagy: Calcium-Induced O-GlcNAc-Dependent Signaling. *Hepatology* **69**, 446-448 (2019).

180. Zhou, J. *et al.* FOXO3 induces FOXO1-dependent autophagy by activating the AKT1 signaling pathway. *Autophagy* **8**, 1712-1723 (2012).

181. Zhao, Y. *et al.* Cytosolic FoxO1 is essential for the induction of autophagy and tumour suppressor activity. *Nat. Cell Biol.* **12**, 665-675 (2010).

182. Liu, H.-Y. *et al.* Hepatic Autophagy Is Suppressed in the Presence of Insulin Resistance and Hyperinsulinemia: INHIBITION OF FoxO1-DEPENDENT EXPRESSION OF KEY AUTOPHAGY GENES BY INSULIN. *J. Biol. Chem.* **284**, 31484-31492 (2009).

183. Zhang, J. *et al.* Histone deacetylase inhibitors induce autophagy through FOXO1-dependent pathways. *Autophagy* **11**, 629-642 (2015).

184. Cheng, Z. The FoxO-Autophagy Axis in Health and Disease. *Trends Endocrinol. Metab.* **30**, 658-671 (2019).

185. Tong, X. *et al.* DDB1-Mediated CRY1 Degradation Promotes FOXO1-Driven Gluconeogenesis in Liver. *Diabetes* **66**, 2571-2582 (2017).

186. Toledo, M. *et al.* Autophagy Regulates the Liver Clock and Glucose Metabolism by Degrading CRY1. *Cell Metab.* **28**, 268-281.e264 (2018).

187. Rubinsztein, D.C. & Frake, R.A. Yoshinori Ohsumi's Nobel Prize for mechanisms of autophagy: from basic yeast biology to therapeutic potential. *J. R. Coll. Physicians Edinb.* **46**, 228-233 (2016).

188. Ohsumi, Y. Historical landmarks of autophagy research. *Cell Res.* **24**, 9-23 (2014).

189. Klionsky, D.J. *et al.* Guidelines for the use and interpretation of assays for monitoring autophagy (3rd edition). *Autophagy* **12**, 1-222 (2016).

190. Dancourt, J. & Melia, T.J. Lipidation of the autophagy proteins LC3 and GABARAP is a membrane-curvature dependent process. *Autophagy* **10**, 1470-1471 (2014).

191. Metlagel, Z., Otomo, C., Ohashi, K., Takaesu, G. & Otomo, T. Structural insights into E2-E3 interaction for LC3 lipidation. *Autophagy* **10**, 522-523 (2014).

192. Nath, S. *et al.* Lipidation of the LC3/GABARAP family of autophagy proteins relies on a membrane-curvature-sensing domain in Atg3. *Nat. Cell Biol.* **16**, 415-424 (2014).

193. Tanida, I., Ueno, T. & Kominami, E. LC3 conjugation system in mammalian autophagy. *The international journal of biochemistry & cell biology* **36**, 2503-2518 (2004).

194. Homewood, C.A., Warhurst, D.C., Peters, W. & Baggaley, V.C. Lysosomes, pH and the anti-malarial action of chloroquine. *Nature* **235**, 50-52 (1972).

195. Mizushima, N. & Yoshimori, T. How to Interpret LC3 Immunoblotting. *Autophagy* **3**, 542-545 (2007).

196. Yoshii, S.R. & Mizushima, N. Monitoring and Measuring Autophagy. *Int. J. Mol. Sci.* **18**, 1865 (2017).

197. Zhang, X. *et al.* Effect of siRNA-induced Atg7 gene silencing on the sensitivity of ovarian cancer SKOV3 cells to cisplatin. *American journal of translational research* **12**, 2052-2061 (2020).

198. Su, L.-Y. *et al.* Atg5- and Atg7-dependent autophagy in dopaminergic neurons regulates cellular and behavioral responses to morphine. *Autophagy* **13**, 1496-1511 (2017).

199. Dhingra, A., Alexander, D., Reyes-Reveles, J., Sharp, R. & Boesze-Battaglia, K. Microtubule-Associated Protein 1 Light Chain 3 (LC3) Isoforms in RPE and Retina. *Adv. Exp. Med. Biol.* **1074**, 609-616 (2018).

200. Bai, H., Inoue, J., Kawano, T. & Inazawa, J. A transcriptional variant of the LC3A gene is involved in autophagy and frequently inactivated in human cancers. *Oncogene* **31**, 4397-4408 (2012).

201. Koukourakis, M.I. *et al.* Autophagosome Proteins LC3A, LC3B and LC3C Have Distinct Subcellular Distribution Kinetics and Expression in Cancer Cell Lines. *PLoS One* **10**, e0137675-e0137675 (2015).

202. Lattin, J.E. *et al.* Expression analysis of G Protein-Coupled Receptors in mouse macrophages. *Immunome Res.* **4**, 5 (2008).

203. He, H. *et al.* Post-translational Modifications of Three Members of the Human MAP1LC3 Family and Detection of a Novel Type of Modification for MAP1LC3B*. *J. Biol. Chem.* **278**, 29278-29287 (2003).

204. Stokkermans, T.J., Goyal, A., Bansal, P. & Trichonas, G. Chloroquine And Hydroxychloroquine Toxicity, in *StatPearls* (StatPearls Publishing Copyright © 2021, StatPearls Publishing LLC., Treasure Island (FL); 2021).

205. Liu, J. *et al.* Hydroxychloroquine, a less toxic derivative of chloroquine, is effective in inhibiting SARS-CoV-2 infection in vitro. *Cell Discovery* **6**, 16 (2020).

206. Li, X. *et al.* Epigallocatechin Gallate Inhibits Hepatic Glucose Production in Primary Hepatocytes via Downregulating PKA Signaling Pathways and Transcriptional Factor FoxO1. *J. Agric. Food Chem.* (2019).

207. Zhang, K. *et al.* Hepatic suppression of Foxo1 and Foxo3 causes hypoglycemia and hyperlipidemia in mice. *Endocrinology* **153**, 631-646 (2012).

208. Yang, W. *et al.* Glucagon regulates hepatic mitochondrial function and biogenesis through FOXO1. *J. Endocrinol.* **241**, 265-278 (2019).

209. Towers, C.G. & Thorburn, A. Therapeutic Targeting of Autophagy. *EBioMedicine* **14**, 15-23 (2016).

210. Moulis, M. & Vindis, C. Methods for Measuring Autophagy in Mice. *Cells* **6**, 14 (2017).

211. Pattison, J.S., Osinska, H. & Robbins, J. Atg7 induces basal autophagy and rescues autophagic deficiency in CryABR120G cardiomyocytes. *Circ. Res.* **109**, 151-160 (2011).

212. Hanson, R.W. & Garber, A.J. Phosphoenolpyruvate carboxykinase. I. Its role in gluconeogenesis. *Am. J. Clin. Nutr.* **25**, 1010-1021 (1972).

213. An, N. *et al.* Chloroquine Autophagic Inhibition Rebalances Th17/Treg-Mediated Immunity and Ameliorates Systemic Lupus Erythematosus. *Cell. Physiol. Biochem.* **44**, 412-422 (2017).

214. Festa, B.P. *et al.* Impaired autophagy bridges lysosomal storage disease and epithelial dysfunction in the kidney. *Nature communications* **9**, 161-161 (2018).

215. Sands, M.S. AAV-mediated liver-directed gene therapy. *Methods Mol. Biol.* **807**, 141-157 (2011).

216. Wang, L. *et al.* Systematic evaluation of AAV vectors for liver directed gene transfer in murine models. *Molecular therapy : the journal of the American Society of Gene Therapy* **18**, 118-125 (2010).

217. Wang, Y. *et al.* Targeted disruption of the CREB coactivator Crtc2 increases insulin sensitivity. *Proc. Natl. Acad. Sci. U. S. A.* **107**, 3087-3092 (2010).

218. Zhang, Z. *et al.* Autophagy regulates turnover of lipid droplets via ROS-dependent Rab25 activation in hepatic stellate cell. *Redox Biology* **11**, 322-334 (2017).

219. Popli, P., Sun, A.J. & Kommagani, R. The Multifaceted Role of Autophagy in Endometrium Homeostasis and Disease. *Reprod. Sci.* (2021).

220. Kang, R., Zeh, H.J., Lotze, M.T. & Tang, D. The Beclin 1 network regulates autophagy and apoptosis. *Cell Death Differ.* **18**, 571-580 (2011).

221. Wang, T. *et al.* Expression and phosphorylation of FOXO1 influences cell proliferation and apoptosis in the gastrointestinal stromal tumor cell line GIST-T1. *Exp. Ther. Med.* **15**, 3197-3202 (2018).

222. Xue, R. *et al.* Melatonin alleviates deoxynivalenol-induced apoptosis of human granulosa cells by reducing mutually accentuated FOXO1 and ER stress. *Biol. Reprod.* (2021).

223. Wei, C. *et al.* miR-221-3p regulates apoptosis of ovarian granulosa cells via targeting FOXO1 in older women with diminished ovarian reserve (DOR). *Mol. Reprod. Dev.* **88**, 251-260 (2021).

224. Wanitpongpun, C. *et al.* Tamoxifen enhances romidepsin-induced apoptosis in T-cell malignant cells via activation of FOXO1 signaling pathway. *Leuk. Lymphoma*, 1-15 (2021).

225. Li, W., Zhu, Q., Xu, X. & Hu, X. MiR-27a-3p suppresses cerebral ischemia-reperfusion injury by targeting FOXO1. *Aging (Albany N. Y.)* **13**, 11727-11737 (2021).

226. Perrault, R., Molnar, P., Poole, J. & Zahradka, P. PDGF-mediated activation of CREB in vascular smooth muscle cells alters cell cycling via Rb, FoxO1 and p27(kip1). *Exp. Cell Res.*, 112612 (2021).

227. Ye, R.Y. *et al.* KCTD12 promotes G1/S transition of breast cancer cell through activating the AKT/FOXO1 signaling. *J. Clin. Lab. Anal.* **34**, e23315 (2020).

228. Huang, P. *et al.* Hematopoietic-Specific Deletion of Foxo1 Promotes NK Cell Specification and Proliferation. *Front. Immunol.* **10**, 1016 (2019).

229. He, Q. *et al.* FoxO1 Knockdown Promotes Fatty Acid Synthesis via Modulating SREBP1 Activities in the Dairy Goat Mammary Epithelial Cells. *J. Agric. Food Chem.* **68**, 12067-12078 (2020).

230. Kim, D.H. *et al.* Altered FoxO1 and PPARγ interaction in age-related ER stress-induced hepatic steatosis. *Aging (Albany N. Y.)* **11**, 4125-4144 (2019).

231. Nagai, S., Matsumoto, C., Shibano, M. & Fujimori, K. Suppression of Fatty Acid and Triglyceride Synthesis by the Flavonoid Orientin through Decrease of C/EBPδ Expression and Inhibition of PI3K/Akt-FOXO1 Signaling in Adipocytes. *Nutrients* **10** (2018).

232. Kandror, K.V. Mammalian target of rapamycin complex 1 and FoxO1 in the transcriptional control of lipolysis and de novo lipogenesis. *Curr. Opin. Endocrinol. Diabetes Obes.* **24**, 326-331 (2017).

233. Sato, T. *et al.* Acute fructose intake suppresses fasting-induced hepatic gluconeogenesis through the AKT-FoxO1 pathway. *Biochem Biophys Rep* **18**, 100638 (2019).

234. Zhang, X., Jiang, L. & Liu, H. Forkhead Box Protein O1: Functional Diversity and Post-Translational Modification, a New Therapeutic Target? *Drug Des. Devel. Ther.* **15**, 1851-1860 (2021).

235. Cathy, A.G. & Shaodong, G. Insulin receptor substrate signaling controls cardiac energy metabolism and heart failure. *J. Endocrinol.* **233**, R131-R143 (2017).

236. Oh, K.-J., Han, H.-S., Kim, M.-J. & Koo, S.-H. CREB and FoxO1: two transcription factors for the regulation of hepatic gluconeogenesis. *BMB reports* **46**, 567-574 (2013).

237. Janah, L. *et al.* Glucagon Receptor Signaling and Glucagon Resistance. *Int. J. Mol. Sci.* **20**, 3314 (2019).

238. He, L. *et al.* Metformin and insulin suppress hepatic gluconeogenesis through phosphorylation of CREB binding protein. *Cell* **137**, 635-646 (2009).

239. Puigserver, P. *et al.* Insulin-regulated hepatic gluconeogenesis through FOXO1-PGC-1alpha interaction. *Nature* **423**, 550-555 (2003).

240. Lee, J.M. *et al.* AMPK-dependent repression of hepatic gluconeogenesis via disruption of CREB.CRTC2 complex by orphan nuclear receptor small heterodimer partner. *J. Biol. Chem.* **285**, 32182-32191 (2010).

241. Beale, E.G., Harvey, B.J. & Forest, C. PCK1 and PCK2 as candidate diabetes and obesity genes. *Cell Biochem. Biophys.* **48**, 89-95 (2007).

242. Hanson, R.W. & Reshef, L. Regulation of phosphoenolpyruvate carboxykinase (GTP) gene expression. *Annu. Rev. Biochem.* **66**, 581-611 (1997).

243. Leithner, K. *et al.* PCK2 activation mediates an adaptive response to glucose depletion in lung cancer. *Oncogene* **34**, 1044-1050 (2015).

244. Banka, S. & Newman, W.G. A clinical and molecular review of ubiquitous glucose-6-phosphatase deficiency caused by G6PC3 mutations. *Orphanet J. Rare Dis.* **8**, 84-84 (2013).

245. Singh, P., Han, E.H., Endrizzi, J.A., O'Brien, R.M. & Chi, Y.I. Crystal structures reveal a new and novel FoxO1 binding site within the human glucose-6-phosphatase catalytic subunit 1 gene promoter. *J. Struct. Biol.* **198**, 54-64 (2017).

246. Hutton, J.C. & O'Brien, R.M. Glucose-6-phosphatase Catalytic Subunit Gene Family *. *J. Biol. Chem.* **284**, 29241-29245 (2009).

247. Guo, S., Dunn, S.L. & White, M.F. The Reciprocal Stability of FOXO1 and IRS2 Creates a Regulatory Circuit that Controls Insulin Signaling. *Mol. Endocrinol.* **20**, 3389-3399 (2006).

248. Livak, K.J. & Schmittgen, T.D. Analysis of relative gene expression data using real-time quantitative PCR and the 2(-Delta Delta C(T)) Method. *Methods* **25**, 402-408 (2001).

249. Cao, R. *et al.* Prevention of HIV protease inhibitor-induced dysregulation of hepatic lipid metabolism by raltegravir via endoplasmic reticulum stress signaling pathways. *The Journal of pharmacology and experimental therapeutics* **334**, 530-539 (2010).

250. Walker, D.K. *et al.* Insulin increases mRNA abundance of the amino acid transporter SLC7A5/LAT1 via an mTORC1-dependent mechanism in skeletal muscle cells. *Physiol Rep* **2**, e00238 (2014).

251. Zhang, W. *et al.* FoxO1 regulates multiple metabolic pathways in the liver: effects on gluconeogenic, glycolytic, and lipogenic gene expression. *J. Biol. Chem.* **281**, 10105-10117 (2006).

252. Gao, Y., Moten, A. & Lin, H.-K. Akt: a new activation mechanism. *Cell Res.* **24**, 785-786 (2014).

253. Sarbassov, D.D., Guertin, D.A., Ali, S.M. & Sabatini, D.M. Phosphorylation and regulation of Akt/PKB by the rictor-mTOR complex. *Science* **307**, 1098-1101 (2005).

254. Tzivion, G., Dobson, M. & Ramakrishnan, G. FoxO transcription factors; Regulation by AKT and 14-3-3 proteins. *Biochim. Biophys. Acta* **1813**, 1938-1945 (2011).

255. You, B.R. & Park, W.H. Proteasome inhibition by MG132 induces growth inhibition and death of human pulmonary fibroblast cells in a caspase-independent manner. *Oncol. Rep.* **25**, 1705-1712 (2011).

256. Zhang, L. *et al.* MG132-mediated inhibition of the ubiquitin–proteasome pathway ameliorates cancer cachexia. *J. Cancer Res. Clin. Oncol.* **139**, 1105-1115 (2013).

257. Wang, S. *et al.* The ubiquitin-proteasome system is essential for the productive entry of Japanese encephalitis virus. *Virology* **498**, 116-127 (2016).

258. Takahashi, S.-s. *et al.* Loss of autophagy impairs physiological steatosis by accumulation of NCoR1. *Life Science Alliance* **3**, e201900513 (2020).

259. Saito, T. *et al.* Autophagy regulates lipid metabolism through selective turnover of NCoR1. *Nature Communications* **10**, 1567 (2019).

260. Tsai, W.C., Bhattacharyya, N., Han, L.Y., Hanover, J.A. & Rechler, M.M. Insulin inhibition of transcription stimulated by the forkhead protein Foxo1 is not solely due to nuclear exclusion. *Endocrinology* **144**, 5615-5622 (2003).

261. Perrot, V. & Rechler, M.M. Characterization of Insulin Inhibition of Transactivation by a C-terminal Fragment of the Forkhead Transcription Factor Foxo1 in Rat Hepatoma Cells *. *J. Biol. Chem.* **278**, 26111-26119 (2003).

262. Nakae, J., Park, B.-C. & Accili, D. Insulin Stimulates Phosphorylation of the Forkhead Transcription Factor FKHR on Serine 253 through a Wortmannin-sensitive Pathway*. *J. Biol. Chem.* **274**, 15982-15985 (1999).

263. Brunet, A. *et al.* Akt promotes cell survival by phosphorylating and inhibiting a Forkhead transcription factor. *Cell* **96**, 857-868 (1999).

264. Valenti, L. *et al.* Increased Expression and Activity of the Transcription Factor FOXO1 in Nonalcoholic Steatohepatitis. *Diabetes* **57**, 1355 (2008).

265. Shen, M. *et al.* Involvement of the Up-regulated FoxO1 Expression in Follicular Granulosa Cell Apoptosis Induced by Oxidative Stress *. *J. Biol. Chem.* **287**, 25727-25740 (2012).

266. Vincow, E.S. *et al.* Autophagy accounts for approximately one-third of mitochondrial protein turnover and is protein selective. *Autophagy* **15**, 1592-1605 (2019).

267. Komatsu , M. *et al.* Impairment of starvation-induced and constitutive autophagy in Atg7-deficient mice. *J. Cell Biol.* **169**, 425-434 (2005).

268. Yang, Z., Huang, J., Geng, J., Nair, U. & Klionsky, D.J. Atg22 recycles amino acids to link the degradative and recycling functions of autophagy. *Mol. Biol. Cell* **17**, 5094-5104 (2006).

269. Onodera, J. & Ohsumi, Y. Autophagy is required for maintenance of amino acid levels and protein synthesis under nitrogen starvation. *J. Biol. Chem.* **280**, 31582-31586 (2005).

270. Scalise, M., Galluccio, M., Console, L., Pochini, L. & Indiveri, C. The Human SLC7A5 (LAT1): The Intriguing Histidine/Large Neutral Amino Acid Transporter and Its Relevance to Human Health. **6** (2018).

271. Fukuhara, D. *et al.* Protein characterization of NA+-independent system L amino acid transporter 3 in mice: a potential role in supply of branched-chain amino acids under nutrient starvation. *Am. J. Pathol.* **170**, 888-898 (2007).

272. Zhang, N. *et al.* Increased Amino Acid Uptake Supports Autophagy-Deficient Cell Survival upon Glutamine Deprivation. *Cell Rep.* **23**, 3006-3020 (2018).

273. Collins, J.K. *et al.* Watermelon consumption increases plasma arginine concentrations in adults. *Nutrition* **23**, 261-266 (2007).

274. Landauer, K. Designing media for animal cell culture: CHO cells, the industrial standard. *Methods Mol. Biol.* **1104**, 89-103 (2014).

275. Salazar, A., Keusgen, M. & von Hagen, J. Amino acids in the cultivation of mammalian cells. *Amino Acids* **48**, 1161-1171 (2016).

276. Schneider-Poetsch, T. *et al.* Inhibition of eukaryotic translation elongation by cycloheximide and lactimidomycin. *Nat. Chem. Biol.* **6**, 209-217 (2010).

277. Sharma, P., Nilges, B.S., Wu, J. & Leidel, S.A. The translation inhibitor cycloheximide affects ribosome profiling data in a species-specific manner. *bioRxiv*, 746255 (2019).

278. Park, Y. *et al.* Versatile Synthetic Route to Cycloheximide and Analogues That Potently Inhibit Translation Elongation. *Angewandte Chemie International Edition* **58**, 5387-5391 (2019).

279. Kim, K.H. *et al.* Autophagy deficiency leads to protection from obesity and insulin resistance by inducing Fgf21 as a mitokine. *Nat. Med.* **19**, 83-92 (2013).

280. Zhang, N. *et al.* Increased Amino Acid Uptake Supports Autophagy-Deficient Cell Survival upon Glutamine Deprivation. *Cell Rep.* **23**, 3006-3020 (2018).

281. Ling, A.V. *et al.* FoxO1 Is Required for Most of the Metabolic and Hormonal Perturbations Produced by Hepatic Insulin Receptor Deletion in Male Mice. *Endocrinology* **159**, 1253-1263 (2018).

282. Pan, X., Zhang, Y., Kim, H.G., Liangpunsakul, S. & Dong, X.C. FOXO transcription factors protect against the diet-induced fatty liver disease. *Sci. Rep.* **7**, 44597 (2017).

283. Zhang, B. *et al.* SIRT3 overexpression antagonizes high glucose accelerated cellular senescence in human diploid fibroblasts via the SIRT3-FOXO1 signaling pathway. *Age (Dordr)* **35**, 2237-2253 (2013).

284. Wang, Y. *et al.* Regulation of SIRT3/FOXO1 Signaling Pathway in Rats with Non-alcoholic Steatohepatitis by Salvianolic Acid B. *Arch. Med. Res.* **48**, 506-512 (2017).